SCUOLA DI DOTTORATO

UNIVERSITÀ DEGLI STUDI DI MILANO-BICOCCA

Dipartimento di / Department of

Fisica G. Occhialini

Dottorato di Ricerca in / PhD program Fisica e Astronomia Ciclo / Cycle XXXVII

Curriculum in (se presente / if it is) Fisica Subnucleare e Tecnologie Fisiche

Development of prototype PVDF-based ultrasound transducer for thermoacoustic and iono-acoustic imaging

Cognome / Surname BAIG Nome / Name Mirza Hassan

Matricola / Registration number 883870

Tutore / Tutor: Prof. Giuseppe Chirico

Cotutore / Co-tutor: Dr. Elia Arturo Vallicelli
(se presente / if there is one)

Supervisor: Dr. Marcello De Matteis
(se presente / if there is one)

Coordinatore / Coordinator: Prof. Stefano Ragazzi

ANNO ACCADEMICO / ACADEMIC YEAR 2023/2024

Table of Contents

List of Table

List of figures

Abstract

This work presents the comprehensive design, development, and experimental validation of two prototype ultrasound piezoelectric sensors. These sensors are specifically developed for the purpose of thermoacoustic imaging and ionoacoustic tomography , respectively. Both sensors utilize polyvinylidene fluoride (PVDF) as the piezoelectric material. PVDF was chosen for its outstanding characteristics, compared to the state-of-the-art PZT ultrasound sensor. The relationship between the physical structure and the acoustic characteristics of the PVDF transducer was simulated using both a Finite Element Model (FEM) and an Analytical Model. The simulations demonstrated that most relevant sensor variables, such as the frequency response and sensitivity, are significantly influenced by the physical arrangement of the transducer. Printed circuit board (PCB) technology was used to accurately define the sensor's active area, while simultaneously reducing the complexity and cost. The first sensor is developed by using PVDF material with a thickness of 20 μm. It is specially designed for thermoacoustic imaging and has an active area of 0.3x10mm millimeters, which has the bandwidth of 10MHz. The sensor is configured with a Multichannel array design. This design is crucial for achieving optimal imaging results with resolution in the range of 10 microns. At the same time multichannel format allows for future applications of bioimaging. The second sensor utilizes PVDF-TrFE material with a thickness of 1.2mm, which is specifically designed for ionoacoustic tomography in hadron therapy. The scope of this sensor is to accurately measure the deposition of dose during treatment. This sensor has a bandwidth of 1 MHz and is equipped with three parallel channels, each of which has dimensions of 3x30 mm. The design of these sensors was carefully developed using analytical modeling and finite-element simulations to optimize their directivity, frequency response, and sensitivity. Both sensors were subjected to acoustic behavior validation, and preliminary experimental findings were provided to confirm the acoustic behavior of both sensors. Such a sensor would be used for further acoustic characterization by using an amplifier and finally used as a potential candidate for sensing of cells in photoacoustic bioimaging or in hadron therapy monitoring.

Chapter 1.

State of the art sensors and Thesis Motivation

1.1 Overview of State of the art sensors

Piezoelectric features like high sensitivity and energy conversion make PZT (lead zirconate titanate) sensors popular in thermoacoustic imaging (TAI). They create powerful signals, making them ideal for medical imaging and industrial non-destructive testing. PZT sensors have flexibility, mechanical impedance, and wearable device integration issues. Brittleness renders them unsuitable for biological applications that need conformal or flexible surfaces. Inefficient coupling with biological tissues due to high acoustic impedance reduces soft tissue imaging sensitivity.

Table 1: State-of-the-art PZT sensor comparison

Sensor PZT	frequency	Sensitivity(V/Pa)	Band width	Resolution	Reference
HIFU PZT sensor (1-3)	1-5 MHz	100 mV/Pa	40%	500 µm	Brown et al., Ultrasonics, 2020
CMUT-PZT hybrid transducer	3-10MHz	120 mV/Pa	60%	300 µm	Kim et al., IEEE Trans. Biomed. Eng., 2019
Polymer-PZT Composite Senso	0.5-2.5MHz	75 mV/Pa	30%	600 µm	Beard, P.C. (2011), *Biomedical Optoacoustic Imaging*, Physics Review
Piezoelectric single element	5-20MHz	150 mV/Pa	70%	200 µm	Kim et al. (2014), *High-Resolution Photoacoustic Imaging*, Appl. Phys. Lett.
3D PZT Matrix Array	1–20 MHz	180mV/Pa	50%	250 µm	Wang, L.V., & Hu, S. (2010), *3D PZT Transducers in PAI*, IEEE Transactions

PVDF sensors are more flexible, have lower acoustic impedance, and are more mechanically adaptable. PVDF's compliance improves tissue matching and TAI signal reception, especially on curved or uneven surfaces**[4]**. Although PVDF has lesser piezoelectric efficacy than PZT, its mechanical adaptability and enhanced tissue interaction benefit certain TAI circumstances. Despite its lesser sensitivity than PZT, PVDF sensors are promise for flexible and integrated applications.

The table 1.1 presents a comparative analysis of advanced PZT (Piezoelectric) sensors, emphasizing frequency range, sensitivity, bandwidth, resolution, and pertinent references. Each sensor type exhibits unique advantages and disadvantages, contingent upon its specific application. For instance, the HIFU PZT sensor demonstrates a sensitivity of 100 mV/Pa and a resolution of 500 µm. In contrast, the CMUT-PZT hybrid transducer exceeds these metrics with a sensitivity of 120 mV/Pa and a resolution of 300 µm; however, its broader frequency range may affect performance consistency throughout that range. The polymer-PZT composite sensor demonstrates reduced sensitivity (75 mV/Pa) while providing the widest resolution (600 µm). Piezoelectric single-element sensors and 3D PZT matrix arrays exhibit high sensitivity (150 mV/Pa and 180 mV/Pa, respectively) and enhanced resolutions; however, challenges persist in achieving a balance between wide bandwidth and precision across a broadband frequency range. The limitations of these sensors involve trade-offs among sensitivity, bandwidth, and resolution, with improvements in one parameter frequently resulting in compromises in another. The identified trade-offs underscore the necessity for progress in material science and design to develop sensors that exhibit a more balanced performance across various biomedical applications.

Table 2: State of the Art in Ionoacoustics comparison [5]

	Assmann et al, 2015 [4]	Patch et al, 2016 [5]	Hayakawa et al, 1995 [3]	Jones et al, 2016 [6]	Lehrack et al., 2017 [7]
Beam Type	Protons	Protons	Protons	Protons	Protons
Beam Energy	20 MeV	49 MeV	100 MeV	190 MeV	220 MeV
Absorber	Water tank	Water tank, inhomogeneous target	Hepatic cancer patient	Water tank	Water tank
Particle Range	4.1 mm	21 mm	70 mm	238 mm	320 mm
Beam Diameter (FWHM of spot size at BP)	1.6 mm	4 mm	n.a.	22 mm	7.5 mm at water tank entrace
Particles/shot	10^6	$19 \cdot 10^6$	n.a.	$56 \cdot 10^6$	
Dose/shot	1.6 Gy	2 Gy	3 mGy	34 mGy	10 mGy
dP at Bragg Peak	250 Pa	200 Pa	n.a.	~ 6 Pa	~ 1 Pa
BP-Sensor Distance	25.4 mm	6.5 mm	120 mm	50 mm	75 mm
dP at sensor	n.a.	n.a.	500 mPa	32 mPa	8 mPa
Signal frequency	2 MHz	700 kHz	170 kHz	45 kHz	< 50 kHz
Detector	1 channel PZT, 3.5 MHz resonant frequency	94-ch PZT ultrasound array, 1-4 MHz pass-band	10 uV/Pa hydrophone	Commercial omnidirectional hydrophone	Commercial hydrophone
Analog Front-end	General purpose 60 dB, 10 MHz BW LNA	Medical ultrasound array	80 dB gain LNA and passive RC low-pass filter	Commercial charge amplifier	Commercial low-noise amplifier
N shots	16	1024	100-700	200	1000
Precision	45 µm	n.a.	n.a.	2.2 mm	1 mm
Accuracy	< 100 µm	1.2 mm	2 mm	4.5 mm	

The table compares proton beam treatment systems based on various experimental settings and characteristics. Each research employs a distinct set of beam intensities, absorbers, detectors, and signal processing equipment to quantify typical parameters such as particle range, dosage per shot, and accuracy. For example, Assmann et al. (2015) employed a 20 MeV proton beam with a water tank absorber to reach a 4.1 mm particle range, but Lehrack et al. (2017) used a higher 220 MeV proton beam, resulting in a substantially wider particle range of 320 mm. Detectors range from highly specialized 94-channel PZT ultrasonund arrays (Patch et al., 2016) to commercial hydrophones with different signal frequency and sensitivity. While each configuration yields useful insights into proton beam characterization, many limits emerge from the investigations. Especially, differences in beam intensity and detecting systems add discrepancies that make direct comparisons difficult. Furthermore, there are major trade-offs between particle range, accuracy, and detector type (e.g., PZT arrays versus commercial hydrophones). Higher precision systems, like Jones et al. (2016)'s 45 µm accuracy, may necessitate more complicated and specialised equipment, making them unsuitable for many

clinical contexts. The issue remains in maximising both accuracy and convenience of use across a wide variety of beam intensities and experimental settings, emphasising the need for more standardised measurement techniques.

1.2 Thesis outline

This thesis is organized in three main sections. First one is about general and historical overview of acoustic sensor and second is about introduction to addresses fundamental topics concerning thermoacoustic imaging and the development of piezoelectric materials, emphasizing its applications in acoustic sensing. Thermoacoustic imaging, a method retaining acoustic signals produced by pulsed laser, provides high-resolution biomedical imaging. The identification of piezoelectric materials has facilitated the advancement of diverse sensing technologies, resulting in the creation of both inorganic and organic piezoelectric substances. Polyvinylidene Fluoride (PVDF) polymers have gained considerable interest owing to their advantageous characteristics, including flexibility, elevated piezoelectric constants, and acoustic impedance compatibility with biological tissues, rendering them suitable for pressure sensing applications. The viability of PVDF as an acoustic sensor is examined, emphasising its application in ultrasonic transducers, particularly piezoelectric-based ultrasound transducers (pUT), which are contrasted with capacitive-based ultrasound transducers (cUT). The discussion encompasses the structural components and active layer characteristics of piezoelectric ultrasonic transducers, including piezoelectric constants, electromechanical coupling, and the application of matching layers to enhance sensitivity. The concepts of piezoelectric transduction, including the piezoelectric effect and the incorporation of a supporting layer in annular array configurations, are also highlighted. This section discusses the resolution capabilities of 1-D ultrasound transducers, emphasising axial and lateral resolution, and explores the issues in developing high-frequency ultrasound transducers. The last section examines the produced acoustic effect, which is essential to the operation of these devices. This thorough introduction establishes the groundwork for an in-depth examination of PVDF-based sensors within the realm of advanced acoustic sensing applications.

The chapter 3 of the thesis describes the development of broad-band Polyvinylidene Fluoride (PVDF)-based ultrasound sensor array designed for biomedical thermoacoustic imaging applications, such melanoma detection for the preliminary results along with its modelling and experimental validation. The construction and performance of the PVDF transducer were studied by using Finite Element Modelling (FEM). The 3.6 μV/Pa sensitivity and 56 MHz resonant frequency were attained using the developed PVDF sensor. Because of the PVDF

materials key characteristics, which include an acoustic impedance that is similar to biological tissues differently than other materials like PZT, do not require the complex acoustic matching layers that are necessary. Our prototype had a multichannel array with a modest active area for each channel, which was made via a low-cost PCB-based fabrication method. The electrical and acoustic performance of the sensor was experimentally tested, revealing a close agreement with the FEM predictions. According to the results, the PVDF sensor may make inexpensive, high-resolution, non-invasive biomedical imaging possible.

Chapter 4 of the thesis discuss the details of the development and testing of an ultrasound sensor array based on polyvinylidene fluoride (PVDF) for ionoacoustic tomography in hadron treatment, a method for accurately mapping particle beam dose deposition. Pulsed particle beams produce ionoacoustic signals that, with a spatial resolution of sub-millimeter, reveal details on the energy deposition. In order to address the issues with poor sensitivity and narrow bandwidth with conventional PZT sensors, we developed the PVDF-TrFE sensor array. In order to achieve wide frequency response and minimise signal distortion, I focused on manufacturing of 3-channel prototype with a 1 MHz bandwidth. The experimental setups and FEM simulations were used to characterize the sensor's acoustic behavior, which confirmed that PVDF could acquire weak acoustic signals at different energy levels and revealed a sensitivity of 480 μV/Pa. The concept highlights the possibility of adaptive hadron treatment in real-time using sensors based on photovoltaic diode arrays, which might provide precise and low-latency dosage mapping.

Finally, the obtained results will be discussed, and conclusions will be drawn.

Chapter 2.

Introduction

2.1 Thermoacoustic Imaging

Thermoacoustic Imaging (TAI) is a developing biological imaging method. In TAI excitation sources use far-infrared light laser source. It offers increased imaging depth as a result of the use of distinct non-invasive infrared radiation[6]. TAI technology can take image at deeper depths than other optical visible imaging methods and offers better spatial resolution than ultrasound imaging. This type of imaging modality, which makes advantage of the photoacoustic effect, quick and concentrated energy depositions by infrared pulsed laser by exploiting the acoustic signal that the deposition itself produces. When energy deposition over the time shorter than the thermal relaxation time , measured in tens or hundreds of nanoseconds, the absorber experiences a rise in temperature. This phenomenon, in turn, causes an increase in pressure, which may be detected by specialised sensors through the propagation of an acoustic signal. By employing suitable techniques (such as beamforming), the information on the variation in the acoustic wave's arrival time to create an image of the acoustic source through the use of multichannel sensors (linear arrays or matrices), allows to Commercial ultrasound sensor arrays designed for medical ultrasonography are often used in thermoacoustic imaging research. However, these arrays have unique characteristics. There is a need to manufacture of specific sensors with the following characteristics.

- Well-acoustically connected with biological tissues for maximum sensitivity and ability to detect weak acoustic signals.
- Multichannel with tailored geometry for different application.
- Thermoacoustic detectors may be manufactured using industrial procedures, allowing for economies of scale and multiple use.
- Advanced detectors apply etching processes to remove metallization from PVDF and define channel areas. This is in contrast to the traditional etching technique of discussing the novel design and validation of an ultrasonic sensor using printed circuit technology (PCB) to specify the geometry of a single channel.
- Use of a PVDF with metallization on one side (ground plane) and gluing it to a PCB with exposed pads (equivalent to sensor channel area) allows for a rapid and cost-effective acoustic sensor with a precise active region specified by the PCB pad.

- This method uses a consolidated industrial technology to create a sensor with high accuracy (a few micrometres) without requiring additional technical stages[7].

There are numerous applications of ultrasound detectors in the medical field but the most emerging and concerning application in medical imaging application is the Melanoma diagnosis. Early detection is crucial for successfully treating melanoma, a malignant skin cancer that resembles a cutaneous nevi. A pulsed laser with adequate wavelengths can map endogenous chromatophores (e.g. melanin) and reconstruct a 3D picture by mapping the absorption coefficient. This is not achievable with typical optical methods at depths of several millimeters[8].

In the past ten years, Photoacoustic imaging (PAI) has achieved notable advancements in several pre-clinical and clinical applications as a result of improved instrumentation, such as innovative optoacoustic transducer designs, and the incorporation of enhanced reconstruction algorithms[9, 10]. In addition, due to the same detection platform with widely used ultrasound imaging, researchers have created integrated ultrasound and photoacoustic imaging systems with handheld devices. These systems allow for the simultaneous display of morphological and molecular differences in tissue. The current standard in all these applications is bulk piezoelectric transducers. However, in order to create wearable, portable, or micro-endoscopy photoacoustic imaging (PAI) devices, it is necessary to utilize small ultrasound transducers and seamlessly integrate them with optical components and the corresponding front-end electronics. Micromachined ultrasonic transducer (MUT) arrays, created utilizing micro-electro-mechanical systems (MEMS) technology, can be easily attached to application specific integrated circuits (ASICs)[11]. These arrays are highly suitable for tiny devices. The compact size of integrated MUT-ASICs allows for the efficient placement of optical components, like as fiber coupled lasers, to effectively transfer light into deep tissue. MUTs should possess both a cost-effective nature and excellent reproducibility as a result of batch fabrication processing[12]. As a result of decreased power needs and the convenience of on-chip processing, these systems will also enable the shrinking of necessary electronics and power subsystems[13]**.** Cost-effective portable PAI devices have the potential to enhance point-of-care imaging applications and serve as a valuable addition to conventional imaging technologies like MRI and PET.

High-frequency transducers which are spherically focused, have a large frequency bandwidth spanning from 10 MHz to more than 150 MHz. In both of cases, 9 um-thick piezoelectric

PVDF (polyvinylidene fluoride) film is used. Anticipating that the phase velocity of longitudinal waves may be determined using a flat transducer composed of the same piezoelectric PVDF film is a reasonable expectation. It may be used to study very thin materials due to its high-frequency bandwidth. We created a flat PVDF transducer and successfully measured the phase velocity of the longitudinal mode propagating in the thickness direction of a very thin glass slide and stainless steel shim by using it as a generator and detector of ultrasound waves[14]. A modified sampled technique that is tailored to the flat PVDF transducer aligned parallel to a very thin-plate specimen and uses water as a coupling medium is of particular interest, even though both a broadband pulse and a tone burst of different carrier frequencies are used for this purpose. This technique sweeps frequency over the effective bandwidth of the PVDF transducer.

2.2 Discovery of piezoelectric materials

Four external forces determine the life cycle of a material or product which are known as environmental forces acronym as STEP (social/culture, technology, economic, and political forces). The development of piezoelectric material depends on the support of these external forces. Pierre and Jacques Curie discovered the direct piezoelectric action in single crystal quartz in 1880. Under pressure, quartz generates electrical charge/voltage from other materials. The term "piezo" means "pressure" in Greek, hence the original meaning of piezoelectricity is "pressure electricity." Materials exhibiting this effect have a geometric strain proportional to the applied electric field[15]**.** Gabriel Lippmann discovered the converse piezoelectric effect in 1881. Pierre Curie's understanding of the link between the two occurrences led to his groundbreaking thoughts on the importance of symmetry in physics.
The Curie brothers used this discovery to create the piezoelectric quartz electrometer, which could measure tiny electric currents. This let Pierre's wife, Marie Curie, do early research 20 years later. Several materials have been found to exhibit piezoelectricity. For example, both inorganic and biological piezoelectric materials exhibit the piezoelectric effect[16]. Inorganic piezoelectric materials lack inversion symmetry, resulting in uneven distribution of positive and negative charges. Mechanical stress on a material induces ion displacement, leading to the creation of an electric field[17]. Organic piezoelectric materials comprise polar molecules with a permanent electric dipole moment. Applying stress causes electric polarization as molecular dipoles align in the stress direction[18].

2.3 Organic Piezoelectric materials

The world of organic piezoelectric materials incorporates both natural and synthetic origins. Natural organic piezoelectric materials embrace small biomolecules namely amino acids, long-chain peptides, proteins, polysaccharides, and viruses are examples of macromolecules that can be found in peptides[19]. Some representative examples of synthetic organic piezoelectric materials are polyvinylidene fluoride (PVDF), poly(vinylidene fluoride-trifluoroethylene) (PVDF-TrFE), poly (L-lactic acid) (PLLA), poly (γ-benzyl glutamate) (PBG), poly (3-hydroxybutyric acid-co-3-hydrovaleric acid) (PHBV), etc. [30–33]. These materials have been used for a variety of applications in the field of biomedicine, including biomechanical energy harvesting, biosensing, and the regeneration of cells and tissues[20, 21].On top of that, organic piezoelectric materials have recently emerged as potential options for the development of implanted biomedical devices. The fact that they possess a number of favorable qualities makes it possible for them to be utilized in devices that are on the micro and nanoscale. PLLA and its copolymers are favored over PZT due to their superior biocompatibility and biodegradability. This preference arises from the potential toxicity of PZT's lead concentration to living creatures[22]. Organic piezoelectric materials, like PVDF and PHBV, possess greater flexibility and stretchability, allowing their design to closely align with the mechanical properties of biological tissues. This promotes improved integration and compatibility, unlike inorganic materials which may lack similar tissue-matching capabilities[23].

Organic piezoelectric materials often have a reduced environmental footprint in comparison to several inorganic materials. This is because they may be obtained from renewable sources and frequently involve simpler and more sustainable production techniques. These materials may be produced by solution-based methods like spin coating, inkjet printing, or spray coating. However, inorganic piezoelectric materials necessitate more intricate and costly fabrication procedures such as physical vapor deposition or chemical vapor deposition[24]. It is fascinating that the capacity of organic piezoelectric materials to convert the mechanical energy of internal body movements into electricity has allowed the creation of implantable biomedical devices that are self-powered. This reduces the necessity for external batteries and extends the device's lifespan[25].

Table 3:Comparison of Electromechanical Properties of PVDF, P(VDF-TrFE), PZT[26].

Parameter	**PVDF**	**PVDF-TrFE**	**PZT**
Sound Speed (m/s)	2200	2400	4350
Density (g/cm^3)	1.78	1.88	7.75
Impedance (Mrayl)	3.9	4.5	39.5
Relative-dielectric permittivity	6.0	5.0	1200
Mechanical Q	10	25	75
Electromechanical coupling Coefficient	0.15-0.20	0.3	0.49
Flexibility	Outstanding	Satisfactory	Poor

PVDF and its copolymers revealed itself as extremely beneficial in medical and biological imaging above 15 MHz. Polymer transducers have offered straightforward, small, robust, and diffraction-limited performance, whereas ceramic transducers have suffered with sensitivity, repeatability, beam characteristics, and manufacturing issues. The review paper by Brown is a great place to get reference material on PVDF[27]**.** A comparison of the important material parameters for PVDF, P(VDF-TrFE), and PZT5A is given in Table I. Table I makes a striking contrast in the physical characteristics of the polymers and the ceramic apparent. Ceramics are superior to other materials in a number of crucial aspects, like mechanical Q and electromechanical efficiency, but their extreme brittleness and high acoustical impedance pose a significant barrier in the high-frequency range. For a resonant structure operating at 50 MHz, PZT5A must have a thickness of 43.5 μm. This indicates that the active ingredient is just 6–8 times thicker than the ceramic's grain structure. In addition to resulting in a lower coupling factor and higher electromechanical losses[28]**,** this also makes the structure too delicate to be used as a transducer. PVDF was therefore the perfect material for high frequency imaging because to its low acoustical impedance, mild piezoelectric characteristics, and excellent mechanical flexibility. To accurately estimate the performance of the material, certain features of PVDF, such as its frequency-dependent dielectric and mechanical losses, have to be taken into account. In 1989, Brown and Carlson published helpful models for measuring the dielectric and acoustic characteristics of PVDF.

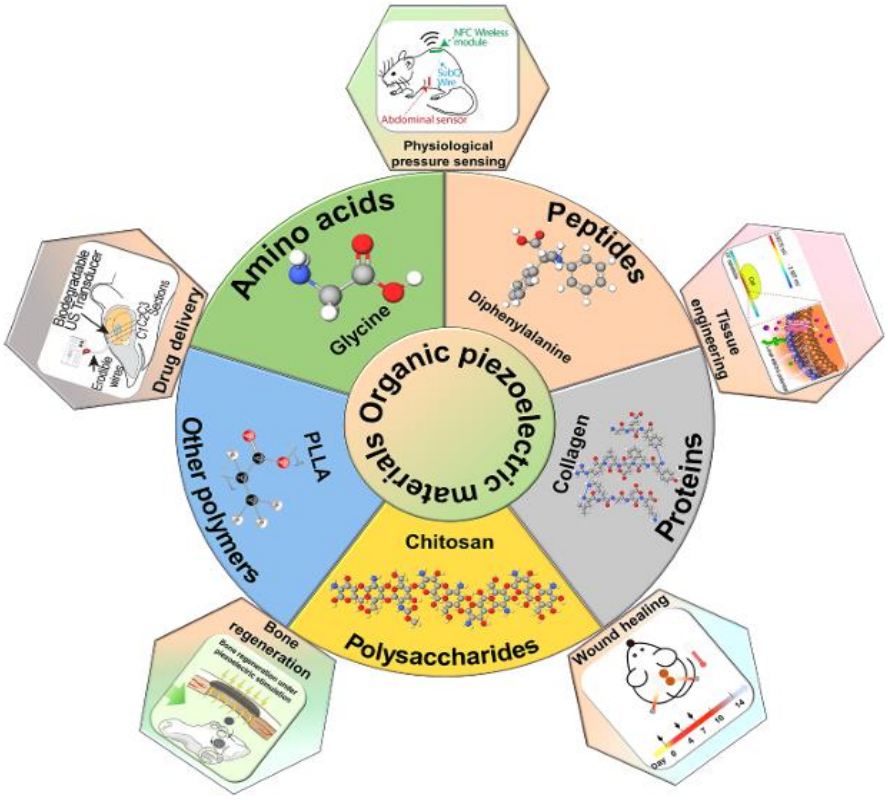

Figure 1:Schematic illustration of different categories of organic piezoelectric materials and their applications in implantable biomedical devices [23].

2.4 PVDF-Polymers

PVDF is a kind of polymer that exhibits semicrystalline properties. In 1969, Japanese scientist Kawai discovered that PVDF has enhanced piezoelectricity when subjected to mechanical stretching and high-voltage polarization[29].

When comparing with other polymers like poly(vinyl chloride) and poly, it can be observed that Carbonate has significantly enhanced piezoelectric activity, indicating a significant advancement in the historical evolution of piezoelectricity in polymer research. Subsequently, the researchers also discovered that PVDF and its copolymers have commendable pyroelectric and ferroelectric properties[30]. PVDF material has excellent electrical properties, which makes it a potential candidate for great use in the field of medical applications. Polyvinylidene fluoride (PVDF) and its copolymers, such as P(VDF-TrFE) and P(VDF-CTFE), are all materials that exhibit ferroelectric behavior, as well as possessing piezoelectric and ferroelectric capabilities. Quartz crystal exhibits limited piezoelectric activity and requires a simple and symmetric manufacturing technique. Lead-based piezoelectric ceramics, such as lead zirconate titanate (PZT), are fatal among the organic piezoelectric materials[31]**.** When compared to inorganic piezoelectric materials, organic polymer materials have clear

advantages in terms of mechanical properties, lightweight, flexibility, chemical stability, ease of processing, non-toxicity, and biocompatibility. As a result, they have rapidly emerged as a highly developed type of piezoelectric functional material over the past two decades[32].

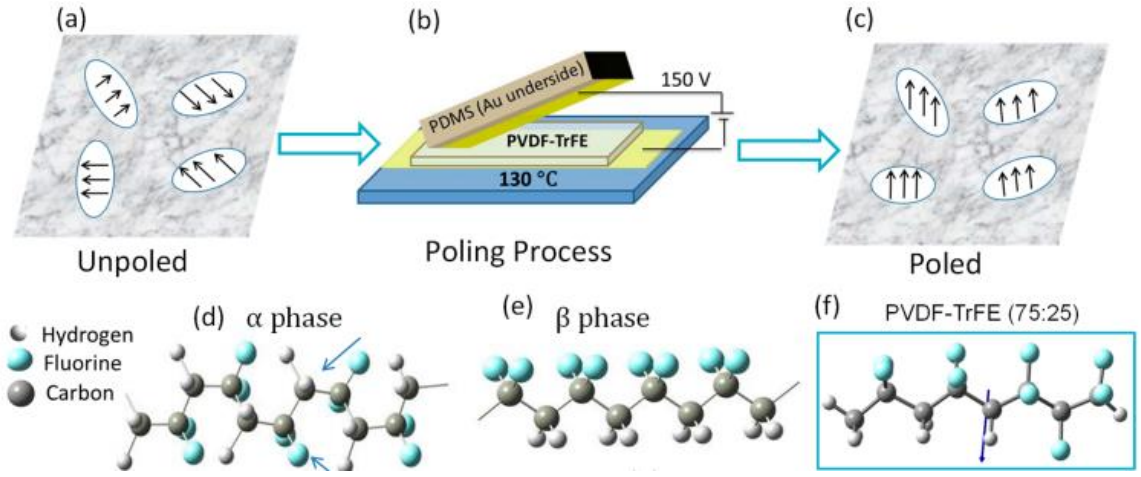

Figure 2: Chemical structure and spectroscopic fingerprint of PVDF. (a) Schematic representation of unpoled PVDF-TrFE. It has crystalline, (b) Application of a vertical electric field while heating the film just above the ferroelectric-paraelectric transition temperature results, (c) an alignment of the net dipole moment. Schematic representation of (d) α PVDF, (e) β PVDF, and (f) β PVDF-TrFE (75:25). (g) Raman spectrum of PVDF-TrFE (75:25)

PVDF and its copolymers are polymers with crystalline dipolar domains surrounded by a noncrystalline matrix (see Figure 2a). During crystallisation at the ferroelectric-paraelectric transition temperature, an electric field is applied to align the dipoles, as seen in Figure 2b,c. Molecular dipoles can be aligned parallel or perpendicular to the film plane by changing the direction of the electric field, a process known as poling[33]**.**The net dipole moment of a molecule is determined by its backbone chain structure. At least four stages have been recognized. The two main phases are paraelectric (α) and ferroelectric (β). The α phase features a backbone conformation of alternating trans-gauche ($TG^{+}TG^{-}$), whereas the β phase is all-trans (TTTT). Figure 2d, e illustrates these two phases, with arrows indicating the direction of the dipole moment. In the α phase, the backbone conformation causes individual dipole moments to cancel out. The β phase exhibits ferroelectricity due to variations in electronegativity between hydrogen and fluorine atoms. This results in a dipole moment for each molecule perpendicular to the backbone of plane.

Polyvinylidene fluoride (PVDF) is mostly known for its high polarity in piezoelectric polymers. The unique conformation of overlapped molecular chains (CF2-CH2) and the arrangement of molecular chains are intimately associated with PVDF. Typically, the molecular chain of PVDF may assume distinct configurations of α, β, γ, and δ, correspondingly. It has been demonstrated

that the β conformation is accountable for the material's favourable ferroelectric and piezoelectric characteristics. However, temperature increases, pressure changes, and other circumstances can readily disrupt the β-phase confirmation of PVDF, which can decrease or even eliminate the piezoelectric feature and negatively impact the stability of the device[]. Consequently, in flexible piezoelectric sectors, PVDF is rapidly being replaced by a PVDF-based copolymer poly (vinylidene fluoride-trifluoroethylene) (P(VDF-TrFE)) that has demonstrated a naturally predominance of β conformation. Along with inheriting PVDF's advantages, P(VDF-TrFE) also has greater piezoelectric characteristics and a larger β phase composition.

Untreated PVDF mostly crystallizes in the form of a phase, with its piezoelectricity primarily dependent on the polarity of the phase. Despite its high flexibility, PVDF has a very tiny piezoelectric constant when compared to inorganic piezoelectric materials. Hence, increasing the concentration of the phase is the primary method to enhance the piezoelectric activity of PVDF. The crystal structure of PVDF has a direct bearing on both its ferroelectricity and piezoelectricity. The unit cell has no net dipole moment due to the antiparallel arrangement of molecular chains in phase. The unit cell in the other three crystal forms has a net electric dipole moment and is capable of spontaneous polarization. The dipoles in the unit cell are parallel to one another and perpendicular to the molecular chain axis. Of them, the phase has the highest piezoelectric coefficient, dielectric permittivity, and dipole moments per chain per repeat unit (2.10 D)[34].

Table 4: Comparison of PVDF and its copolymers performance with inorganic piezoelectric [21].

Material	ε_r	Curie Point (°C)	g33 (10^{-3} Vm/N)	d (10^{-12}C/N)	k_{33}
PVDF	8-12	80	339	d_{33}= 30, d_{31}=20–30	0.20
P(VDF-TrFE)	5-19	90	380	d_{33}= 38, d_{31}=6–12	0.285
PVDF(VDF-CTFE)	12	/	/	d_{33}= -140 d_{31}=6	0.39
Quartz	5	520	50.0	d_{11}=2.0-2.3	/
ZnO	10.9	/	/	d_{33}=12.4 ±1.1, d_{31}= 5.0 ± 0.1	0.48 ±0.05
$BaTio_3$	1200	120	14.1	d_{33}=149	/
PZT-4	1300	380	26.1	d_{33}=289	0.4

The given comparison table 2. illustrate that Pvdf should be a potential candidate for the piezoelectric-based sensors for acquiring appealing applications in medical imaging. Due to their moderate piezoelectric constants and comparatively low Curie points, PVDF-based

polymers (PVDF, P(VDF-TrFE), and PVDF(VDF-CTFE)) are adaptable and appropriate for a wide range of sensor applications. Because of its low piezoelectric constants and extremely high Curie point, quartz is usually utilized in applications requiring reliable frequency control. Higher piezoelectric constants such as those of ZnO and BaTiO3 make them appropriate for applications needing greater sensitivity. PZT-4 is utilized in high-performance applications such as transducers and actuators because of its exceptionally high relative permittivity and piezoelectric constants. In contrast to PZT, Pvdf materials have wide bandwidth and flexibility in their structure, which dominates Pvdf over the PZT in different applications like Sensors for Medical Imaging.

2.5 PVDF as pressure Sensor

PVDF-based piezoelectric materials are being explored for use as pressure sensors in engineering, physiological testing, and micromechanical applications. The polymer's requirements are mostly thin film or nanofiber. The structure is sandwich-like, with electrodes on the top and bottom layers and PVDF-based piezoelectric materials in the center. The pressure sensor will determine if a pipeline valve is routinely turned based on measured pressure changes[35]. The sensor monitors dynamic low-frequency pressure changes due to the delayed discharge of charge on the electrodes caused by foil strain. The advantages of this technology include good aging resistance at low temperatures and pressures, low production costs, short response time, and wide operating temperature and pressure ranges. However, measurement accuracy is limited by the intersection of temperature, thermoelectricity, and temperature sensitivity. Spin-coating the P(VDF-TrFE) copolymer onto a silicon substrate results in a thin film. The tiny form size and biocompatibility of this device allow for integration with catheters to monitor blood flow direction and vascular pressure, opening up new possibilities for implanted medical devices[36].

PVDF can be built as a basic accelerometer, vibrometer, and orientation sensor in addition to applying positive pressure to cause the material to bend and deform to provide piezoelectric response; these applications show promise for usage in sensitive impact detectors and self-balancing robots.

PVDF-based pressure sensors have numerous applications in the field of wearable technologies for human-computer interaction. The piezoelectric sensor incorporates a skin-interactive metal-free spongy electrode. This electrode utilizes highly aligned poly(vinylidene fluoride)

(PVDF) arrays as the piezoelectric active component. Flexible electrodes are created by coating the PVDF nanofibers with conducting polyaniline (PANI) . This design effectively overcomes the shortcomings of poor compatibility and fragility associated with metal electrodes. Additionally, it exhibits excellent mechanical-to-electrical energy conversion properties. As a result, it can accurately detect human finger touch with a high energy conversion efficiency of approximately 53%[37, 38].

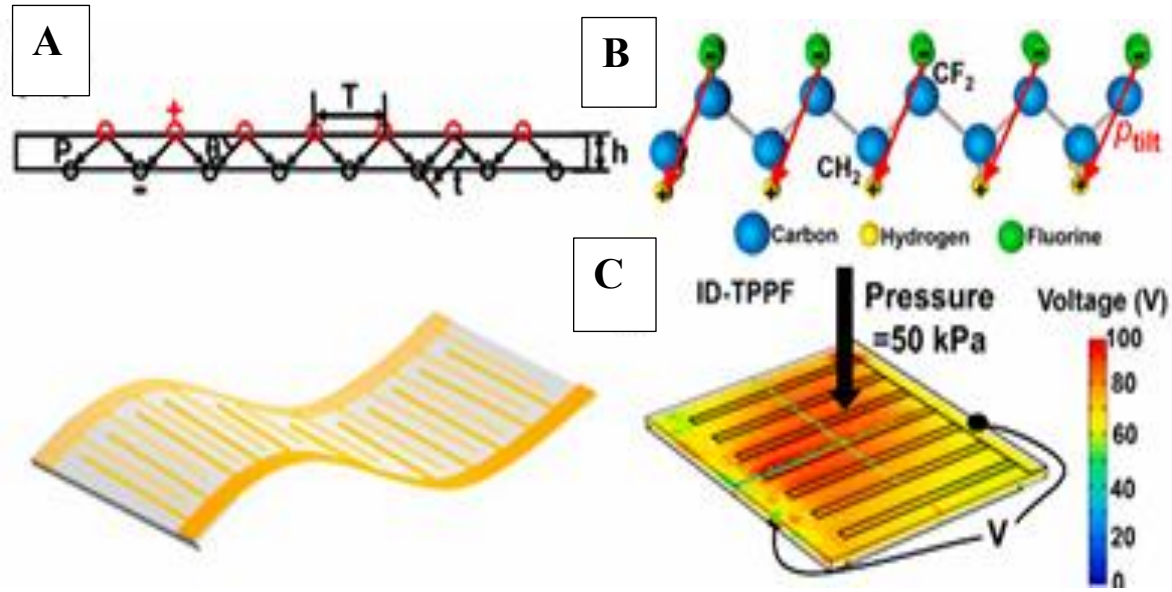

Figure 3:(A) Schematic illustration of alternatively tilt-polarized P(VDF-TrFE) film. (B) Molecular chain arrangement and tilt dipole orientation uptilt of P(VDF-TrFE) polymer(C) The voltage distribution on ID-TPPF under a dynamic pressure of 50 kPa[2].

the P(VDF-TrFE) piezoelectric film by inkjet printing (Figure 3A). Then, by applying a high voltage, multiple alternating oblique polarization regions (Figure 3B,C) are generated inside the cross-sectional area, which exhibits enhanced sensitivity to an external stress stimulation. The patterned electrode can effectively improve the device's sensitivity in addition to changing the material itself[25].

2.6 Feasibility as Acoustic Sensor

Sound detection and recognition sensors (SDRs) utilizing electrostatic, capacitive, electromagnetic, or electrical approaches suffer from drawbacks such as bulky dimensions, internal power requirements, and low electro-acoustic conversion efficiency. On the other hand, the PVDF-based piezoelectric sensor possesses several advantageous features such as compact size, flexibility, self-powering capability, excellent acoustic-electric conversion efficiency, and a high signal-to-noise ratio. These qualities make it suitable for fulfilling the present demands in SDRs applications[39]. The sensing materials must exhibit high sensitivity and excellent flexibility in order to function as piezoelectric acoustic sensors.

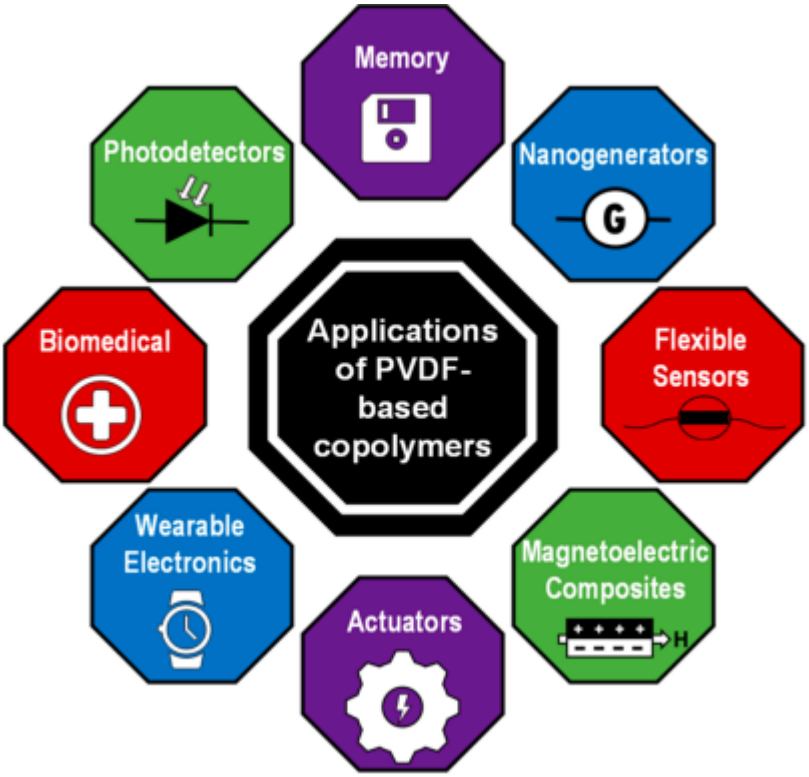

Figure 4:Applications of PVDF-based copolymers [35]

2.7 Ultrasound Transducer Mechanisms

There are two primary methods for artificially producing the ultrasound waves used in medical imaging. First, a capacitive technique known as capacitive ultrasound transducer (cUT) is used. The second method involves creating an acoustic wave with a piezoelectric ultrasound transducer (pUT) [40], which is created by the vibration of a piezoelectric material. These days,

the majority of ultrasound transducers use the pUT technique. The next sections will provide illustrations of the mechanisms behind both cUT and pUT.

2.7.1 Capacitive Based Ultrasound transducer (cUT)

In cUT, a metal-coated membrane made of semiconductor materials by micromachining is subjected to an AC signal, which alters the capacitance of the membrane. The device is also known as a capacitive micro-machined ultrasonic transducer (cMUT) since the change in capacitance produces mechanical vibration, or an ultrasound wave. Because the applied ac signal and the membrane vibration have the same frequency, an ultrasonic wave may be produced in the medium if the applied ac signal has a frequency greater than 20 kHz. Figure 5 depicts the cMUT's construction. Because cMUT employs the micromachining technology, producing an array format with a large number of components in a short space for the purpose of producing a high-resolution image is simple[1]. Strong design, cheap IC manufacturing costs, high integration levels, compactness, ease of making high-frequency devices, and lead-free disposables are some of the benefits of the cMUT. On the other hand, cMUT often produces far less acoustic power than pUT.

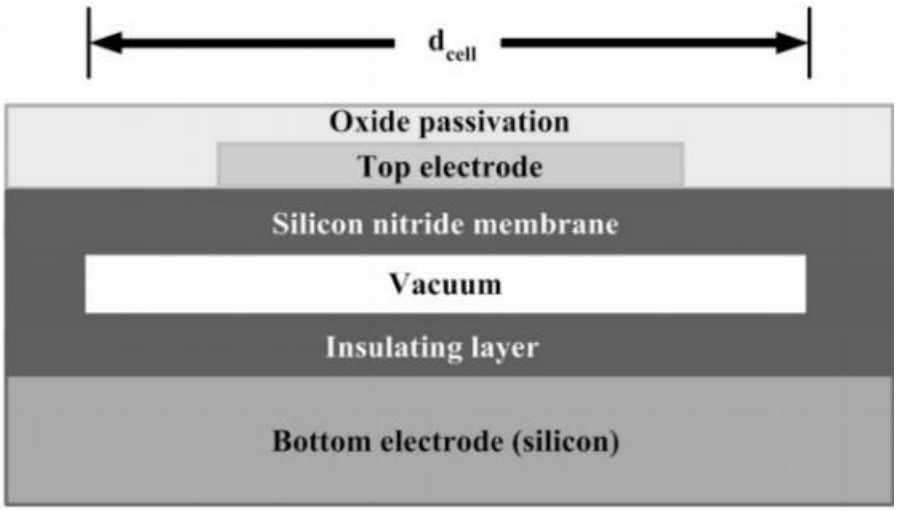

Figure 5: The structure of a single cell cUT[1].

2.7.2Piezoelectric-based Ultrasound Transducer (pUT)

The second method involves the use of a piezoelectric material to generate an ultrasound waves. Materials that have the piezoelectric effect can convert mechanical stress into electric charges on their surfaces or the other way around. The two French scientists Pierre and Paul-Jacques Curie made the initial discovery and demonstration of the piezoelectric phenomenon in 1880. Surface charges that match the internal electric polarization are produced when the material is

subjected to mechanical stress, which causes the lattice to extend or compress**[41].** As a reversible action, the piezoelectric effect can be classified as either the direct or converse piezoelectric effect, depending on whether an electrical or mechanical input is used. Both of the mechanism diagrams are shown in Figure 5**[42].**

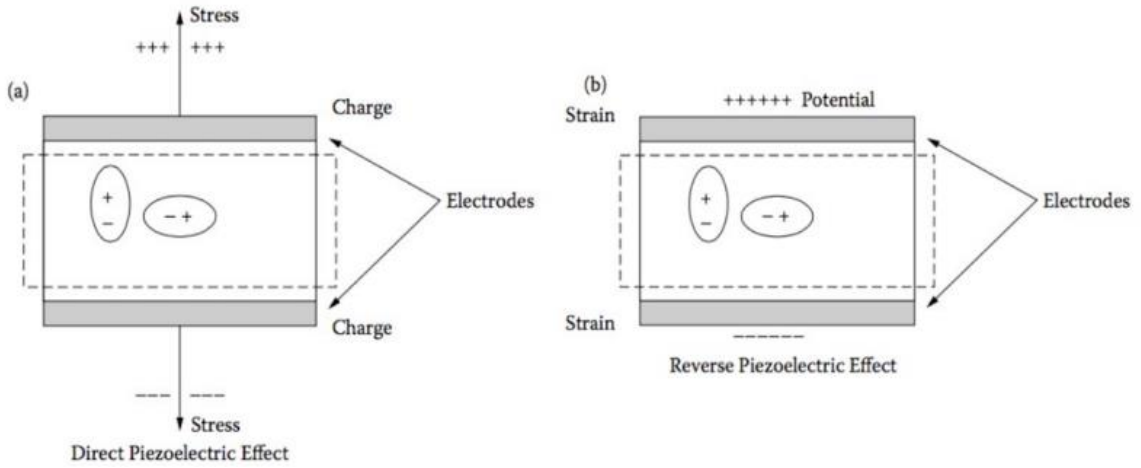

Figure 6: The indication diagram of (a) direct piezoelectric effect by applying an elongation on the material and (b) converse piezoelectric effect by applying an electrical potential on the surface of the material[3].

The direct piezoelectric effect is seen when a piezoelectric material experiences mechanical stress, such as pressure, force, or vibration. This stress causes the dipole moments in the crystal structure of the material to align or deform, resulting in the generation of an internal electric charge distribution. This process induces an electric charge on the material's surface, which may be collected and quantified as a voltage across electrodes. This phenomenon is mainly used in sensing applications, such as pressure sensors, accelerometers, and microphones, where mechanical input is transformed into an electrical signal.

2.8 Characteristics of Piezoelectric Ultrasound Transducer

The elements influencing transducer sensitivity and resolution are explained and thoroughly examined in this part in order to check feasibility of a transducer that is appropriate for biomedical imaging applications.

2.8.1 Structural Components of piezoelectric ultrasound transducer

An ultrasound transducer typically has three primary parts, including an backing layer, matching layer, and active element. The fundamental design of a typical array transducer is shown in Figure 7. Similar to what is described in section 1.8, the active layer's piezoelectric layer converts electrical signals into auditory signals and vice versa by use of the piezoelectric effect. The mechanism by which the piezoelectric material functions as the active layer is based on the piezoelectric effect, which occurs when an external electric field acts on the material and reroutes the dipoles within it. This causes a strain to be generated in either the longitudinal or lateral directions. In a similar way, the piezoelectric material may vibrate when an AC electric field is applied to it. The inherent properties of the piezoelectric material and the frequency of the AC electric field would determine the vibration frequency. As a result, when the piezoelectric material vibrates, the molecules in the surrounding medium also vibrate. This causes the piezoelectric material's resonance frequency to be used to produce an auditory pulse. Figure 7. shows the double matching layer array transducer's basic construction. The primary function of the matching layer is to increase the ultrasound wave's rate of transmission between the coupling medium and the active layer. One way to lessen the impedance gradient is to place one or more matching layers between them. The increased transmission rate would raise the energy of the acoustic waves being sent and received, increasing the sensitivity of the Second matching initial corresponding Active Layer transducer for ultrasound**[40].** The supporting layer, which makes up the third component, functions similarly to the matching layer in terms of mechanism. The sole distinction is that the backing layer's purpose is to absorb sound waves that are traveling in the opposite direction of the target through the ultrasound transducer's backside.

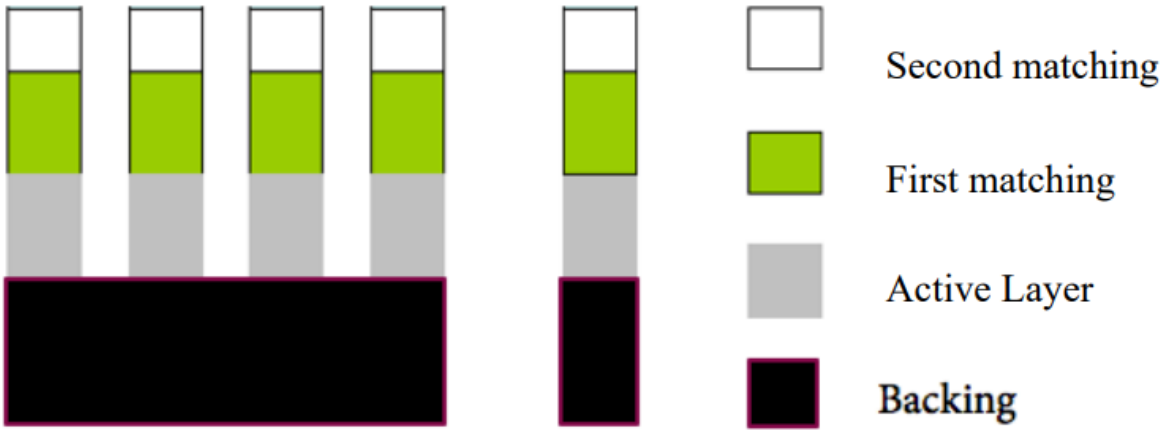

Figure 7: Basic structure of Array transducers with multiple matching layers

2.8.2 Properties of Active Layer of Piezoelectric

The material's piezoelectric qualities, the matching layer, and the electrical connection all have an impact on the UT's performance. The strength of the piezoelectric effect is caused by piezoelectric characteristics. It has an impact on the transducer's resolution in addition to its sensitivity. Stronger piezoelectric materials have the ability to exert more strain on the loading medium while converting with comparatively less energy loss.

2.8.3 Piezoelectric constant

The piezoelectric constant is one of the factors influencing the UT's performance. The strength of the piezoelectric effect conversion under various conditions and orientations is shown by four distinct types of piezoelectric constants. The factor g_{ij} represents the direct piezoelectric effect used to convert an ultrasound signal to an electrical signal. Furthermore, factor d_{ij} is the opposite piezoelectric effect that produces the ultrasound signal. When considering a piezoelectric material with high g_{ij} values and dij, where as i and j are the vectors of the inducer and trigger. It is possible to produce an ultrasound signal that is transmitted or received with greater strength. As a result, employing a material with a high g_{ij} or d_{ij} will enable the UT to be more sensitive.

2.8.4 Electromechanical Coupling

Another piezoelectric parameter that illustrates the effectiveness of a piezoelectric material's transition from electrical to acoustic is the electromechanical coupling coefficient (kij) of the piezoelectric layer, as opposed to the piezoelectric constant. The coupling coefficient, which can also represent a fraction of the energy conversion, has a value between 0 and 1.

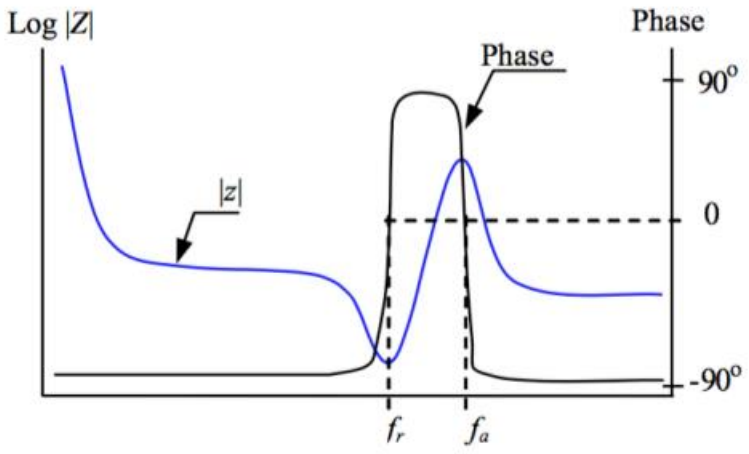

Figure 8:Impedance (blue line) and phase angle (black line) responses of a typical bulk piezoelectric material[42].

The following Figure 8. displays the formulae for the electromechanical coupling coefficients based on the frequency and direction dependency phenomena. The permittivity under constant stress is represented by ε_{ij}, the piezoelectric constant by d_{ij}, and the material's antiresonance and resonance frequencies by fr and fa, respectively. If the transducer is made of a material with a greater electromechanical coupling coefficient, the sensitivity might be higher. The coefficient is proportional to the frequency difference between the resonance and anti-resonance when the equation is evaluated at high frequencies. Since the quality factor is inversely related to the frequency difference between resonance and anti-resonance, it is likewise inversely related to the $k$ij. The quality factor that displays the material's mechanical loss and amplitude sharpness over the frequency range. The following diagram 9. shows the link between quality factor, bandwidth, and mechanical loss (tan δm):

$$\tan(\delta m) = 1/Qm \quad \text{.....(1)}$$

Conversely, the mechanical response's center frequency and bandwidth are represented by the values of $\omega 0$ and $\Delta\omega$ respectively. The relationship between the mechanical coupling coefficient and the piezoelectric material's frequency bandwidth is proportional. The bandwidth is displayed in Figure 9. variation with the expansion of the electromechanical coupling coefficient**[43]**. Furthermore, when the quality factor increases, Figure 9 also demonstrates that the band edge gets sharper (indicating a smaller loss), which might potentially have an impact on the pUT's frequency bandwidth. Therefore, one of the key variables influencing pUT's sensitivity and resolution is the $k$ij coefficient.

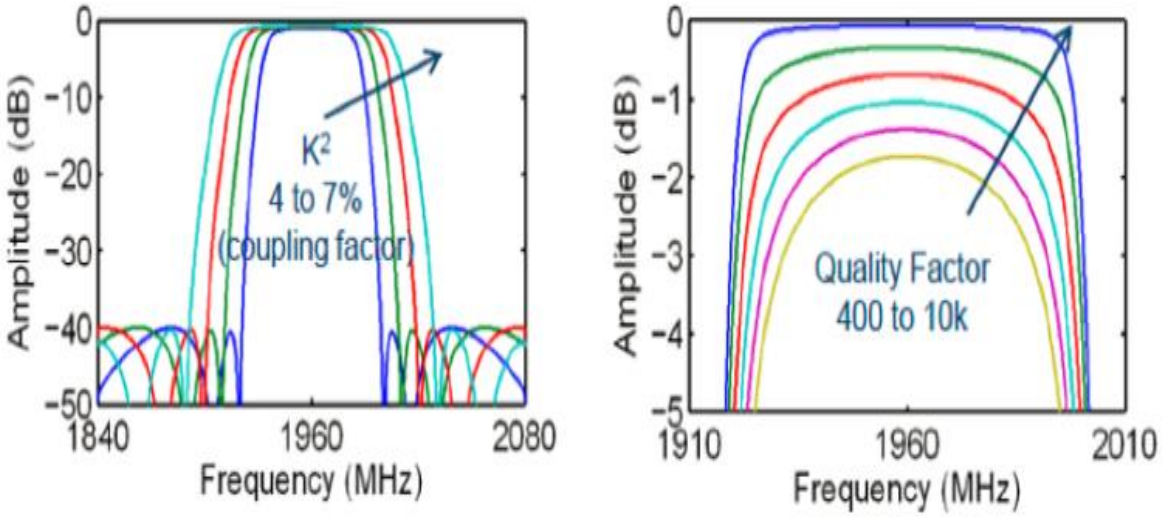

Figure 9: The relationship between (Left) electromechanical coupling coefficient and bandwidth, and (Right) the band peak shape and quality factor[2].

2.8.5 Matching Layer

A matching layer significantly improves the sensitivity of the pUT. The matching layer adjusts the UT's sensitivity and bandwidth during emission and reception processes.

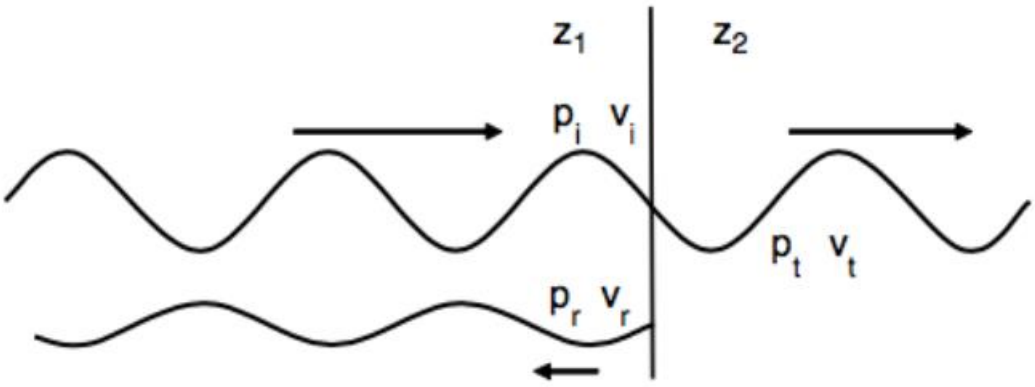

Figure 10: Induction of the acoustic reflection due to the acoustic impedance mismatch

The acoustic impedance mismatch between two media affects the coefficients of reflection (Ri) and transmission (Ti).

$$Ri = \frac{Zc-Zp}{Zc+Zp} \text{.....(2)}$$

$$Ti = \frac{2Zp}{Zc+Zp} \text{.....(3)}$$

Where Zc and Zp are the acoustic impedance of the coupling medium and the piezoelectric material, respectively Figure 2.10 depicts an acoustic wave propagating across two materials with varying impedances (Zc and Zp)**[44].**

Table 5: Acoustic impedance of different body tissue

Body tissue	Acoustic Impedance MRayl
Air	0.0004
Lung	0.18
Fat	1.34
Liver	1.65
Blood	1.65
Kidney	1.63
Muscle	1.71
Bone	7.8

The equations for reflecting and transmission coefficients are provided below. In clinical ultrasound imaging, human tissues have an impedance of 1.5 MRayl, while most piezoelectric materials have an impedance of 32 MRayl, only PVDF piezoelectric material has a good matching impedance condition (3.3 MRayl) which gives maximum absorption of acoustic waves. So don't need to use any matching layer in case Pvdf as piezoelectric materials. Whereas in other materials a direct contact between the ceramic-based piezoelectric material and the coupling medium can reflect up to 80% of the signal intensity. To improve propagation intensity, use an acoustic impedance medium between the piezoelectric layer and the coupling medium. Therefore, to optimize the propagation intensity, a medium with acoustic impedance value in between the piezoelectric layer and the loading is required.

2.9 Sensitivty of Pizeoelctric Ultasound Tranducer

The sensitivity and resolution of an ultrasound transducer impact its performance in biomedical imaging applications. The electro-acoustic transducer's energy conversion efficiency can be used to quantify sensitivity. It is possible to define sensitivity as the relationship between the amplitudes of the input and output. A network converts the amplitudes of voltage (V, I) and current at the electrical port of the ultrasound transducer used in biomedical imaging to the amplitudes of force and velocity (F, v) at the acoustic port. The sensitivity is defined as the product of the transmission sensitivity and the reception sensitivity since the transducer serves as both a transmitter and a receiver[45]. The logarithmic units of sensitivity are often defined

$$S= 20\log_{10}(V_{out}/V_{in})\text{……..(4)}$$

where Vout is the voltage signal from the transducer that was received and Vin is the electrical voltage that was supplied to excite the transducer. The receiving transducer and the transmitting transducer are the same in ultrasound imaging. As a result, the Vout is now the transmission transducer's receiving voltage at the initial location where it picked up the acoustic signal that was reflected by a reflector.

2.10 Principle of Piezoelectric Transducer

A piezoelectric transducer works by using the piezoelectric effect, which refers to the capacity of certain materials to transform mechanical energy into electrical energy (direct effect) and vice versa (inverse effect).

2.10.1Piezoelectric Effect

The application of an electric field to a piezoelectric material causes a reorientation of dipole moments, resulting in the generation of a mechanical strain inside the material. This particular strain induces the material to either increase or decrease in size, resulting in a mechanical movement. The phenomenon of inverse effect is used in actuators, such as piezoelectric motors, inkjet printer heads, and precise positioning devices. In these devices, electrical energy is transformed into regulated mechanical motion.

A piezoelectric transducer typically consists of three layers: the matching layer, the backing layer, and the piezoelectric layer. The acoustic performance of a piezoelectric transducer is significantly influenced by the piezoelectric coefficient (d33) and the electromechanical coupling coefficient (kt) of the piezoelectric materials. One of the most crucial characteristics of a piezoelectric material is the piezoelectric coefficient (d_{33}). It measures how much electric charge a material can produce in reaction to mechanical stress. Whereas the electromechanical coupling coefficient (kt) of a piezoelectric material is an important quantity that measures how well the material transfers electrical energy into mechanical energy (and vice versa). It is a critical indicator of the efficiency of the piezoelectric effect in that material. To be specific, the acoustic impedance of biological tissues is around 1.5MRayl, whereas if acoustic impedance of piezoelectric materials is higher than the Coupling medium (water). Ultrasound waves will reflect at the interface due to an acoustic impedance mismatch, making it impossible for the ultrasound wave to pass through the interface[46]. As a result, the acoustic matching layer is necessary, which can raise the transducer's sensitivity, bandwidth, and energy transfer efficiency. The impedance matching layer is proposed to have a thickness of λm/4, where λm represents the matching layer's sound wavelength. The forward propagating sound wave can potentially pass through the acoustic matching layer fully when its acoustic impedance matching with the corresponding materials. According to equation 5.

$$Z_{matching}=\sqrt{Zp.Zc} \quad \ldots\ldots\ldots(5)$$

Here, Zp and Zc stand for the piezoelectric material's and the coupling medium's (i.e. water) respective acoustic impedances[47]**.** To lessen the duration of the pulse and absorb some of the energy from the backward sound wave, the transducer's backing layer (such as conductive epoxy) can be applied on the back[44, 48]. Typically, piezoelectric transducer design uses an equivalent circuit (FEM). A set of limited-length transmission lines with a frequency-dependent

electroacoustic coupling transformer is how a piezoelectric transducer is defined in the FEM model; in this case, planar acoustic waves travel in both directions[44].

Table 6: Effect of different backing layers on Pvdf transducer performance[45].

Device	Backing material	Impedance (Z_b)	Center Frequency (CF)	IL (dB)
1	Epoxy+ Al_2O_3	6	44	-56.3
2	Epoxy+Microballon	1	65	-50
3	Epoxy+Tungsten	16	40	-54
4	Epoxy	13	50	-44.34

Table 7: Comparison of different parameters of PVDF and PZT[45].

Material Parameter	PVDF	PZT
Density (g/cm^3)	1.78	7.75
Sound velocity v (m/s)	2200	4350
Acoustic impedance ρ_o v_o (10^6 kg/m^2s)	3.9	33.7
Coupling coefficient k	0.17	0.49
Dielectric constant ε (at 100 Hz)	10	830
Piezoelectric constant e (C/m^2)	0.14	15.8

2.11 Backing layer For Annular Array Design

There are many transducers designed to optimize the backing layer effect to enhance their properties using pulse-echo testing, centre frequencies between 2 and 65 MHz at -6dB bandwidths. The echo amplitudes varied based on the backing and electrical impedance matching, from 100mVpp to 940mVpp.The ultrasonic device has a backing material consisting of two parts Al_2O_3 and one part epoxy Epo-Tek 301 (Epoxy Technology, Incorporated), which produced a backing impedance of 6MRayl. The response had a bandwidth of 16% at -6 dB and was centred at 44 MHz. This apparatus did not employ electrical impedance matching, and the echo amplitude was I80mV. An ultrasound transducer with Epoxy and Tungsten as backing material had impedance16 MRayl when this epoxy was combined with four parts tungsten powder to provide a higher impedance backing. The result was a frequency shift to 40 MHz

with a 94% bandwidth of -6 dB, but with a significant gain in sensitivity. The backing material for ultrasonic device was applied only using epoxy. This caused the frequency to increase to 50 MHz with a bandwidth of 107%. So in conclusion there is a trade-off arises between depth of field and lateral resolution, even though single-element transducers can offer strong axial resolution. An annular array architecture was used in order to provide both a large depth of field and good lateral resolution. So according to the schematic diagram 5, easily analyse the different possible shades of piezoelectric materials of the ultrasound transducer. Which are playing a vital role in the field of biomedical imaging.

2.12 Resolution of 1-D Ultrasound Transducers

A 1-D array transducer has spatial resolution in two directions: axial and lateral. Both resolutions define the ability to resolve two points of an object along a single direction. The spatial resolution of transducers. Figure 11[49]. shows three different directions.

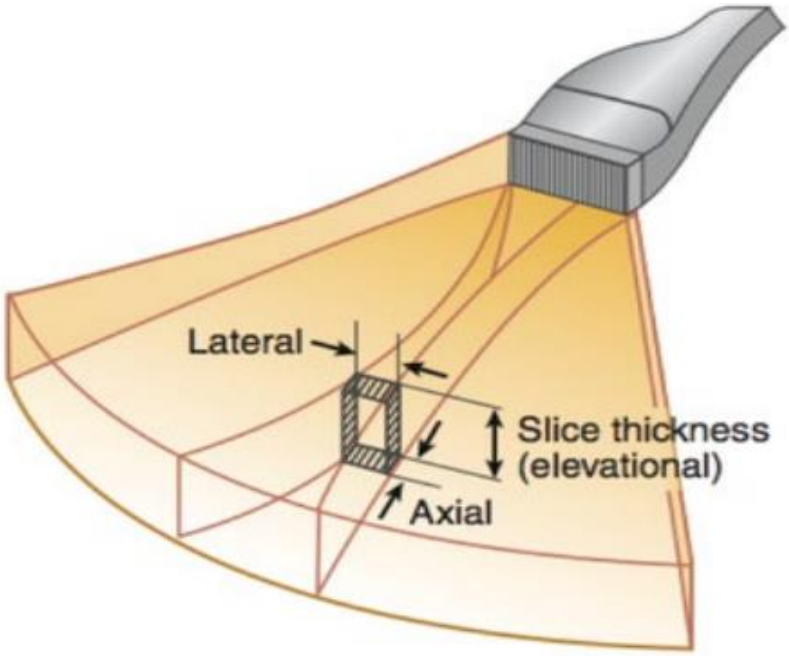

Figure 11: Array transducer resolution

2.13 Axial resolution

The resolution along the direction of propagation of an ultrasonic pulse, which is defined as half the pulse length, is known as the axial resolution. The echo reflected by the first item may be separated from the echo reflected by the subsequent object, which is situated deeper in the transducer's axial direction, with a shorter pulse duration. After signal processing, the first and

second echoes may be distinguished as two separate signals and shown in the image. The fast Fourier transform (FFT) is used to convert the echo signal from the time domain to the frequency domain as it is difficult to determine the pulse duration in the time domain. The spectrum -6 dB bandwidth serves as a representation of the pulse length in the frequency domain. The signal with an amplitude less than half of the input is not counted in the pulse length, as -6 dB indicates half of the input value, according to the equation below.

$$dB = -20\log_{10}(V_{out}/V_{in}) \ldots\ldots\ldots (6)$$

The acoustic pulse length has inversely proportional connection with the breadth of the function at the frequency at -6 dB. Consequently, the axial resolution of the transducer rises concurrently with the -6 dB frequency bandwidth, so it may be found scientifically rather than by time domain computation of the pulse length. The axial resolution expressed in terms of bandwidth follows this formula

$$Raxial = \frac{c}{2BW} \ldots\ldots\ldots\ldots\ldots (7)$$

Where c is the acoustic wave velocity in the medium and BW is the -6 dB frequency bandwidth of the transducer, Consequently, raising the resonance frequency of the Piezoelectric Ultrasound Transducer will help to attain a high axial resolution (shot pulse length). The frequency bandwidth is greatly reliant on the Piezoelectric Ultrasound Transducer resonance frequency. The Piezoelectric Ultrasound Transducer center frequency is mostly determined by the thickness and acoustic velocity of the piezoelectric layer in the resonance mode.

2.14 Lateral Resolution

The beam breadth of the transducer is a factor that influences the lateral resolution. The resolution is enhanced by the ability to identify adjacent objects when the beam width is reduced. The acoustic beam emitted by the transducer is defined as the beam width:

$$\text{Beamwidth} = \lambda L/D \ldots\ldots\ldots\ldots\ldots\ldots (8)$$

In equation (8), the wavelength of the acoustic pulse in the medium is denoted by λ, the distance between the transducer and the target is denoted by L, and the aperture size of the transducer is denoted by D.

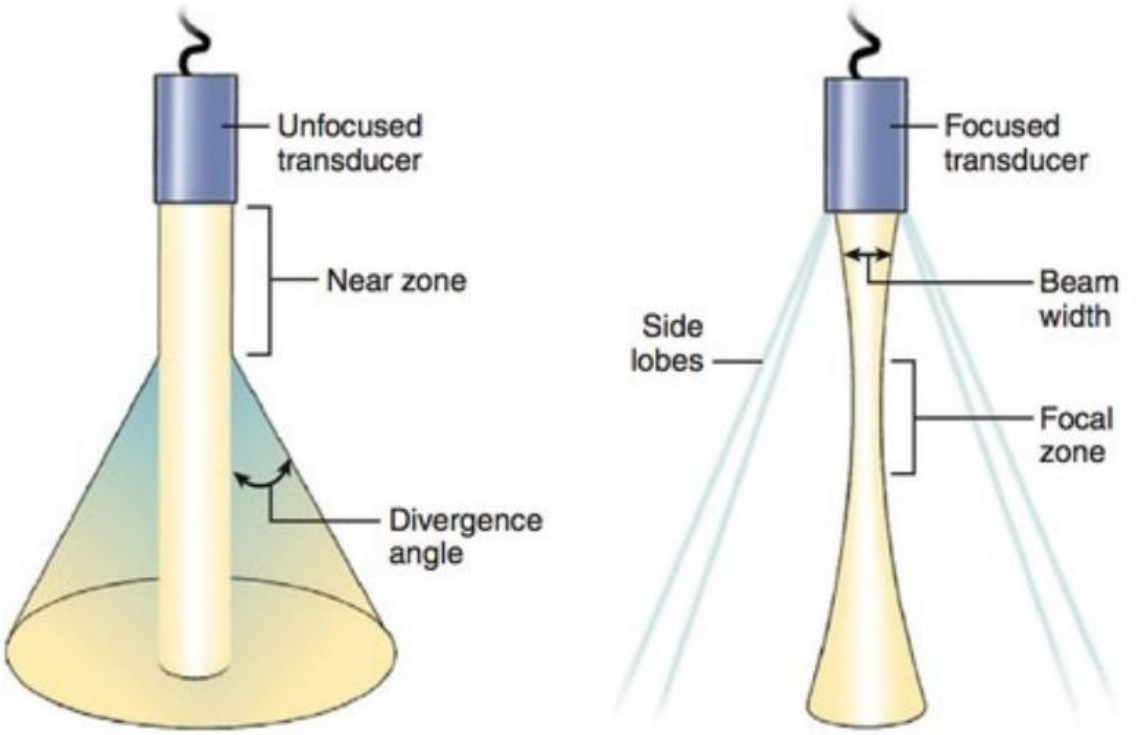

Schematic diagrams of acoustic beams emitted by the unfocused and focused single-element transducer are depicted in Figure 12[49], respectively.

Figure 12: Single element focused and unfocused transducer Beam profile

It is demonstrated that the unfocused acoustic beam is nearly parallel (equal beam width) within the near-field zone (also known as the Fresnel zone) and disseminated with a specific divergence angle to the infinite distance beyond the near-field zone. Consequently, the lateral resolution of the unfocused transducer is nearly identical within the near-field zone. The resolution is at its highest at the near-field-far-field transition point; however, it decreases progressively along the axial direction of the transducer after the transition point. In contrast, the focused transducer has the narrowest beam width (and, consequently, the maximum resolution) in the focal zone near and far zones. The focused single-element transducers are not suitable for medical imaging due to the limited range. The beam breadth of the 1-D array transducer is illustrated in Figure 12. The lateral resolution of an array transducer is contingent upon the main beam lobe angle θ, as represented by the following equation:

$$\text{Sin } \theta = \text{lateral resolution}/L = \lambda/w \ldots\ldots\ldots\ldots\ldots\ldots (9)$$

where L is the focal length of the beam. This equation is comparable to that of a single element; however, the aperture size factor is substituted with the array's total breadth. The lateral resolution of an array is also proportional to the element number, kerf widths, and element widths, as indicated by its structure.

2.15 High-Frequency Ultrasound Transducer

Single-element focused transducers using polyvinylidene fluoride (PVDF) membranes as its active acoustic layer were employed in the first high-frequency ultrasound (HFU) transducer research[50]. Although these transducers were not too difficult to construct, the PVDF material had a somewhat high two-way insertion loss (IL) of about 40 dB. As a result, efforts have been directed towards ways to enhance the IL through electrical matching and drive electronics optimization. Simultaneously, techniques for creating single-element HFU transducers using ceramic materials were being improved, and several devices were successfully constructed to function in the HFU regime[51]. Due to their significantly reduced IL, these devices offer an intrinsic advantage over PVDF-based transducers. Nonetheless, the most popular transducer option for HFU applications remains to be single-element PVDF transducers. PVDF and ceramic transducers have both been employed with excellent results in dermatological, ophthalmology, and small animal imaging fields[52]. The focus of HFU transducers at the moment is mostly on array technology. Through the use of an array, electrical focusing is made possible, which enhances the device's depth of field and makes it possible to create a two-dimensional (2-D) picture without the need for mechanical transducer scanning. There is research being done on technologies such as capacitive micromachined ultrasonic transducers (CMUT), micro electrical mechanical systems (MEMS) , and more conventional ceramic materials[53]**.** All of these techniques seek to create individual array elements on the order of $\lambda/2$; in order to fully apply the technologies, these tiny dimensions require advancements in electronics and interconnects.

A more sensible course of action, to create annular arrays with element sizes comparable to those of existing single-element transducers. An annular array's benefit is that it may provide a greater depth of field along a line focus with a comparatively small number of components. The main disadvantage is that in order to create a 2-D picture, it needs to be mechanically scanned. Annular arrays with passive focus and those without focus are currently being researched. Since

ceramic materials are hard to mold into curved patterns, they are usually employed for flat arrays[54]**.** In this regard, a PVDF membrane is more beneficial as it offers a higher acoustic impedance match to biological tissue and can be press-fitted into curved shapes with ease[55]**.** Although a PVDF annular array could be created,were unable to produce pictures or carry out all of the array's functions.

The slower development of commercial applications for these arrays might likely be due to the higher dielectric constants and larger electromechanical coupling efficiency of piezo-ceramics, namely PZT. However, PZT-based transducer arrays become difficult to produce at the high pitch needed at frequencies exceeding 10 MHz. Therefore, it is feasible that the simplicity with which array transducers based on PVDF may be built in comparison to PZT [56]will lead to the development of a PVDF-based imaging system that is clinically beneficial and will coincide with the usage of single-element PVDF transducers at higher frequencies. The impedance matching specifications of each transducer element in the array is a major problem. PVDF transducer components with different dimensions, constructed from 28μm PVDF film, have an electrical impedance of around 3kΩ at 20MHz[57]. Given the application of common impedance matching methods, this may essentially exclude the usage of PVDF . Furthermore, the usefulness of building tiny PVDF components is limited, even in the case of local amplification. To get around these issues for the sake of this study, transducers with components on a pitch of 3λ were constructed, and the transducer was closely coupled to amplifier and pulser circuits[58]. There are also some test findings for a transducer prototype that operates at frequencies higher than 20 MHz measured.

Alternative to PVDF, inorganic piezoelectric lead zirconate titanate (PZT) series ceramics and single crystals are the most widely used materials for ultrasonic transducers[59]. These materials have an excellent high-frequency response but a small frequency domain. Furthermore, flexible equipment made of these inorganic materials is difficult to construct and is brittle. In contrast to inorganic materials, newly suggested piezoelectric polymers exhibit remarkable benefits such ultra thinness, lightweight, flexibility, and easy or moderate processing conditions. As a result, transducer sensors and actuators are showing a lot of interest in these materials.

2.16 Challenges In High-Frequency Transducer Design

The primary difficulty in the design and construction of a high-frequency imaging array is in the intricate specific dimensions of its components. The technologies employed in commercial arrays have been reached a pretty advanced stage of development and extensively reported in

the literature[60]**.** However, in several cases, it is impracticable to only proportionally adjust miniaturizing a gadget. Methods for producing and testing composites, elevation focusing that is appropriate, and acoustic analysis at a small scale. Materials that can be matched and designs that can accommodate variations in thickness.

Modification, and functional electrical adjustment and connection methods are necessary. When developing or implementing piezo-composites, it is crucial to take into account the spatial size of the components. A one-dimensional array utilizes a composition of layer of different materials, which consists of backing material (pads and glue) and piezoelectric polymer placed layer by layer. This arrangement allows for a significant increase in thickness. Coefficients of coupling and high volume percentages of polymers to get the highest possible device parasitic capacitance. In addition, pairing the reduction in the thickness-extensional mode is substantial. Thus, a layer-by-layer composite is the recommended choice for high-frequency applications. Software programs within a composite array element, only the thickness mode is present. If additional modes are stimulated inside the composite microstructure, the coupling of the thickness mode will be disrupted, leading to the emergence of undesired resonances in the time-domain response. These resonances can be seen as the outcome of acoustic waves being reflected by the composite material. The microstructure is discussed in the references[61] .The amplitude of the signal is significantly reduced throughout a range of frequencies close to the resonance, which is referred to as the stopbands. The stopband margins are dictated by the spatial size and the coupling between the piezoelectric elements. Edge resonances, commonly known as lateral resonances, must be eliminated to achieve optimal composite performance. The distance of both the ceramic part and the polymer must be considered. In order to position something, it needs to be smaller than a fraction of a wavelength. The resonance frequencies at the stopband edge are significantly higher than the resonance frequencies related to the thickness, due to the piezoelectric coupling. Various approaches, such as dynamic models of guided waves [62] and finite element modeling [63] have been employed to establish the maximum permissible spatial scale for periodic composites. Without these models, which frequently need to complete range of component characteristics, Several elementary computations may be employed to roughly estimate Calculate the maximum permissible spatial scale for polymer composites. These recommendations accept that the composite material is integrated into a transducer with a wide frequency range. Consequently, the lateral resonances are maintained at a frequency that is at

least double the core frequency of the device[61]**.** Designed for individuals with low to moderate use levels the initial lateral resonance of fractions is determined by the piezoelectric coupling and corresponds to the half-wavelength resonance.

2.17 Induced Acoustic Effect

Both thermal expansion and acoustic waves are produced by the deposition of energy of specifically non-ionizing radiation. The photoacoustic (PA) effect was identified in 1880 and was brought about by light stimulation. Since the first practical laser based on ruby was created in Hughes Research Laboratories on May 16, 1960, the PA effect has been the subject of increased research, and several technologies have been created for use in physics, chemistry, and biology. The PA signal can be used in biomedical engineering to scan biological tissues[64]. In the broadband aspect, the PA effect to reveal about the biological tissue architecture. The visible spectrum is just one part of the electromagnetic radiation spectrum that may be employed to activate acoustic waves in biological tissues. EM radiation may be used for a variety of imaging purposes due to the varied wavelengths at which tissues absorb and penetrate light. Thermoacoustic tomography (TAT), which we first investigated to study of microwave-induced acoustic waves in biological tissues[65].This technique was then refined into photoacoustic tomography (PAT), which substitutes a laser pulse for the microwave pulse. For use in biomedical applications, both microwave and visible or near-infrared (NIR) laser light are safe forms of non-ionizing radiation.

Chapter 3.

Methodology For Design and Experimental Validation of PVDF-Based Ultrasound Sensors.

This chapter explores the design, development, and experimental validation of Polyvinylidene Fluoride (PVDF) ultrasound sensors specifically engineered. The advantage of the acoustic impedance of PVDF, which closely aligns with that of biological tissues and water, renders it an ideal material for transducers in high-frequency applications. The sensor design utilizes economical manufacturing techniques, such as printed circuit board (PCB) technology, to accurately portray the sensor's active region while reducing complexity and production expenses. Experimental validation confirmed the sensors' ability in both electrical and acoustic domains, highlighting their potential in novel biomedical applications, especially in photoacoustic melanoma detection. This chapter describes the modeling, sensitivity, frequency response, and noise characteristics, underscoring the sensor's efficiency for imaging applications necessitating high resolution and sensitivity.

There are three main steps followed for developing the sensor.

- Analytical Model: To describe the basic formulation for the Prototype sensor.
- Finite Element Model: To check the behavior of each layer including for development.
- Model Acoustic test: Preliminary Test to validate its acoustic behavior.

3.1 Analytical-Model

The reaction of piezoelectric materials to various mechanical and electrical conditions can only be understood by modeling and modeling these materials. For numerical computation, visualisation, and programming, MATLAB is the right interactive tool and programming language to use. Intricate systems, like piezoelectric materials, to modeled and simulated with its powerful capabilities. The main goal of this thesis is to develop a formulation by MATLAB model that faithfully represents the operation of piezoelectric devices constructed from PVDF. In this work, we first establish the applicable material characteristics for PVDF including its piezoelectric constant(d_{33}), relative permittivity(ε_r) as well as elastic piezoelectric voltage coefficient (g_{33}) in a MATLAB Model that solves the constitutive equations for given input pressure source and electric field combine these features.

In this work, the use of Polyvinylidene fluoride (PVDF) as a piezoelectric material is proposed due to its advantages over commonly used piezoceramic materials like Lead-Zirconate-Titanate (PZT), particularly in terms of bandwidth, piezoelectric, acoustic, and construction characteristic PVDF can be easily processed and manufactured in different shapes and arrays due to its plastic nature, and its acoustic impedance (3.3 MRayl w.r.t 35 MRayl for PZT) is close enough to water acoustic impedance (1.5 MRayl) that no matching layer is needed, minimizing ringing behavior and thus obtaining a flatter frequency response and wider bandwidth, while PZT sensors typically have a narrow bandwidth around their resonance frequency. This enables a single PVDF sensor design to acquire ionoacoustic signals with varying bandwidths, making them suitable for different clinical and pre-clinical scenarios. Additionally, the wide band of PVDF helps preserve the signal shape without introducing distortion or ringing

Moreover, the MATLAB model enables the modeling of other possibilities including: Dynamic analysis i.e. Simulating the time-dependent response of PVDF to oscillatory or impulsive forces.

Parametric Studies i.e. Investigating PVDF-based device performance under varying material parameters and external circumstances.

3.1.1Frequency Response

The resonance frequency of piezoelectric material (PVDF) depends on the frequency coefficient N (Hz·m) and on the thickness TH of the piezoelectric material according to equation (1).

$$f_R = \frac{N}{TH} \dots\dots\dots\dots\dots\dots\dots 1$$

Consider a PVDF foil 20 μm thickness has been chosen for achieving a 56MHz resonant frequency. This relation basically demonstrates that thicker the foil more will be the resonance frequency. By using this relation, one can easily get an idea about resonance frequency of proposed prototype sensor.

3.1.2 Transmission Coefficient and Sensitivity

The sensitivity value is usually reduced to around 80% due to the acoustic impedance mismatch between the water (acoustic signal propagation medium) and the piezoelectric material itself. In fact, whenever an acoustic wave traveling in one medium encounters another medium with different mechanical properties, it is partly transmitted and partly reflected. The transmission coefficient (η_T) depends on the acoustic impedances of the materials (Z, defined as the product between density (ρ) and speed of sound (c)in the medium) as and is equal to:

$$\eta_T = \sqrt{1 - (\frac{Z_2 - Z_1}{Z_2 + Z_1})^2} \dots\dots\dots\dots\dots\dots\dots\dots 2$$

$$S_{PVDF} = \eta_T . g_{33} . TH \dots\dots\dots\dots\dots\dots\dots\dots\dots\dots 3$$

Water and soft tissues have an acoustic impedance of around 1.5 MRayl, very close to the 3.3 MRayl of the PVDF, and therefore in a direct interface between the two materials above 80% of the wave amplitude is transmitted, causing a relatively low loss of sensitivity and SNR (-2 dB).The in-band sensitivity obtained 3 μV/Pa by using equation (3), where g33 is the piezoelectric voltage coefficient, equal to 200 mV/(Pa·m).

3.1.3Sensor Capacitance and Noise Power

Due to the capacitive nature of piezoelectric sensors, approximation to kT/C demonstrates their output referred noise power. Specifically, the formula of parallel plate capacitor is used to calculate the capacitance for thin piezoelectric material, according to the equation.

$$C = \varepsilon_r \varepsilon_o \frac{A}{TH} \dots\dots\dots\dots\dots\dots\dots\dots 4$$

. Thus, the output-referred noise power of the sensor channel is:

$$ORN = \sqrt{KT/C} \text{.....5}$$

$$ORN = \sqrt{\frac{KT.TH}{\varepsilon_r \varepsilon_o . A}} \text{... ... ...6}$$

Considering the physical parameters of the PVDF, the single channel capacitance is equal to 115 pF, leading to an output referred noise power of 6 μV_{RMS}.

$$IRN = \frac{ORN}{S} \text{... ... ... 7}$$

Finally, the input referred noise power can be obtained by dividing the ORN by the sensitivity and is equal to 2 Pa_{RMS}.

These factors allow to evaluate the performance of the prototype proposed sensor. The capacitance of the sensor determines how much electrical charge it can hold. This is an important characteristic of PVDF sensors because the charge produced in response to acoustic pressure is transformed into a voltage that can be measured. The 56MHz band-width of sensor confirms the range of frequencies that the sensor is able to detect acoustic signals, the sensor can record sounds in this range of frequencies, which makes it appropriate for high-frequency uses such as ultrasound imaging.

The output voltage is 245.1μV of the sensor per unit input, generated at a specific acoustic 34 Pa pressure. It describes how well the sensor can interpret changes in pressure into an electrical output. The particular pressure at which the sensor is being assessed is indicated by a value of 34.6 Pa.When the sensor is exposed to a certain pressure, the output voltage shows the signal that the sensor produced. Where as noise power19.6 μV_{RMS} at the sensor's output is measured by RMS (Root Mean Square). The overall signal quality is improved when the noise power is lower since there is less noise in the system.

The distribution of noise power over frequency is described by the noise power spectral density (PSD) at the output. An indication of the noise performance throughout a range of frequencies is provided by a value of 2.61 nV, which indicates that the noise level is 2.61 nV/√Hz of bandwidth. This is the noise power's RMS value as it relates to the sensor's input. It helps in evaluating the effectiveness of the sensor and its readout circuitry by describing the equivalent

noise present at the sensor's input. A result of Input referred noise (IRN) indicates that the noise level at the sensor's input is 0.36 μV/√ Hz.The signal-to-noise ratio (SNR) on one channel for a single pulse. This shows the degree to which the sensor can separate noise from the acoustic signal.

$$SNR = 20*\log10(dV/ORN)^{-3} \text{ …….8}$$

When a signal has an SNR of 18.9 dB, it depicts that it is around 18.9 dB greater than the noise level.In a multichannel system, this is the signal-to-noise ratio calculated over 32 channels for a single pulse. Because many channels combine data from several sensors, they considerably enhance signal quality, as seen by the large increase in SNR (48 dB) above single-channel SNR. The SNR of the proposed prototype sensor is still 48dB if we used 1000 pulses. Which indicating that the multichannel configuration's noise levels are already so low that adding more pulses doesn't improve the SNR. It shows that proposed prototype multichannel PVDF sensor is quite sensitive and appropriate for applications involving high-frequency ultrasound wave detection. By decreasing noise through channel aggregation, the multichannel arrangement (like 32 channels) considerably enhances the SNR, enabling the system to identify weak acoustic signals.

3.1.4 Analytical Model Directivity

Refraction affects the directivity of the PVDF (Polyvinylidene Fluoride) sensor was measured by using the analytical Model. Directivity measures the sensor's sensitivity to acoustic impulses originating from various angles. Directivity measures the sensor's sensitivity to acoustic signals originating from various angles by field view of 45.

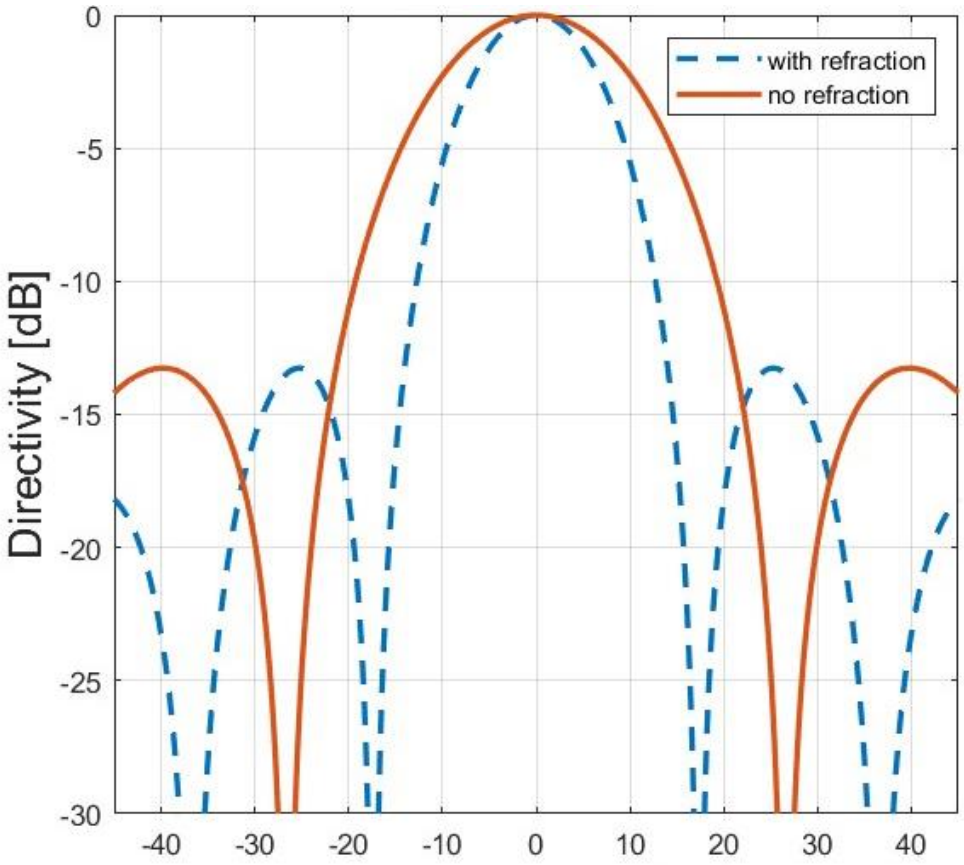

Figure 13: Analytical Model predicted Directivity

The directivity diagrams show the performance of a PVDF sensor, when acoustic waves pass from water to the PVDF material. The blue dotted curve shows refraction, while the red curve shows expecting result. A thorough analysis of the effects of refraction shows the bending of sound waves as they go through various media, on performance may be achieved by taking into account several aspects.

While blue and red curve reveal how the passage of acoustic waves from water to the PVDF material affects the performance of a PVDF sensor.

Red Curve: The sensor is extremely sensitive to head-on (perpendicular) auditory impulses since its greatest sensitivity is at 0°. At this angle, the directivity plot has a strong peak close to 0 dB, suggesting that the sensor is best suited for picking up signals that are directly along the axis of arrival.

Blue curve: A considerable reduction in the peak response at 0° is observed, with the peak falling by several dB in comparison to the red curve. This decrease implies that the total sensitivity for direct (on-axis) signals is lost as a result of refraction. The sensor's ability to

detect signals coming from the front is reduced as the sound waves refract as they pass from the water to the PVDF material.

Sensitivity Loss this would decrease the sensor's ability to identify direct signals in applications where the sensor must detect signals directly (e.g., underwater sonar or targeted ultrasound sensing). This can be an issue in settings when maximal detection sensitivity and exact directionality are essential.

Main Lobe: The lobe broadening lessens the capacity to distinguish between signals arriving from closely spaced angles for applications needing high angular resolution (directed sonar, imaging systems, etc.). Because the sensor will now be able to detect signals from a larger angular range, it will be more difficult to discriminate between two sources that are near in angle. This loss of resolution might distort the detection accuracy.

Side Lobe Behaviour: At approximately ±15° and above, the blue curve displays pronounced side lobes. The undesirable sensitivity of these side lobes to signals coming from off-axis angles may cause interference or noise to be picked up. Includes Refraction the side lobes are significantly more noticeable in the red curve. The side lobes have also increased in amplitude, corresponding with the main lobe's broadening; this suggests that refraction adds additional sensitivity to signals arriving from angles that are farther out from the central axis (±20° to ±40°).

Impact on Performance: By enabling the detection of additional off-axis noise or interference, increased side lobe levels brought on by refraction might impair the sensor's performance. When there are several sources of acoustic signals present in an area, there is a chance that the sensor would identify unwanted signals, which would lower the overall signal clarity and cause false detections. This impact can be particularly significant in noisy circumstances when accurate detection depends on the system's capacity to reject off-axis inputs.
The major lobe predominates throughout a rather small ±25° angular sensitivity range for the sensor.

The sensor can now respond to signals over a larger range, expanding the effective angular sensitivity beyond ±40°, as shown by the red curve.

In addition to the PVDF sensor's shape, the frequency of the incoming acoustic signal also affects the refraction effect. The refraction and diffraction effects are usually more noticeable at higher frequencies, and this might further change the directivity patterns. Refraction may cause frequency-dependent distortions in wideband applications where the sensor must function well over a variety of frequencies. The side lobe augmentation and lobe widening may intensify

at higher frequencies, although the directivity may be less influenced at lower frequencies. This frequency fluctuation may make it more difficult for the sensor to operate consistently in a variety of acoustic situations, particularly when detecting or resolving multi-frequency signals. Refraction-induced alterations may have a detrimental effect on performance for applications like as underwater sonar or acoustic imaging, where sharp directivity and high resolution are essential. The widened response, however, may be useful in settings where the objective is to monitor a large range of angles or capture signals from many directions. Refraction effects may be reduced by adjusting the impedance characteristics of the PVDF. The provided directivity graph reflects how much refraction affects wave propagation and highlights the need for a k-wave model simulation. The "no refraction" and "with refraction" curves show how refraction modifies wave behavior, causing side lobes to move and energy to be dispersed. Because of the complexity of wave dynamics, especially in heterogeneous media, it is crucial to describe wave propagation properly using k-wave simulations, accounting for elements such as energy loss, scattering, and refraction. Accurate wave behaviour prediction in complicated contexts is made possible by the k-wave model, which is essential for applications like acoustics, medical imaging, and other wave-based technologies.

3.2 Finite Element Model (FEM)

To characterize the behavior of the proposed sensor in the acoustic domain, a finite element model has been developed using the Matlab k-Wave toolbox. This approach is very excellent at recording phenomena such as refraction, diffraction, and scattering, which are critical in acoustic sensing situations. Engineers may use the k-wave model to simulate the sensor's reaction to acoustic waves, which allows them to optimize sensor design and performance. The model also allows for high-resolution examination of directivity patterns, sensitivity, and noise interference, making it essential for developing accurate and dependable acoustic sensors for use in medical diagnostics, sonar, and industrial applications.

In addition to the ultrasound measurements, the free source software package k-Wave was used for the numerical calculation of the ultrasonic fields. Finite element method (FEM), which has been used in many disciplines, was created and evaluated over a 20-year period. The FEM approach is very appropriate for implementing complex geometries in many physical contexts because of its inherent properties as well as the abundance of solvers and grid generators that come with the system. The constructed prototype transducer was therefore selected to be modelled as a two-dimensional (2D), symmetric model of piezoelectric PVDF film. To simulate

the transducer water backing, an upper epoxy layer has also been included to the FEM model, since the multilayer transducer would normally be immersed in water reveal that how a signal acquire by dedicated sensor and to observe the effect of different layers on the incoming acoustic signal.

A comprehensive MATLAB toolkit for modeling the propagation of acoustic waves in complex or heterogeneous media is the k-Wave toolbox. It is extensively utilized in non-destructive testing, environmental acoustics, and medical ultrasonography. The toolkit is ideal for modeling a range of acoustic wave phenomena because it utilizes a grid-based methodology and the finite-difference time-domain (FDTD) method to solve the acoustic wave equations.

Key Parameters of k-Wave:

- **Simulation-Based on Grids**:

k-Wave discretizes the simulation domain using a standard Cartesian grid. This makes it possible to simulate the propagation of waves in detail, including intricate interactions like diffraction, scattering, reflection, and refraction. To balance computational efficiency and accuracy, the time step and grid resolution may be changed.

- **Time-Domain Simulation**:

The k-wave describes how waves change over time by solving the acoustic wave equation in the time domain. This allows it to capture dynamic phenomena including wavefronts, pulse-echo interactions, and transient behaviors.

- **Heterogenous Media**:

k-Wave is a comprehensive toolbox of simulations for different mediums with spatially variable characteristics like absorption, density, and sound speed. When imitating real-world circumstances with non-uniform materials, this is very helpful. k-Wave, for instance, may know how sound waves travel through various tissue types, each of which has a unique set of acoustic characteristics, in imaging by ultrasound transducer.

- **Apply Perfectly Matching Layer**:

The toolbox applies perfectly matched layer (PML) boundary conditions, which reduce reflections from the simulation domain's borders and absorb outgoing waves. This is essential to simulate an open domain without fake reflections.

- **Simulation of Broadband Pulses**

Broadband pulse simulations are supported by k-Wave enabling users to simulate and examine wave propagation over a variety of frequencies (1MHz to 30MHz). This is crucial for uses like ultrasound imaging, where various frequencies might yield various kinds of data.

- **Modeling of Sensors and Sources**:

Within the simulation area, users may design sensors and acoustic sources, such as PVDF arrays transducer or point sources. The sources can be configured to output waveforms, sinusoidal, or other waveforms. Particle velocity, pressure, and other wavefield properties can be recorded using sensors.

- **Post-Processing and Visualization**:

k-Wave offers visualization tools, including pressure fields, wavefronts, and time-series data, for the simulation results. It also provides post-processing tools for analysis, including the ability to determine focus points, calculate acoustic intensity, and create beam profiles.

3.2.1 Basic steps of K-wave:

- **Define the Medium:** Establish the simulation grid and specify the medium's characteristics, such as sound speed, density, and absorption.
- **Model the Sensors and Sources**: Identify the sensors and acoustic source type and positions within the grid.
- **Run the Simulation**: To capture data at the sensor sites, use k-Wave functions to propagate the acoustic waves across the medium.
- **Visualize and Examine**: Visualize wave propagation using the toolbox's visualization capabilities, and then use post-processing methods to analyze and understand the findings.

Acoustic wave simulations find the k-Wave toolbox a versatile resource, providing powerful tools for understanding complicated wave phenomena and fine control over simulation parameters. k-Wave offers the resources you need to accurately model and understand acoustic wave behavior, whether you're enhancing medical imaging methods, researching wave interactions in diverse materials, or creating novel sensor technologies.

To maximize the transducer's performance, two-dimensional FEM simulations were conducted. As the FEM model is more relevant to take into account the complex interactions and acoustic behavior between various materials (Pvdf) and layers (epoxy, Cu traces), this was done to fine-tune the transducer design that was initially based on the 1D predictions. Finding the transducer layer thicknesses of Pvdf 20μm that would maximize the bandwidths up to 30MHz of the

transducer. It was discovered that the 20 µm ideal layer thicknesses were used to optimize the relevant properties of the proposed prototype-designed Ultrasound sensor.

3.2.2 Signal Propagation in K-wave

The diagram given below shows that the signal generation and acquisition procedure in a system that used for sensing that is stimulated by laser-induced acoustic waves. There are flow-work describe below:

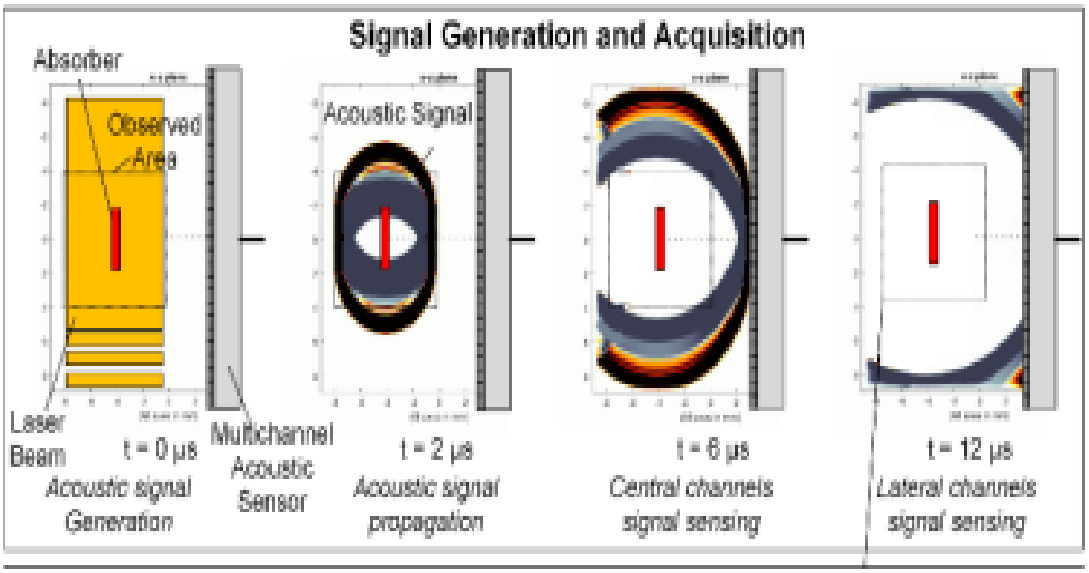

Figure 14:K-wave simulation overview of signal acquisition

- **Generation of Acoustic Signals (t = 0 µs)**

A laser beam is focused on an absorber, that effectively absorbs laser energy or just a substance. The absorber quickly heat up after absorbing the laser energy, follow the adiabatic expansion which results in thermoelastic expansion and the production of an acoustic (ultrasound) wave.

- **Propagation of Acoustic Signals (t = 2 µs)**

The sound wave that is produced starts to travel away from the absorber. The sensor finds the acoustic signal that is propagating and may be made up of several channels. The various hues in this section of the figure most likely depict the shifting phase or strength of the propagating sonic waves.

- **Channels Sensing Signal (t = 6 µs)**

As the acoustic signal continues to travel, the center channels of the acoustic sensor array pick it up at a given sensing point. The interaction of the signal with the channels is illustrated, which probably demonstrates the evolution of the wavefront over time.

- **Signal Sensing at Multichannel (t = 12 µs)**

The acoustic wave has now propagated further, and the signal is detected by the sensor array's, which are situated further away from the center channels. This stage illustrates how the wave gradually reaches various locations inside the sensor array. The progression of the figure illustrates how the acoustic wave changes over time at various intervals of time (0 µs, 2 µs, 6 µs, and 12 µs).

Detection of the acoustic signal at two distinct points (central and lateral), the acoustic sensor array contributes to the construction of a more comprehensive image of the wavefront and, ultimately, the object or region being imaged. This technique uses sound waves to find weaknesses in constructions or materials.

To summarize that the diagram shows the creation, propagation through a medium, and detection over time by various components of a multi-channel sensor array of a laser-induced acoustic signal, enabling comprehensive signal capture and analysis.

3.2.3 Directivity results

The development of the acoustic sensor begins with a fundamental acoustic requirement that constrains the physical dimension of each channel, namely the directivity (i.e. the sensitivity as a function of the angle of arrival of the acoustic wave). when the wave hits with an arrival angle different from 0 ° concerning to the normal one, it will stimulate different parts of the single channel at different moments the more the size of the channel is large compared to the wavelength, leading to destructive interference. In other words, each channel must be small enough w.r.t the acoustic wavelength to behave as an almost omnidirectional sensor, at least in the range of arrival angles foreseen by the experimental scenario.

To measure the proposed prototype PVDF sensor directivity response using a single frequency approach, the sensor-active element must be accurately aligned with the center of propagation. Small placement mistakes can significantly affect observed directional responses. Measuring the directional response of sensors in a array posses a challenge since each PVDF element requires a unique centre of axis. For elements near the array's edge, it might be challenging to establish separate degrees of freedom.

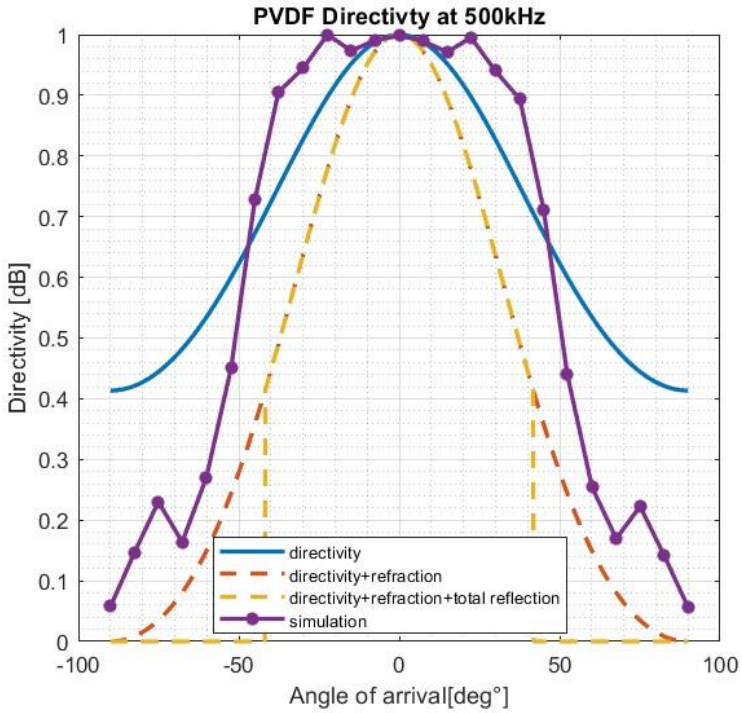

Figure 15:Directivity response of PVDF Sensor at 500KHz with 1.2mm Thickness

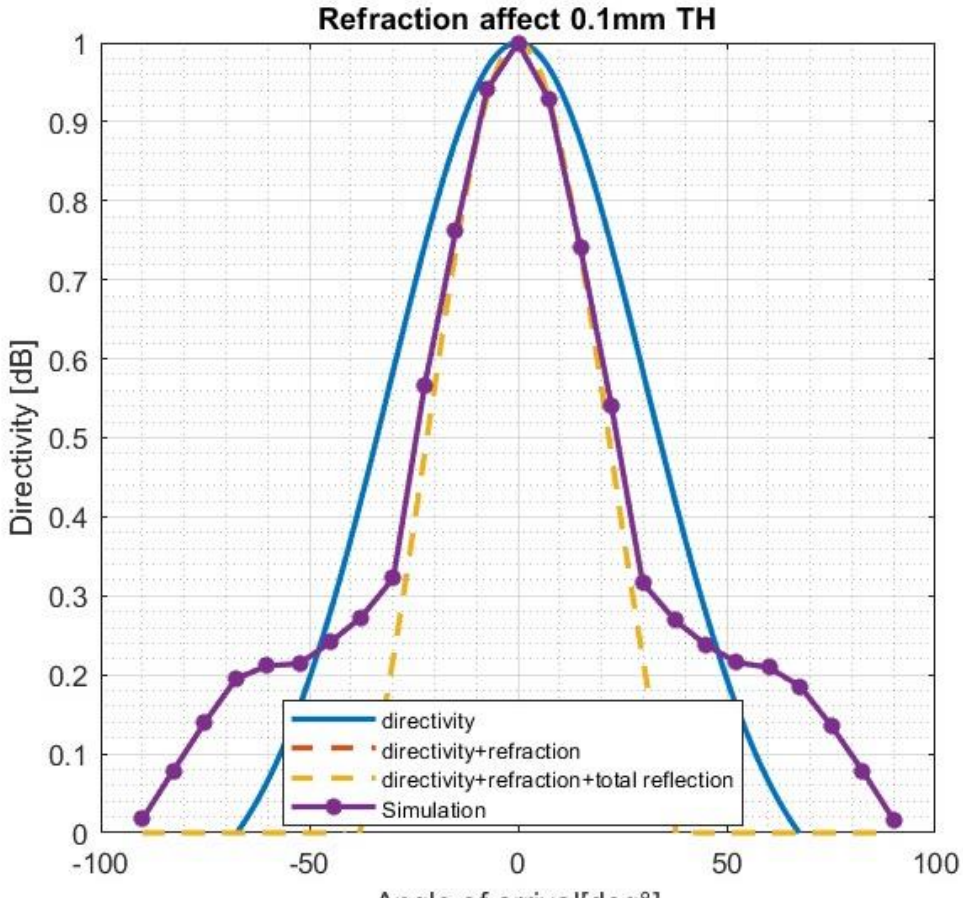

Figure 16:Directivity response of PVDF Sensor at 500KHz with 0.1mm Thickness

The presented plots reveal the influence of refraction on the directivity of an acoustic sensor across varying thicknesses of the sensing layer (1.2 mm and 0.1 mm). The initial plot at 500 kHz and 1.2 mm thickness reveals a significant alteration in directivity upon the inclusion of refraction analysis. The directivity curve (blue) without refraction displays a more concentrated and symmetrical pattern centred around the angle of arrival (0°), showing minimal attenuation. As refraction (dashed orange line) and total reflection effects (dashed yellow line) are incorporated, the pattern exhibits a broadening, which suggests a reduction in sensor directionality. The simulation outcomes (purple line) align closely with the integrated refraction and total reflection model, confirming the wider directivity pattern.

The second plot at 500 kHz and 0.1 mm thickness shows a notable decrease in refraction effects on directivity. The refraction (orange) and total reflection (yellow) curves exhibit a close alignment with the original directivity curve (blue), resulting in minimal deviation. The overall pattern is consistently narrow and sharply concentrated, with the simulation (purple) adhering to this trend as well.

From a design perspective, decreasing thickness from 1.2 mm to 0.1 mm lessens the impact of refraction on directivity, thereby enhancing the sensor's capability to concentrate on signals coming from a more restricted range of angles. This suggests that thinner sensors are advantageous in this scenarios that demand enhanced directivity and precision, as they preserve a closer alignment with the original directivity curve and demonstrate reduced distortions caused by refraction. The presented plots describe the influence of refraction on the directivity of an acoustic sensor across varying thicknesses 1.2 mm to 0.1 mm of the sensing layer.

3.3 Sensor Design and Acoustic Validation

Piezoelectric materials are used to transduce pressure into voltage and can be used as acoustic sensor. Polyvinylidene Fluoride is a polymer material which has an acoustic impedance very close to water and tissues. As compared to Lead-Zirconate-Titanate (PZT) sensors, PVDF does not need any complex matching layer to optimize acoustic signal transmission from the biological sample into the sensor material. In opposite to ceramic materials, PVDF can be easily manufactured in thin layers of few tens microns which are required for high frequency applications.

Mostly PVDF materials have metallization on both sides which act as electrodes and define the active area of the acoustic sensor. In this paper, only one side of the PVDF is covered by a thin 100 nm Au/Cu metallization (attached to ground plane and in common to all the channels). The other side of the PVDF is glued to a PCB whose exposed copper pads act as the second electrode and define each channel area. Fig 13. shows the cross-section view and layers of the proposed sensor. Starting from the bottom, the PCB passive substrate (grey) has exposed PCB copper pads/traces that act as the sensor bottom electrodes and define the sensor's active area. A PVDF film is glued to the PCB using an epoxy glue and the PVDF top metallization is then bonded to a dedicated ground pad on the PCB.

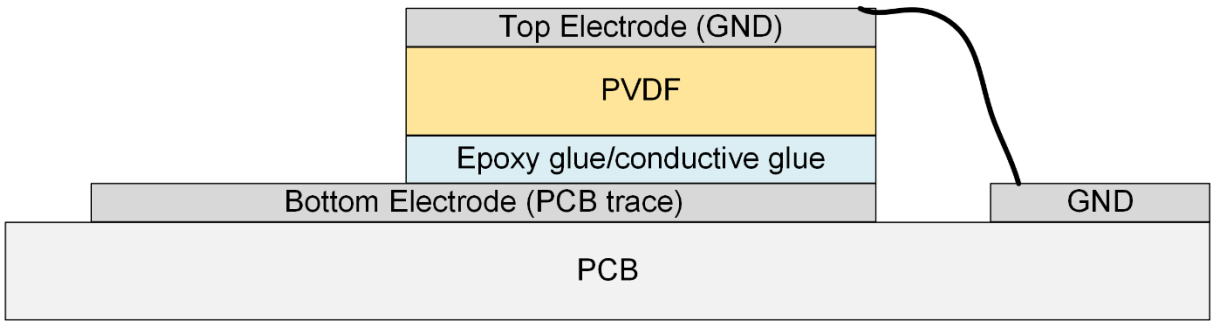

Figure 17 :Sensor design by stacked layers

The grey color rectangular shape in figure 17. is known as the Printing circuit board (PCB) which behaves as the substrate of the receiver signal setup. Receiver signal basically the actual part of this setup which is designed for acquiring the acoustic signals. That part is composed of four different layers which is already demonstrated in the fig 7. The concept about working of four layers is to penetration of the acoustic pressure wave to Pvdf material and its subsequent. This causes the piezoelectric material to vibrate and polarise, resulting in the generation of an electric signal that is sent through a conductor. The epoxy and copper in this context serve as an impedance-matching layer for the acoustic transducer array, while the PCB behaves as a membrane layer.

3.4 Printing Circuit Board (PCB) Layout

PCB layout for the proposed sensor (highlighted by the red box at the bottom) as well as two analog switch electrode arrays, that route each of the 8 channels to an SMA connector for testing purposes. There are three possible phases of proposed geometry for manufacturing of sensor active area and for testing of its acoustic behavior. Below the sensor, a large GND pad is used to connect the top electrode of the sensor to the PCB ground plane. A planned printed circuit board (PCB) layout for an acoustic sensor prototype as shown in Fig 18. The system's geometry is arranged as follows:

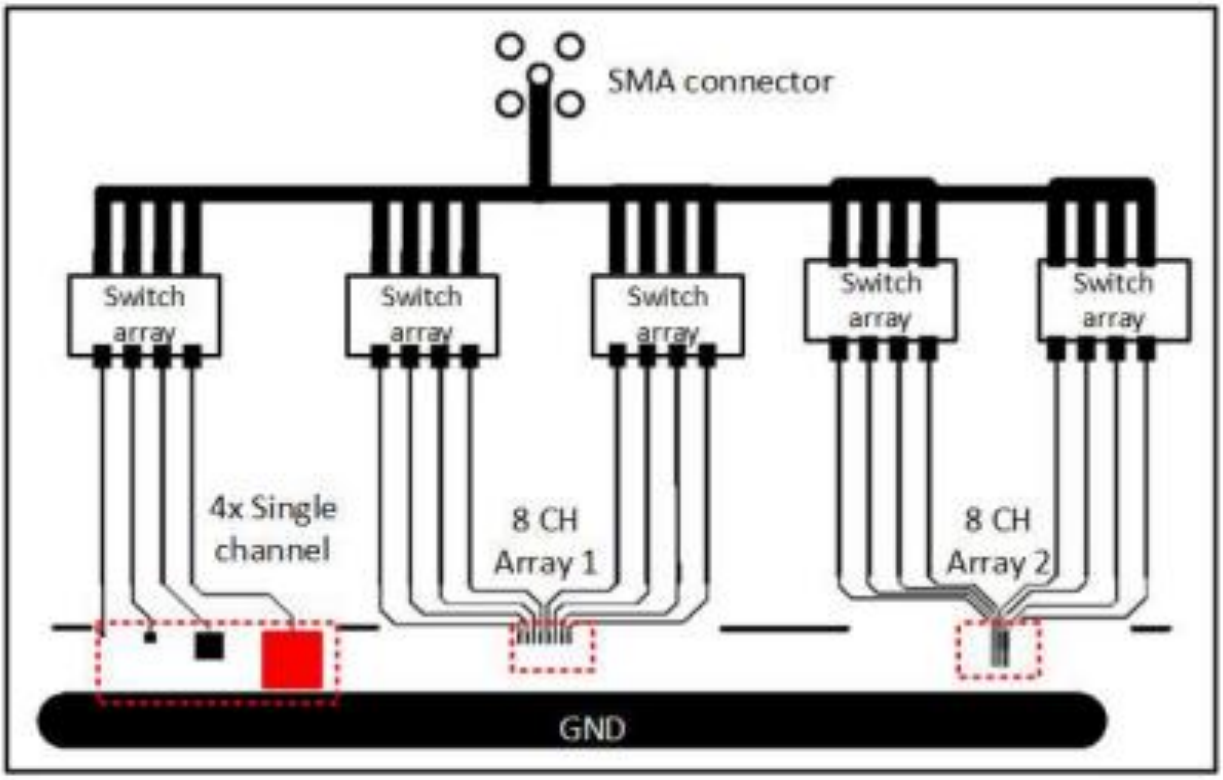

Figure 18 : Proposed PCB layout for Prototype Acoustic Sensor

- **Overall Layout**: - To emphasize organization and modularity, the PCB is built with several linked components placed linearly and symmetrically.
- **Central Component**: - The SMA connector, which is located in the upper center of the layout and is utilized for signal input or output, acts as a crucial interface for the whole sensor system.
- **Switch Arrays**: - Directly linked to the SMA connection via conductive lines, there are four switch arrays arranged horizontally. The signals that are sent to or from the sensor arrays must be routed and controlled by these arrays.

- **Sensor Channels**: - The labeled parts show which sensor channels the PCB supports. 4 Single Channel layout's left side shows four separate sensor channels with the dimensions of 10x10mm (red box), 5x5 (black one) and 3x3mm (small black) joined together.

  8 CH Array 1: This is an eight-channel sensor array that is positioned in the center with dimensions of length into width composed of (3x10)mm respectively. They have a pitch distance of 0.328mm between the channels.

  8 CH Array 2: Mirroring the arrangement of Array 1, but it is situated on the right side with the same dimension but the pitch distance is different 0.128mm .
- **Grounding (GND)**: To provide adequate grounding and reduce electrical noise throughout the circuit, a large ground (GND) plane is positioned horizontally down the bottom of the PCB.
- **Connection Paths**: - A series of parallel lines, which most likely represent electrical traces of Copper (Cu) material on the PCB, link each sensor array or single channel to its corresponding switch array. This PCB design's shape allows for simple expansion or change by adding or deleting channels or sensor arrays.
- **Signal Routing**: An important aspect of acoustic sensor systems is regulated signal transmission, which is why switch arrays and SMA connectors are included in this design. The broad grounding plane indicates that noise reduction should be carefully considered. This is important to preserve signal integrity in sensitive acoustic measurements.

This design demonstrates a multi-channel acoustic sensing system that is well-organized and places a high priority on signal management, noise reduction, and adaptability.

The proposed PCB layout is designed because of its simplicity, efficiency, and ease of implementation, the rectangular form of an acoustic sensor array is sometimes seen to be better to a spherical shape in certain applications. Rectangular arrays are more practical for many use situations because of their consistent, grid-like layout, which makes physical assembly and signal processing easier. By electrically guiding the array's sensitivity in desired directions, they provide accurate spatial resolution as compared to spherical or cylindrical geometry. This design also makes it easy to scale and adjust to different sizes, which makes it adaptable to a wide range of applications. They necessitate intricate sensor locations, they are frequently more costly and necessity for advanced signal processing techniques. Rectangular arrays are a more cost-effective option in many situations because they provide high directional sensitivity and

resolution at a lower cost and complexity, striking a compromise between performance and biocompatibility.

3.5 Physical Acoustic Setup

Acoustic test set-up is used to acquire the acoustic signals from the transmitter (black one) shown in the given below figure 19. In between the Eight switching buttons, there is a rectangular strip of Pvdf sheet with a thickness of 20 μm is stacked on the copper Pads/traces (35 μm) with the help of non-conductive glue with thickness of around 1μm to avoid shorting to the adjacent channel which behaves as an active area of the designed acoustic sensor.

The image depicts a physical setup that is used to test or demonstrate an acoustic sensor system more precisely, it involves sending and receiving sound waves. The main elements and their functions are explained in detail below:

3.6 Components and their functions

- **PVDF Receiver**: In the configuration, Polyvinylidene Fluoride (PVDF) acoustic sensor serves as the receiver. PVDF sensors are frequently employed to detect ultrasound waves because of their well-known sensitivity to sound. The PVDF sensor is positioned in this configuration to receive the acoustic signals that the PZT sensor transmits.
- **PZT Transmitter**: As the transmitter, the PZT sensor produces acoustic or ultrasound waves that are transmitted via the medium, which is most frequently water, as seen in the diagram. PZT sensors are piezoelectric devices that have the ability to create sound waves by converting electrical signals into mechanical vibrations.
- **Channel Selection Electrodes**: These switches govern which signals are delivered or received by choosing different channels or paths inside the circuit. The user can test different setups or sensors within the same setup thanks to the ability to swap channels.
- **Printed Circuit Board** (PCB): A PCB, which offers the required electrical connections and support, is used to install the components. Switches and sensors are firmly fastened, and the PCB design have been tailored for this particular acoustic test.

- **Medium of Propagation.** The image's refer to "Water" implies that the sensors are being tested underwater. Water transmits sound waves well, especially in ultrasound frequency ranges, hence it's frequently employed as a medium in acoustic testing.

Setup as shown in Fig 19. is used to evaluate how well the PVDF sensor detects acoustic signals that transmit by PZT sensor. Measurements of factors including sensitivity, signal strength, and the effectiveness of signal transmission across water were made using this setup by using the PZT sensor to transmit ultrasound waves and the PVDF sensor to receive ultrasound waves. The electrode switches provide the experimental setup, versatility by enabling the testing of various channels. The apparatus offers a regulated setting for evaluating the performance and reliability of acoustic sensors, especially in fluid media such as water.

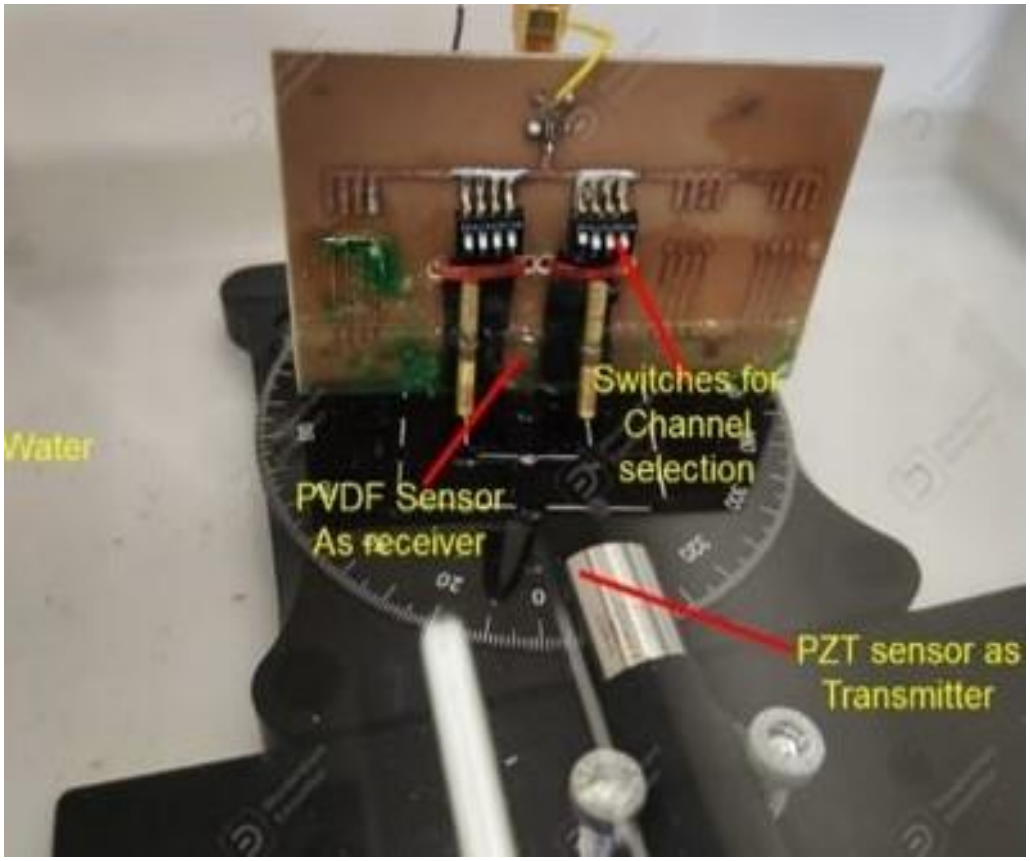

Figure 19 : Physical Acoustic test bench

Chapter 4.

PVDF Ultrasound Array for low and High frequency Application: Design, Optimization, and Validation

Abstract: The chapter 4 presents the design and experimental validation of single-channel polyvinylidene fluoride (PVDF) ultrasound sensor array with variable thickness of 1.2mm and 20 μm which are tailored for ionoacoustic tomography and photoacoustic imaging respectively. Therefore, PVDF sensor array is designed to overcome the limitations of traditional piezoceramic sensors, offering broader bandwidth, reduced signal distortion, and improved sensitivity. The chapter details the design process, including sensor modeling through finite-element simulations, material selection, and performance optimization in terms of frequency response and noise reduction. Experimental results are presented to validate the sensor's capabilities in both electrical and acoustic domains, emphasizing its potential to significantly enhance the precision and adaptability of hadron therapy treatments by accurately mapping dose deposition in real time and for different applications like photoacoustic imaging.

4.1 Ionoacoustic Tomography:

The rapid deposition of energy that occurs along the range of pulsed particle beams generates an increase in temperature and in pressure that propagates in the absorber as an acoustic wave whose frequency depends on the energy of the beam and varies from 300 kHz (60 MeV protons, lowest value in clinical treatment) down to a few tens of kHz (200+ MeV protons, upper value for clinical treatment). In clinical settings, the amplitude of this acoustic signal is a few Pa or fractions of Pa and requires dedicated sensors to be acquired with sufficient signal-to-noise ratio (SNR). The information on the time of flight of the acoustic wave can be used to localize the maximum of dose deposition (Bragg peak) with sub-millimeter precision while applying acoustic imaging algorithms it is possible to obtain a map of the dose deposition.

4.2 Analytical Model.

An analytical MATLAB model for the basic formulation of an acoustic sensor typically involves deriving the governing equations of wave propagation in a medium, often based on the wave equation or acoustic basic discrete equation. The model gives how sensor behave to interact with the sound wave by solving the equations 1 to 8 as directed in chapter No 3. So the below given table define the characteristic parameters of a proposed sensor by using Analytical Model basic formulation.

Table 8: Sensor characteristics parameters

Sensor Parameters	**Value**
Frequency coefficient	1125 Hz.m
Piezoelectric voltage coefficient	400 mV/(Pa·m)
Glue dielectric Constant	3.5
Piezoelectric relative dielectric constant	10.5
Channel width	3mm
Channel length	30mm
PVDF thickness	1.2mm
Water acoustic impedance	1.5 MRayl
PVDF acoustic impedance	3.5MRayl

Table 9: Sensor Performance Parameters

Sensor Parameters	**Value**
Sensor capacitance	5 pF
Sensor bandwidth	800 kHz
Sensor Sensitivity	432 µV
dp @ Sensor	34.6Pa
Output Voltage	14.6µV
Output Referred Noise Power	42 μV_{RMS}
Output Referred Noise PSD	43 nV/sqrt(Hz)
Input Referred Noise Power	97uVrms
Input Referred Noise PSD	99nVrms/sqrt(Hz)

4.3 Pvdf (1.2mm) Sensor Geometry (3x30mm)

The suggested Pvdf multichannel acoustic sensor's shape is defined using the Matlab model. Included in the table are the most important factors about the acoustic PVDF (Polyvinylidene Fluoride) multichannel sensor. By considering these aspects, we may assess how well the suggested sensor prototype works. The amount of charge that a sensor can carry is defined by its capacitance. Because the charge generated in reaction to acoustic pressure is converted into a measurable voltage, this is a crucial feature for PVDF sensors. This sensor is ideal for low-frequency applications like ionoacoustic tomography because to its 800 kHz band-width, which validates the frequency range in which it can detect acoustic impulses and record sounds. At a known acoustic pressure of 34 Pa, the sensor produces an output voltage of 14.6 mV for every unit of input. It explains how accurately the sensor can convert pressure changes into an electrical signal. A number of 34.6 Pa indicates the specific pressure at which the sensor is being evaluated.The output voltage reveals the signal that the sensor generated when subjected to a certain pressure. But the RMS (Root Mean Square) measurement at the sensor's output indicates a noise power of 42 µVRMS. Reducing the noise power improves the signal quality overall since there is less noise in the system.

The output noise power spectral density (PSD) explains the power distribution over frequencies. A noise level of 43 nV/√Hz of bandwidth is shown by a value of 42 uV, which gives an idea of the noise performance across different frequencies. In relation to the input of the sensor, this is the root-mean-squared value of the noise power. For the purpose of assessing the sensor and its readout circuitry, it provides a description of the corresponding noise at the sensor's input. The

input referred noise (IRN) result shows that there is 99 μV/√ Hz of noise at the sensor's input.A single pulse's signal-to-noise ratio (SNR) on a single channel. This reveals how well the sensor can distinguish between the audio signal and background noise. Having a signal-to-noise ratio (SNR) of 47 dB indicates that the signal is about 47 dB elevated above the noise level. This is the signal-to-noise ratio for a single pulse in a multichannel system, computed over 32 channels. The significant improvement in signal-to-noise ratio (SNR) (77 dB) compared to single-channel SNR is evidence that using multiple channels, which aggregate data from several sensors, greatly improves signal quality. Using 1000 pulses does not change the 77dB SNR of the suggested prototype sensor. Therefore, increasing the number of pulses has no effect on the signal-to-noise ratio (SNR) in the multichannel arrangement as the noise levels are already quite low. The results demonstrate the sensitivity and suitability of the suggested prototype multichannel PVDF sensor for use in applications requiring the detection of high-frequency ultrasonic waves. The system is able to detect faint acoustic signals because the multichannel configuration (such as 32 channels) greatly increases the SNR by reducing noise through channel aggregation.

4.4 Refraction affected Directivity

The graph demonstrates the impact of refraction on the directivity of an acoustic sensor array, contrasting performance with and without the influence of refraction. The directivity, expressed in dB, is plotted as a function of the angle of arrival, spanning from -40° to 40°. The "no refraction" curve exhibits elevated peaks and nulls, signifying enhanced directionality and more pronounced responses at specific angles. The "with refraction" curve exhibits a flattened response, characterised by diminished maximum directivity and less distinct nulls. Refraction reduces the sensor's capacity to accurately identify sound sources at particular angles, as the bending of acoustic waves results in a more uniform distribution of energy across those angles.

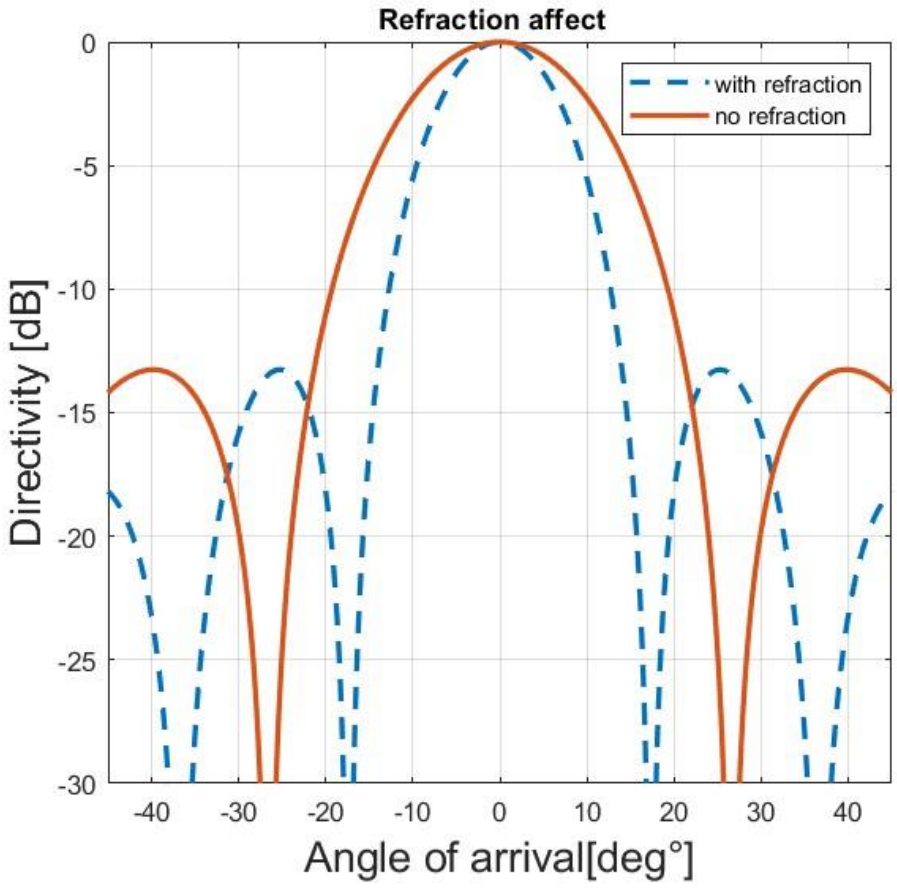

Figure 20: Analytical Model Predicted Directivity

This phenomenon is essential in applications such as ionoacoustic imaging, which necessitates accurate localization of energy deposition. Research by Hurrell and Duck (2000) examined the performance of piezoelectric PVDF arrays and highlighted that environmental factors, such as wave propagation mediums, can significantly influence sensor directivity. Observations in their study emphasized the influence of impedance mismatches and refraction effects on sensor array performance, which must be considered in system design**.**

These parameters allow us to assess the performance of the suggested prototype sensor. The capacitance of the sensor controls the amount of electrical charge it can store. This is an important feature of PVDF sensors because the charge generated in response to acoustic pressure is converted into a voltage that can be measured. The sensor with 1MHz bandwidth indicates the range of frequencies across which it can detect acoustic signals; the sensor can record sounds in this range, making it suitable for lower frequency applications such as Ionoacoustic imaging.

This fundamental approach of Matlab Model shows the feasibility of a sensor array that facilitates omnidirectional functionality through the exploitation of several rectangular PVDF sensors. One may modify the sensor positioning, the quantity of sensors, and the array's radius to enhance omnidirectionality. In practical applications, omnidirectional functionality is typically attained by arranging several sensors in a circular or spherical formation. This enables the sensor array to uniformly acquire acoustic waves from all directions.

4.5 K-Wave-Model

Regarding the Directivity Diagram Revealing the Refraction Effect The influence of wave refraction on the process of acoustic sensors may be better understood with the help of k-Wave modelling. K-Wave is a popular MATLAB package that models how sound waves travel through different types of material. To better forecast the wavefront changes caused by refraction, it is helpful to simulate the interaction between acoustic waves and various materials and their boundaries in this case. To understand how the directivity pattern of the sensor array is affected by the bending of waves as they transition between different media, a k-Wave simulation may be done. In the absence of refraction, the blue curve in the figure represents the increased directivity that would otherwise occur since the waves would follow more predictable routes. Nevertheless, when waves are bent due to refraction, the response becomes more diffuse or hazy, impacting the precision of identifying arrival angles (as shown by the orange curve).

The ability to accurately describe these acoustic behaviours is fundamental to k-Wave simulation, which aids in the optimisation of sensor array design for ionoacoustic imaging applications. When designing for settings where various kinds of tissue or materials could impact wave propagation, designers can foresee and account for performance trade-offs by modelling with and without refraction.

4.5.1 Propagation of Pressure Field in K-wave

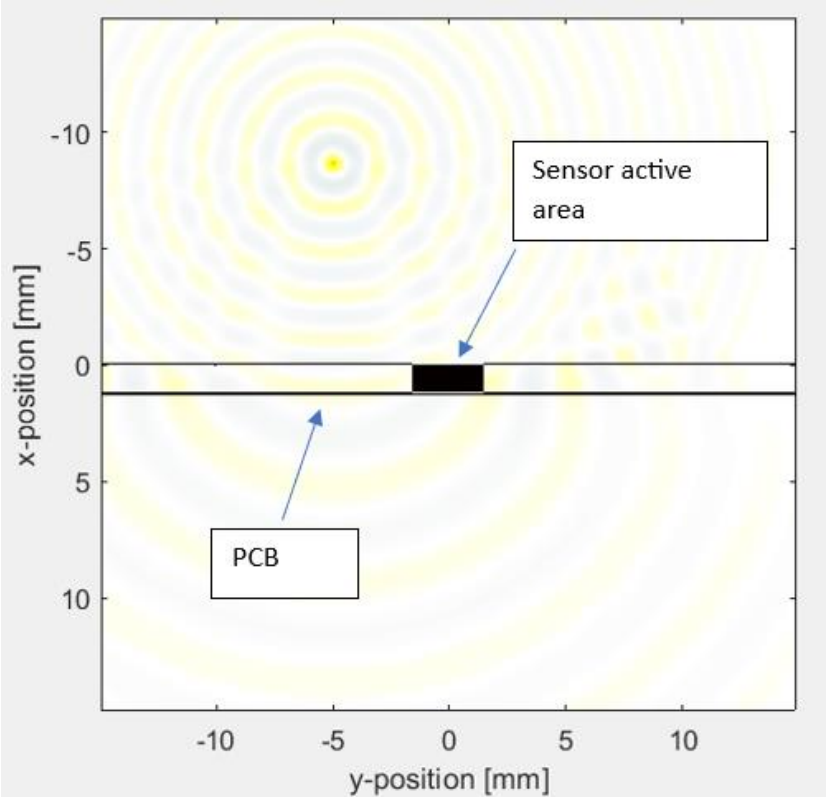

Figure 21: Simulated propagation of wave field

The fig 21. shows the propagation of a pressure field interacting with the active region of an ultrasound sensor. The circular wavefronts demonstrate the pressure waves emanating from a point source located above the sensor, propagating symmetrically. As these waves propagate through the medium, they interact with the sensor's active area, indicated by the black rectangle at the center. Approaching on sensor surface, the pressure waves result in the absorption and conversion of a portion of the wave energy into electrical signals, facilitated by the piezoelectric effect, provided the sensor is constructed from a piezoelectric material such as PVDF. The interaction with the sensor is significantly influenced by the sensor's geometry and the angle of incidence of the wavefronts on its surface. The sensor's directivity influences the extent of wave energy capture and the precision in determining the source's direction.
The simulation demonstrates the impact of sensor placement on the captured signal, emphasizing regions of high and low pressure as the waves propagate. This interaction is

essential for enhancing sensor design in applications like ionoacoustic or photoacoustic imaging, where accurate detection of wavefronts is vital for precise imaging or localization.

4.5.2 Simulated Directivity

The acoustic sensor's development is based upon a core acoustic criterion that determines the physical dimensions of each channel, specifically its directivity (As the sensitivity is in relation to the angle of incidence of the acoustic wave). When a wave stumbles across at an angle other than perpendicular to the surface, it stimulates different fragments of the single channel at different times, particularly when the channel size exceeds the wavelength. This phenomenon elaborated through Fraunhofer diffraction formalism, necessitates constraining the physical size of each channel to ensure unrestricted sensitivity to the acoustic source, regardless of directional constraints. Essentially, each channel must be sufficiently small to operate as an almost omnidirectional sensor, especially within the anticipated range of incident angles. In a linear array setup, channels embrace a rectangular shape to achieve omnidirectional behavior along the array axis and directional sensitivity perpendicular to it.

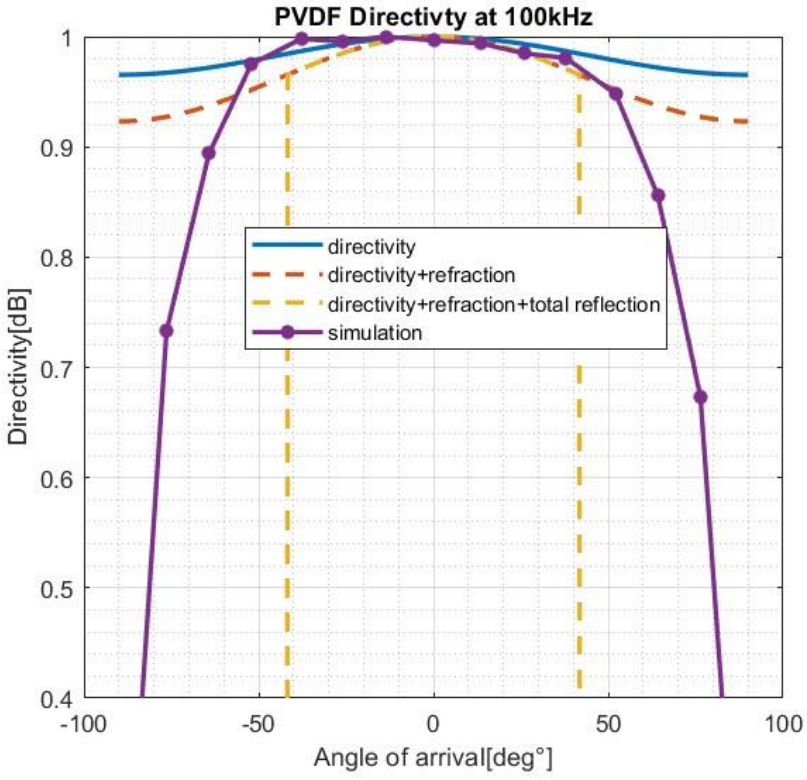

Figure 22:Directivity response of PVDF Sensor at 100kHz

Accordingly, a channel size of 3 mm x 30 mm was selected in this configuration. The diagrams presented in this section provide a detailed analysis of the directivity patterns of a PVDF ultrasound sensor at various frequencies (100 kHz, 300 kHz,500KHz and 800 kHz). These diagrams are necessary for understanding how the sensor responds to acoustic waves arriving from different angles, an essential consideration for applications such as ionoacoustic imaging in hadron therapy.

At 100 kHz in fig 22, the directivity pattern flattens considerably, indicating a broader angular response. The sensor becomes more omnidirectional at this lower frequency, meaning it can detect acoustic waves arriving from a wide range of angles with relatively uniform sensitivity. This is expected, as lower frequencies have longer wavelengths, which makes the sensor's response less dependent on the exact angle of arrival. This omnidirectional behavior is useful in scenarios where detecting sound from multiple directions is important, such as in broader-field imaging or environmental monitoring.

Interestingly, the simulation results (represented by the purple markers) closely match the theoretical directivity curves, demonstrating the model's accuracy in predicting sensor behavior at low frequencies. However, the inclusion of refraction and reflection further modifies the

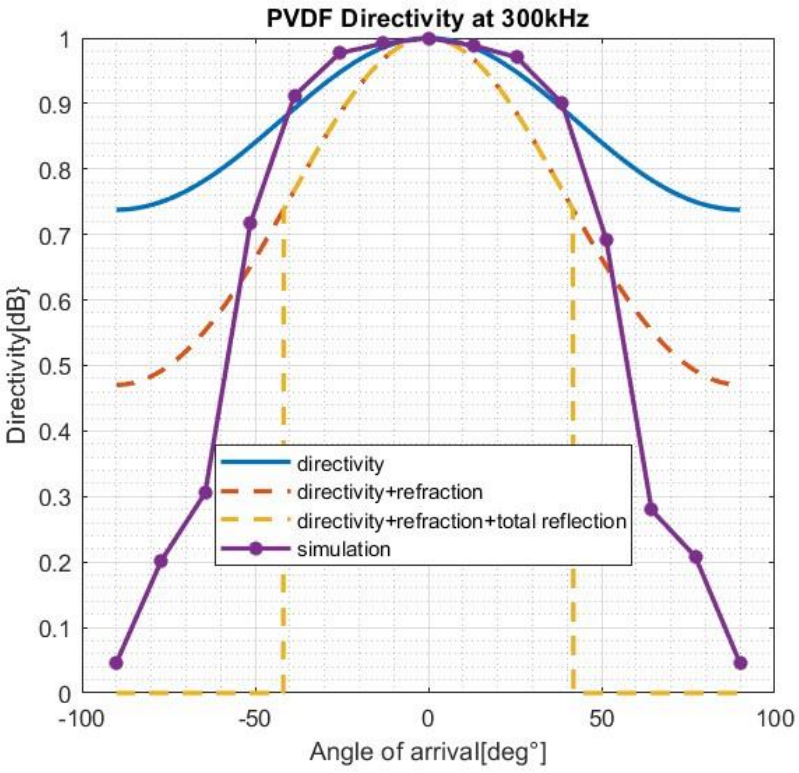

Figure 23:Directivity response of PVDF Sensor at 300kHz

directivity, indicating that the real-world performance of the sensor will still be influenced by the medium through which the waves propagation.

The directivity pattern at 300 kHz in fig 33. represents an intermediate case, where the sensor shows a mix of both focused and broader directivity. While the peak response is still around 0°, the broader response compared to 800 kHz suggests that the sensor can detect off-axis signals more effectively. This frequency is ideal for applications requiring both spatial coverage and some degree of directional accuracy, such as in medical imaging where signals may arrive from various angles due to scattering in tissue.

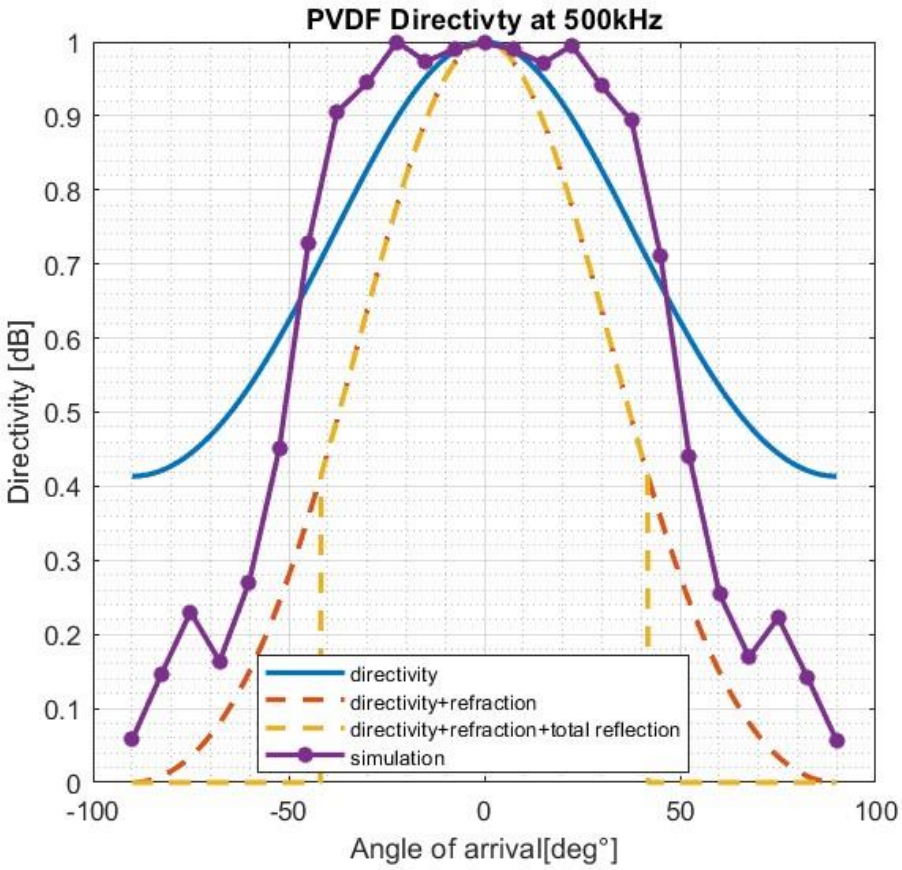

Figure 24:Directivity response of PVDF Sensor at 500kHz

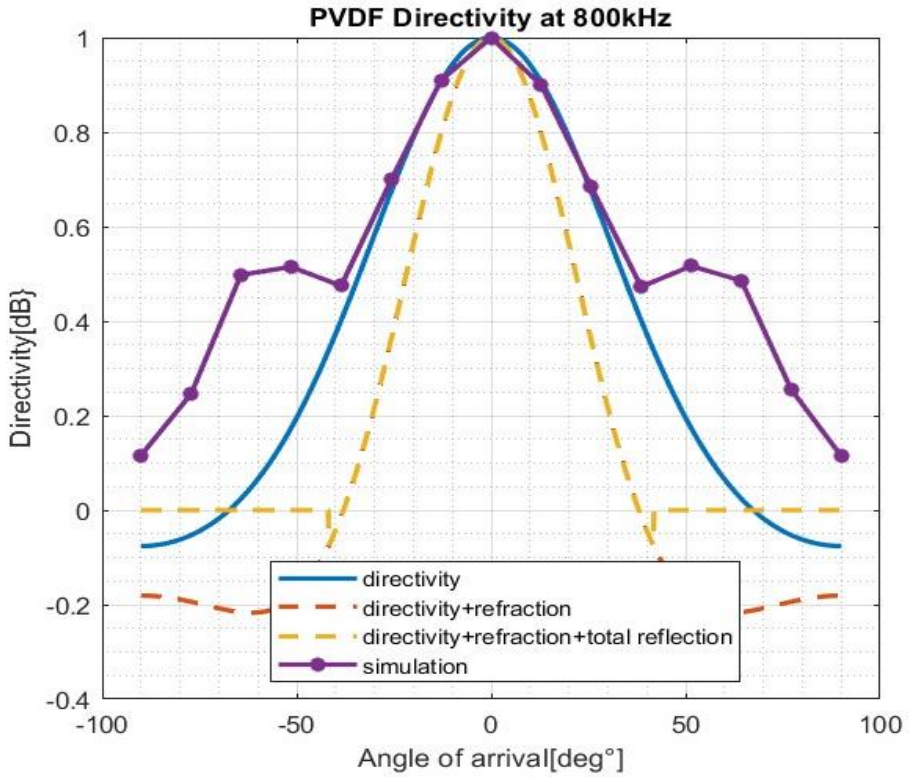

Figure 25:Directivity response of PVDF Sensor at 800KHz

Fig 24 and 25, presents directivity pattern at 500K and 800 kHz, the sensor exhibits a highly focused directivity pattern, with the strongest response occurring around 0° (the angle at which waves arrive perpendicularly to the sensor). The sharp peak indicates that at this high frequency, the sensor is most effective at detecting signals arriving directly from the front, while its sensitivity quickly decreases as the angle of arrival increases. This pattern aligns with established acoustic sensor theory, where higher frequencies correspond to shorter wavelengths, resulting in more focused directivity. This characteristic is particularly valuable for precise localization of energy sources, such as the Bragg peak in ionoacoustic imaging, where millimeter-level accuracy is needed. The influence of refraction and total reflection can be seen in the slightly broader directivity when these effects are considered. This is significant in real-world applications, where the acoustic wave may pass through different media with varying acoustic impedances, bending the wavefronts and altering the angle at which they reach the sensor. Including these factors in the simulation provides a more realistic representation of how the sensor performs in practical scenarios, especially in biological tissues where refractive effects are common.

These directivity patterns highlight the versatility of PVDF sensors in acoustic imaging. The sensor's frequency-dependent behavior makes it suitable for a range of applications, from precise, high-resolution imaging at higher frequencies to broader, more general detection at lower frequencies. The consideration of refraction and reflection effects is particularly important in medical applications, where the acoustic environment is complex, and waves are likely to interact with tissues of different densities and acoustic properties. Studies such as Hurrell and Duck (2000) and others on PVDF sensor arrays confirm the importance of including such effects in modeling to accurately predict sensor performance in real-world conditions

The diagrams offer a comprehensive view of how a PVDF sensor's design and frequency response influence its directivity, providing valuable insights for optimizing sensor arrays used in ionoacoustic imaging and other acoustic sensing applications. By considering not only directivity but also refraction and reflection, these simulations present a more complete picture of the sensor's real-world performance, paving the way for more accurate and reliable imaging technologies.

These directivity patterns provide valuable insights into the behavior of PVDF transducers across a range of frequencies 100 kHz to 800kHz, confirming trends. The results indicate that while higher frequencies offer more focused directivity, the influence of refraction and reflection must be carefully considered to optimize sensor performance in practical applications. These findings provide a foundation for future work in refining the models and adapting PVDF transducers for various sensing and imaging technologies.

4.5.3Frequency Response

The given graph describes the frequency response of a PVDF sensor, indicating its sensitivity in μV/Pa over a broad frequency range from 10^3 Hz to 10^7 Hz. The data demonstrate that the sensor maintains a high and stable sensitivity of approximately 500 μV/Pa across low to mid-range frequencies, reaching up to about 10^5 Hz. This characteristic renders it suitable for applications that necessitate sensitivity in the low-frequency range, including ionoacoustic sensing. As frequency exceeds 10^5Hz, sensitivity significantly decreases, with a marked decline occurring near 10^6 Hz. The sensitivity of the sensor diminishes as it approaches the MHz range and exceeds it. The findings indicate that the PVDF sensor is optimized for low- and mid-frequency applications, maintaining high sensitivity, but is less effective for high-frequency applications exceeding 10^6 Hz.

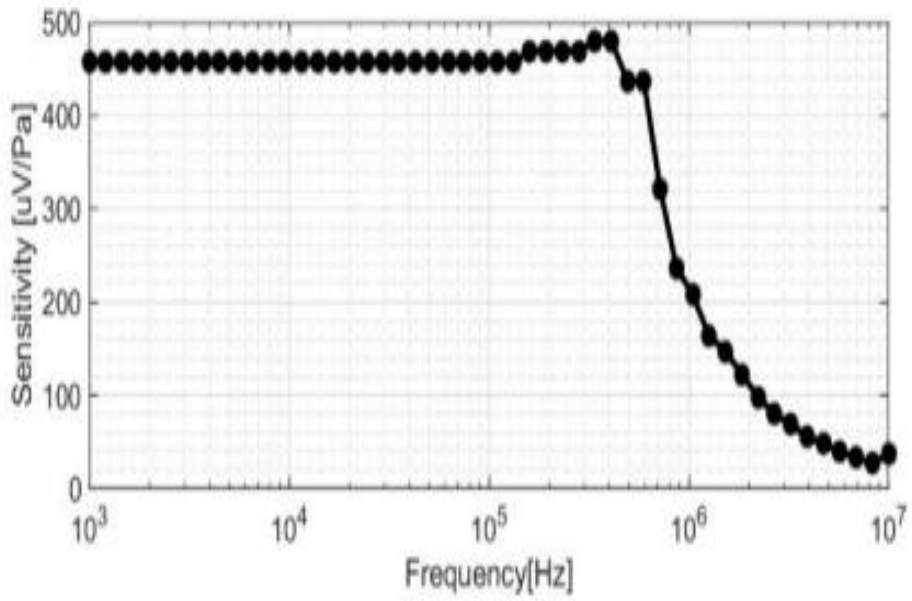

Figure 26:Simulated Frequency Response

The stable sensitivity of the PVDF sensor in the low-frequency range is essential for accurate detection of low-frequency acoustic signals generated by the interaction of ionising radiation with matter in ionoacoustic sensing. The graph indicates that the sensor demonstrates high effectiveness for this application, offering consistent sensitivity within the frequency range pertinent to ionoacoustic uses.

4.6 Experimental Results

4.6.1 Capacitance Measurement

The measurement of Sensor capacitance (Cs) holds significant importance for various reasons:

- Verifying Sensor Construction: The capacitance of PVDF sensors depends on their physical size (area, thickness), and dielectric properties. Therefore, it can be utilized to validate the sensor's construction, detect any discrepancies, and ensure agreement with the theoretical mode.
- Estimating Sensor Noise Performance: Capacitance is closely linked to sensor noise, as explained in Matlab Model.. Consequently, it provides a straightforward means of estimating the sensor's noise performance.

- Facilitating Analog Front-End Design: Piezoelectric sensors commonly employ charge amplifiers in their analog front-ends, where the gain relies on the ratio between Cs and the feedback capacitor.

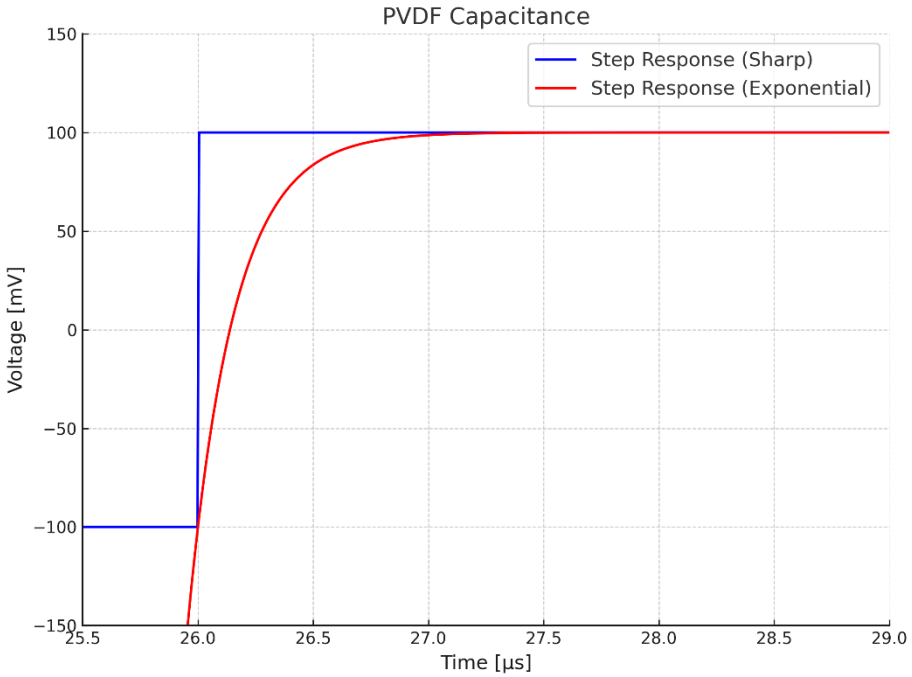

Figure 27: Step response

Thus, accurately characterizing Cs becomes essential for effective gain control and optimal front-end design. Due to the relatively small capacitance, the sensor has been characterized using an RC circuit step response where R is a known resistor (1kΩ) and Cs is the sensor capacitance. The input signal (step, blue) and output signal (exponential charge of the sensor capacitance, red) are shown in Figure 4. The sensor capacitance has been calculated by measuring the time constant of the RC circuit. The capacitance is 5 pF, in agreement with the theoretical value.

4.6.2 Acoustic Testbench

The Acoustic behavior has been tested by using PVDF prototype as a receiver and a piezoelectric sensor with 2 MHz bandwidth has been used as a transmitter. The experimental setup is shown in below Fig 28. The PCB of the PVDF sensor is on the top with the transmitter at the bottom. The transmitter has been excited by a 1 V0-peak signal (a single sinusoidal period at 2 MHz frequency).

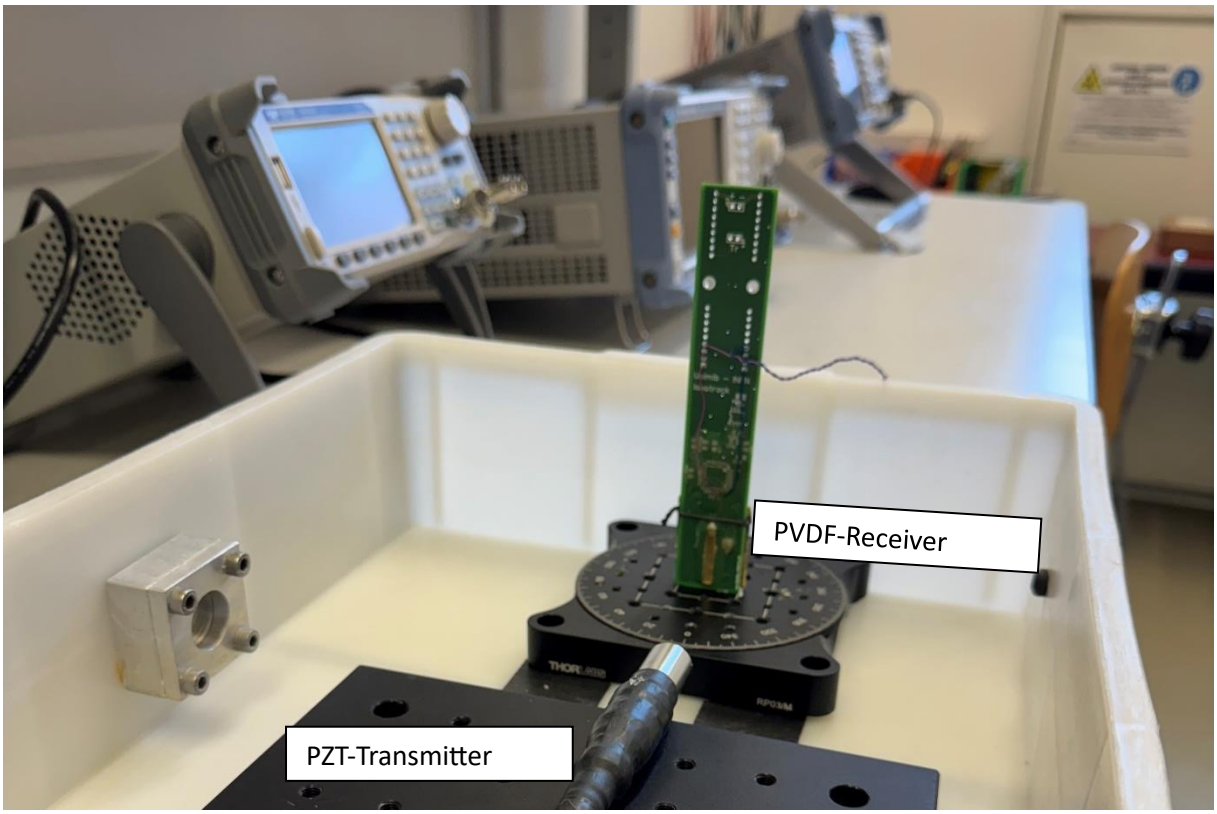

Figure 28: Acoustic Test setup

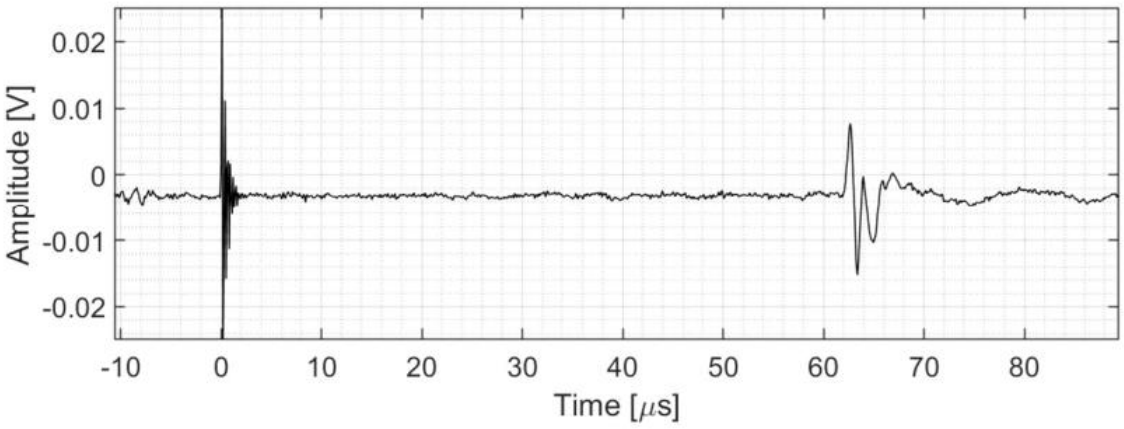

Figure 29: Time Domain Acoustic signal

A significant ringing has been observed with signal amplitude 8 mV0-peak on the receiver which is purely due to characteristic of PZT resonant frequency. The time of flight of acoustic wave has been observed which is 62 microseconds due to wave travel from transmitter to receiver

In this work, the design and experimental validation of a multichannel piezoelectric sensor dedicated to acquiring the weak thermoacoustic signals generated by particle beams in hadron therapy was presented. Acquiring these signals at low noise and preserving their shape allows for high precision and low latency mapping of the dose deposition. Currently the ionoacoustic technique has strong technological limitations due to the low maturity of the detector technology, which uses off-the-shelf components not optimized for the stringent requirements of the application[66]. The acoustic sensor is the element with the greatest impact in the entire acquisition chain as it determines the noise and distortion of the signal. The sensor prototype presented in this work exploits the intrinsic characteristics of PVDF to obtain a wide-bandwidth, low-noise sensor. The sensor was characterized both in the acoustic domain to verify its performance, and in the electrical domain, as knowing its electrical characteristics is of fundamental importance for developing a dedicated and miniaturized acquisition chain in CMOS technology[67].

4.7 PVDF sensor design with 20µm thickness for high frequency applications

4.7.1 Analytical Model

The fundamental equations of wave propagation in a medium, such as the wave equation or the acoustic basic discrete equation, are usually derived in an analytical MATLAB model for the basic formulation of an acoustic sensor. By following the steps outlined in Chapter 3, the model provides an explanation of how the sensor interacts with the sound wave by solving Equations 1 through 8. Following is a table outlining the fundamental formulation of the Analytical Model, which defines the distinctive parameters of the proposed sensor.

Table 10:Sensor Characteristic Parameters

Sensor Parameters	**Value**
Frequency coefficient	1125 Hz.m
Piezoelectric voltage coefficient	200 mV/(Pa·m)
Glue dielectric Constant	3.5
Piezoelectric relative dielectric constant	10.5
Channel width	0.3mm
Channel length	10mm
PVDF thickness	1.2mm
Water acoustic impedance	1.5 MRayl
PVDF acoustic impedance	3.5MRayl

Table 11: Sensor Performance Parameters

Parameters	**Value**
Capacitance	13 pF
Resonance frequency	56 MHz
Sensitivity @ 25 MHz	3.2 μV/Pa
Channels	8
Output referred noise power	18 μVrms
Output referred spot noise @ 25 MHz	1.9 nV/ Hz
Input referred noise power	5.5 Parms
Input referred spot noise @ 25 MHz	596 μPa/ Hz

The acoustic sensor outlined is engineered for high sensitivity and high-frequency applications, rendering it suitable for thermoacoustic imaging. Thermoacoustic imaging is a medical imaging modality that integrates ultrasound and electromagnetic waves to achieve high-resolution visualisation of internal structures, including tissues. Several key parameters delineate the sensor's design and performance, each significantly contributing to its effectiveness for this purpose.

The sensor exhibits a frequency coefficient of 1125 Hz·m, indicating its optimisation for the detection or generation of high-frequency sound waves, which are crucial for acquiring detailed images in thermoacoustic applications. The piezoelectric voltage coefficient of 200 mV/Pa·m indicates the sensor's high sensitivity, allowing for effective conversion of pressure from sound waves into electrical voltage. The high sensitivity is essential for identifying minor pressure variations that arise during the interaction of waves with biological tissues.

The materials of the sensor are selected to enhance its performance. The dielectric constants of the adhesive (3.5) and the piezoelectric material (10.5) facilitate the optimisation of sound wave transmission into electrical signals, thereby ensuring efficient operation. The acoustic impedance values of 1.5 MRayl for water and 3.5 MRayl for the piezoelectric PVDF material

suggest that the sensor is optimised for operation in environments such as water or biological tissues, which exhibit comparable acoustic characteristics.

The sensor's physical design includes channels measuring 0.3 mm in width and 10 mm in length. The small channel dimensions facilitate enhanced spatial resolution, permitting the sensor to acquire more detailed information from sound waves. The selection of a PVDF thickness of 1.2 mm is deliberate, optimising both sensitivity and frequency response to facilitate the detection of high-frequency waves essential for accurate imaging.

The sensor exhibits a resonance frequency of 56 MHz, enabling efficient operation at high frequencies and delivering the requisite resolution for detailed images in thermoacoustic imaging. The sensor exhibits a sensitivity of 3.2 µV/Pa at 25 MHz, enabling it to detect minor pressure variations, which is essential for obtaining clear images. The sensor features 8 channels, which improves its capacity to cover a broader area and deliver more comprehensive imaging data.The design of the sensor effectively reduces noise, which is essential for generating high-quality images. The output referred noise power is 18 µVrms, while the input referred noise power is 5.5 Parms. These values suggest that the sensor contributes minimal interference to the signal, facilitating clearer images. The spot noise levels at 25 MHz validate the sensor's low noise performance, recording 1.9 nV/Hz at the output and 596 µPa/Hz at the input, thereby ensuring accurate signal capture with minimal distortion.

The acoustic sensor, characterised by its selected materials, design parameters, and low-noise performance, is well-suited for thermoacoustic imaging. The capacity to function at elevated frequencies and sense pressure variations enables the generation of detailed, high-resolution images, crucial for medical imaging applications.

4.8 Directivity Results

The development of the acoustic sensor begins with a fundamental acoustic requirement that constrains the physical dimension of each channel, namely the directivity (i.e. the sensitivity as a function of the angle of arrival of the acoustic wave). when the wave hits with an arrival angle different from 0 ° concerning to the normal one, it will stimulate different parts of the single channel at different moments the more the size of the channel is large compared to the wavelength, leading to destructive interference. In other words, each channel must be small enough w.r.t the acoustic wavelength to behave as an almost omnidirectional sensor, at least in the range of arrival angles foreseen by the experimental scenario.

To measure the proposed prototype PVDF sensor directivity response using a single frequency approach, the sensor-active element must be accurately aligned with the center of propagation. Small placement mistakes can significantly affect observed directional responses. Measuring the directional response of sensors in a 2-D array poses a challenge since each hydrophone element requires a unique centre of rotation. For elements near the array's edge, it might be challenging to establish separate degrees of freedom. This alternate technique evaluates directivity patterns based on frequency for a particular angle. This significantly reduces susceptibility to location and temperature stability issues. A modified version of the traditional single frequency approach was used to create a directivity pattern for hydrophone components at the centre of the 2-D array[68]. To compare theoretical directivity patterns, examine the idea of effective. A comprehensive study of this issue may be found elsewhere, and a method for determining effective size has been provided[69].

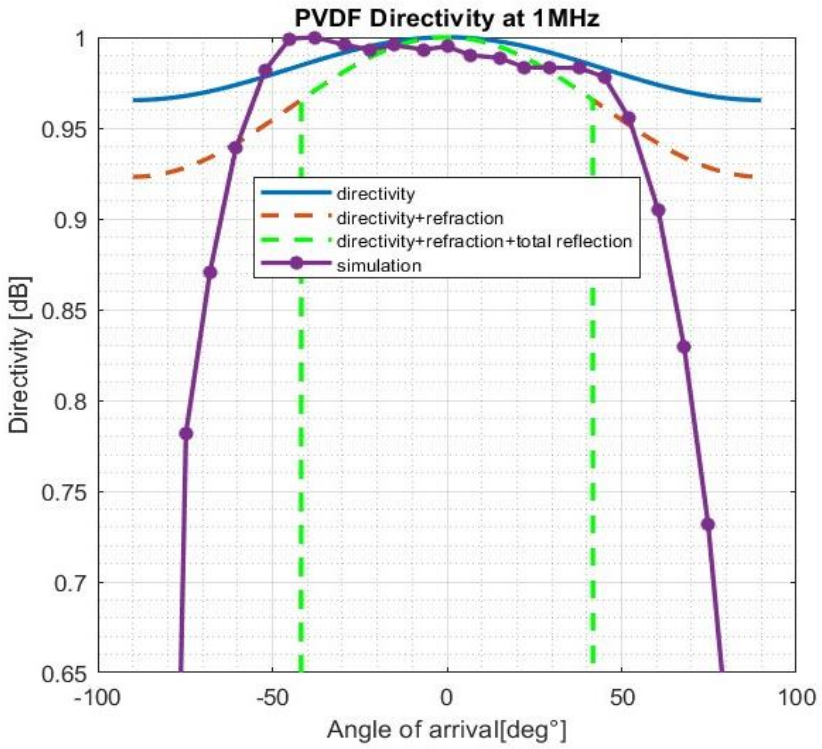

Figure 30: Directivity response of PVDF Sensor at 1MHz

The effect of frequency increase has a significant impact on the directivity of a sensor, especially in the case of a PVDF transducer, enhancing its directional characteristics. As the frequency increases, from 1 MHz to 10 MHz, the directivity pattern narrows, indicating that the sensor becomes more concentrated in detecting signals along its central axis (0 degrees). At 1

MHz, the directivity pattern is wide, enabling the sensor to detect signals from a wide array of angles, maintaining relatively high sensitivity even at ±45 to ±50 degrees, behaving like an omnidirectional sensor. At 10 MHz, the directivity is highly concentrated around the centre, exhibiting a steep decline in sensitivity as the angle deviates from 0 degrees. This indicates that at elevated frequencies, the sensor exhibits reduced sensitivity to off-axis signals, thereby becoming more directional. The increased frequency leads to a decrease in sensitivity to signals coming from broader angles, as the shorter wavelengths associated with higher frequencies

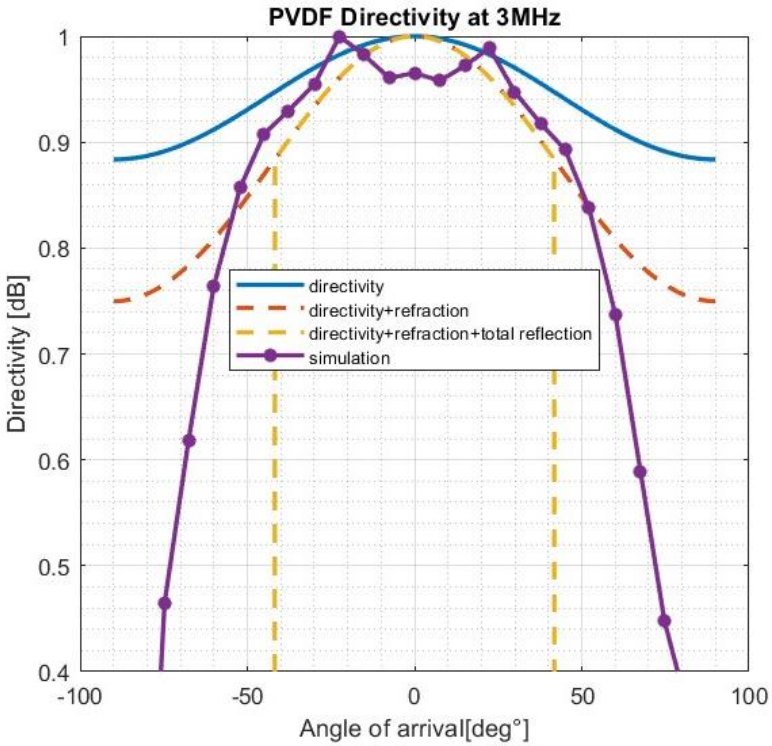

Figure 31:Directivity response of PVDF Sensor at 3MHz

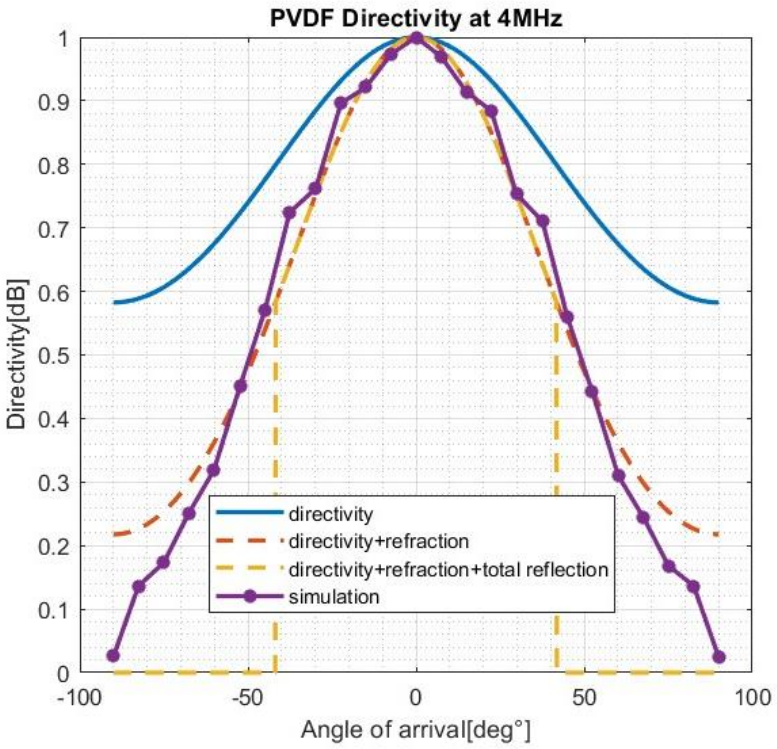

Figure 32:Directivity response of PVDF Sensor at 4MHz

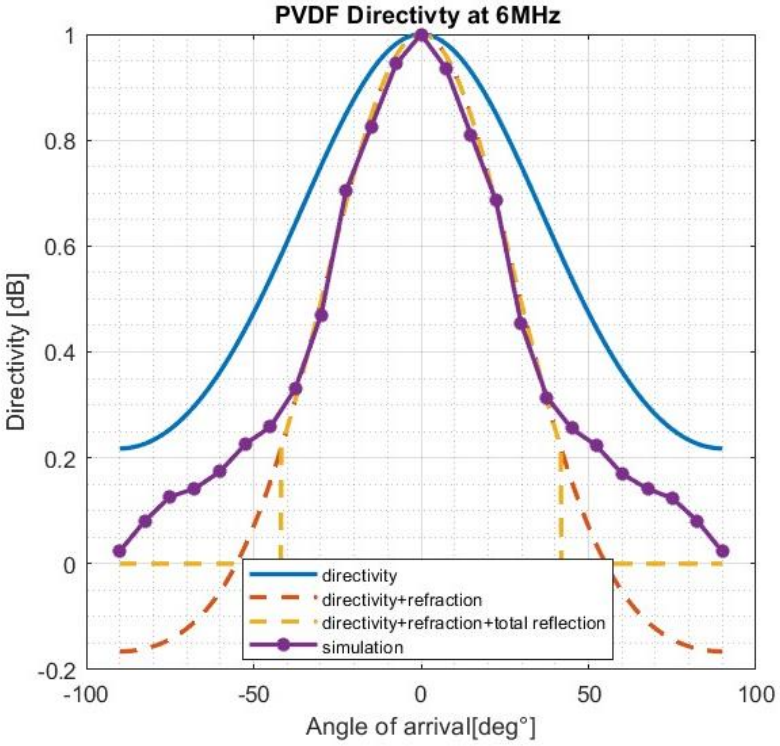

Figure 33:Directivity response of PVDF Sensor at 6MHz

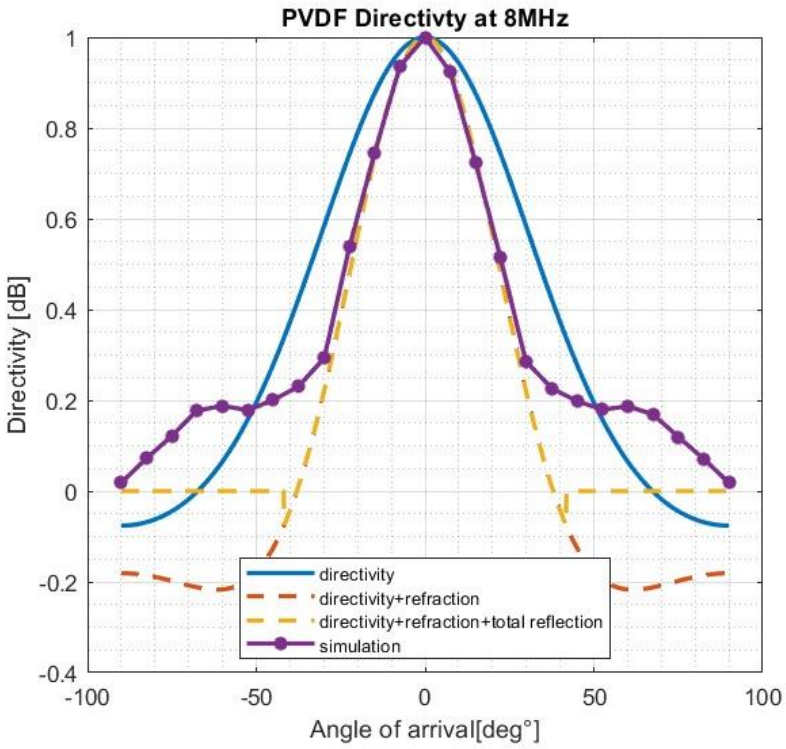

Figure 34:Directivity response of PVDF Sensor at 8MHz

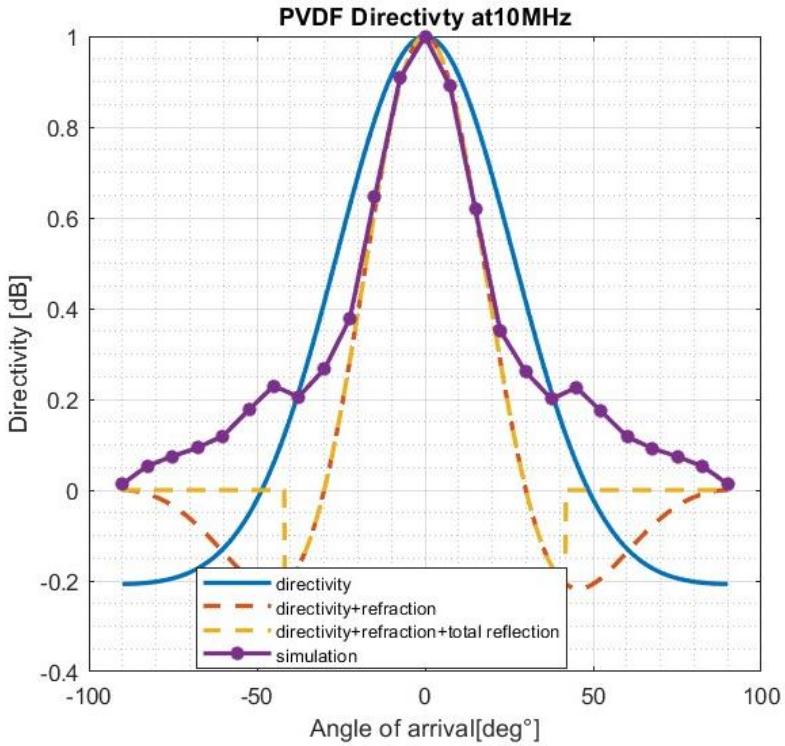

Figure 35:Directivity response of PVDF Sensor at 10MHz

inherently restrict the sensor's capacity to detect signals from directions that stray from the central beam.

Furthermore, refraction and total reflection affect the directivity pattern at both frequencies, their impact is more pronounced at lower frequencies. It happens when an acoustic wave enter from one medium like water lower sound speed (1500 m/s) to another medium like PVDF (2250 m/s) with a higher sound speed face bending inward due to the different sound speeds of both mediums in results acoustic wave refracted. At 10 MHz, the overall pattern stays more focused, despite the continued influence of these factors. while moving from 1 to 10MHz, there is clear trend has been seen that at lower frequency around 1MHz sensor size is smaller as compared to acoustic wavelength which makes it as omnidirectional sensor. While moving towards a higher frequency from 1 to 10MHz, sensor become more directional because at higher frequency wavelength gets shorter gradually as compared to the sensor size (0.3x10mm), the wave hits with an arrival angle different from concerning to the normal one, it will stimulate different parts of the single channel at different moments leading to destructive interference. Such kind of directivity pattern helps a lot to optimize the geometry of sensors for high-frequency applications.

In general, enhancing the frequency leads to an improvement in the sensor's spatial resolution, resulting in greater precision in detecting signals from a limited range of angles. High-frequency transducers, such as those operating at 10 MHz, are more suitable for applications that require pinpoint accuracy and high directivity. In contrast, lower-frequency transducers, like those at 1 MHz, excel in applications that need broader detection over a wider frequency range.

4.9 Frequency Response

The simulated wideband frequency response of a PVDF (Polyvinylidene fluoride) sensor, the power output/input ratio (Pout/Pin) in decibels (dB) as a function of frequency in hertz (Hz).

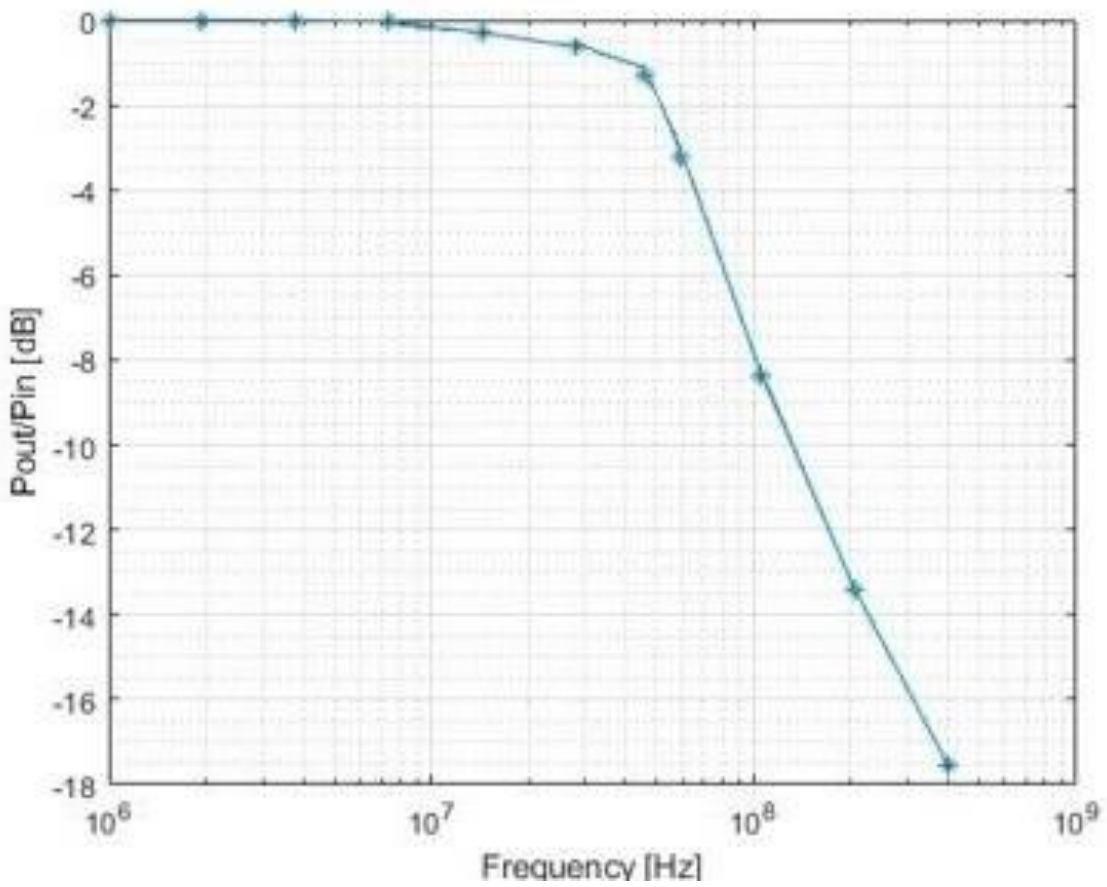

Figure 36: Pvdf sensor Frequency Response

The response stays constant at 0 dB up to roughly up to 10^7 Hz, signifying negligible signal attenuation within this range. Nevertheless, beyond this frequency, a significant decrease is

seen, with the output power diminishing dramatically by approximately -18 dB as the frequency nears 10^9 Hz. This indicates that the PVDF sensor operates effectively in the higher frequency spectrum up to 10MHz but suffers considerable loss and diminished efficiency beyond this higher frequencies as already explained in the analytical model frequency is thickness dependent so 20µm thickness makes him a potential candidate for high frequencies application, especially beyond 10^7 Hz. This behavior is characteristic of wideband sensors, wherein higher frequencies lead to increased attenuation.

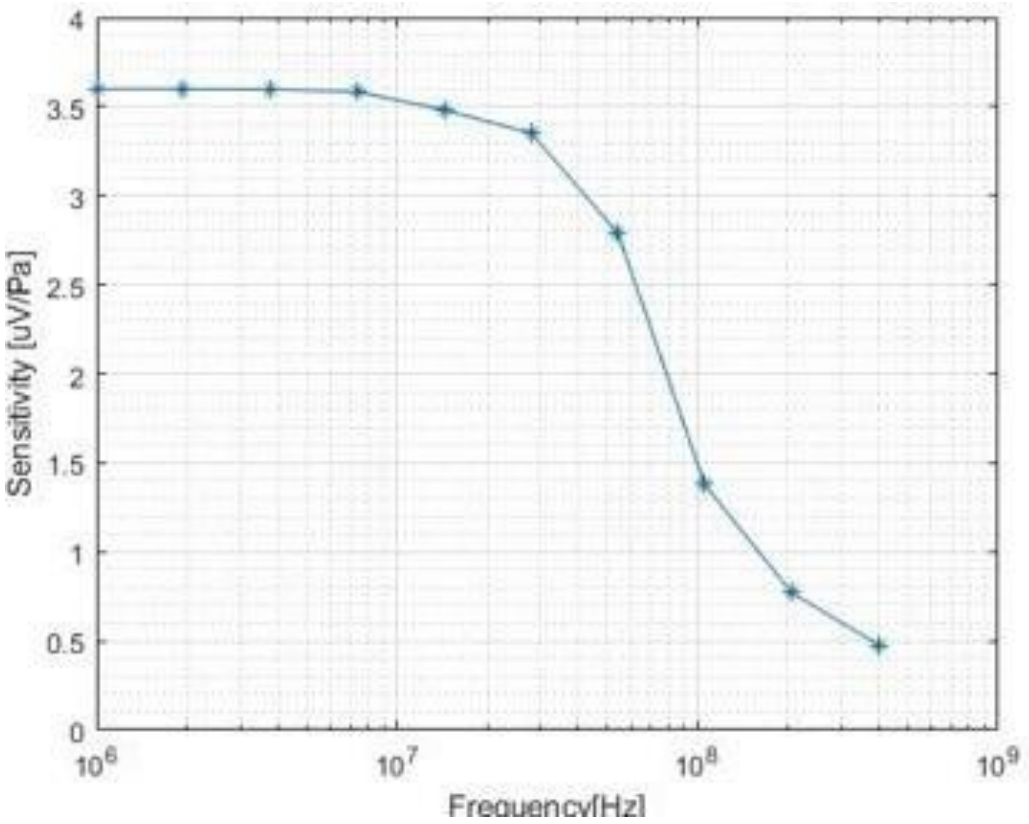

Figure 37: Simulated Sensitivity Response Curve

PVDF, like other piezoelectric materials, has inherent dielectric losses that increase with frequency. At higher frequencies, the molecular dipoles within the PVDF material cannot realign quickly enough to respond to the electric field generated by incoming signals. This leads to higher energy dissipation, which manifests as a reduction in the output power relative to the input, as shown by the drop-off in the response curve beyond At higher frequencies, the wavelength of the acoustic waves decreases, and the acoustic impedance mismatch between the PVDF sensor and the surrounding medium (e.g., air or water) becomes more pronounced. This mismatch results in greater reflection of acoustic energy at the boundaries, causing signal loss

and less effective transmission of power into and out of the sensor. The frequency response graph provided shows that the PVDF sensor maintains a relatively flat response with minimal attenuation. Beyond the resonance frequency point, there is a significant drop in the output/input power ratio, indicating that the sensor's performance degrades rapidly at 10^7 Hz frequencies. For 10 MHz applications, the PVDF sensor is suitable, as the frequency response is still relatively stable and efficient at this frequency. At 10 MHz, the attenuation is minimum, and the output/input power ratio is close to 0 dB, meaning the sensor can efficiently transmit or receive signals without significant loss. However, if the application involves frequencies beyond 10 MHz, the sensor may not perform as well, as shown by the steep decline in response. Since the sensor's frequency response begins to drop sharply past 10 MHz, it is optimal for applications that operate at or below 10 MHz. In such cases, the sensor will provide good sensitivity and energy transfer, making it effective for tasks like ultrasonic imaging, sensing, or communication that rely on frequencies around 10 MHz.

The sensitivity and frequency response graphs show that the PVDF sensor performs well up to 10 MHz, maintaining a steady sensitivity and a low energy loss. Nevertheless, both the output/input power ratio and sensitivity show a discernible decrease above resonance frequency suggesting that the sensor's performance is severely diminished at higher frequencies. As a result, the sensor performs best in low- to mid-frequency applications (up to 10 MHz), with higher-frequency activities reducing its efficiency.

4.10 Experimental Results

4.10.1 Acoustic Test Setup

The experimental setup as shown in Figure 38. with the transmitter on the right side (Black) and the PVDF receiver on the left. The complete setup is under water to validate the acoustic behavior of the designed prototype PVDF based ultrasound transducer. PVDF designed ultrasound transducer composed on flexible circuit which contain multiple channel. Whereas water behave as acoustic propagation medium.

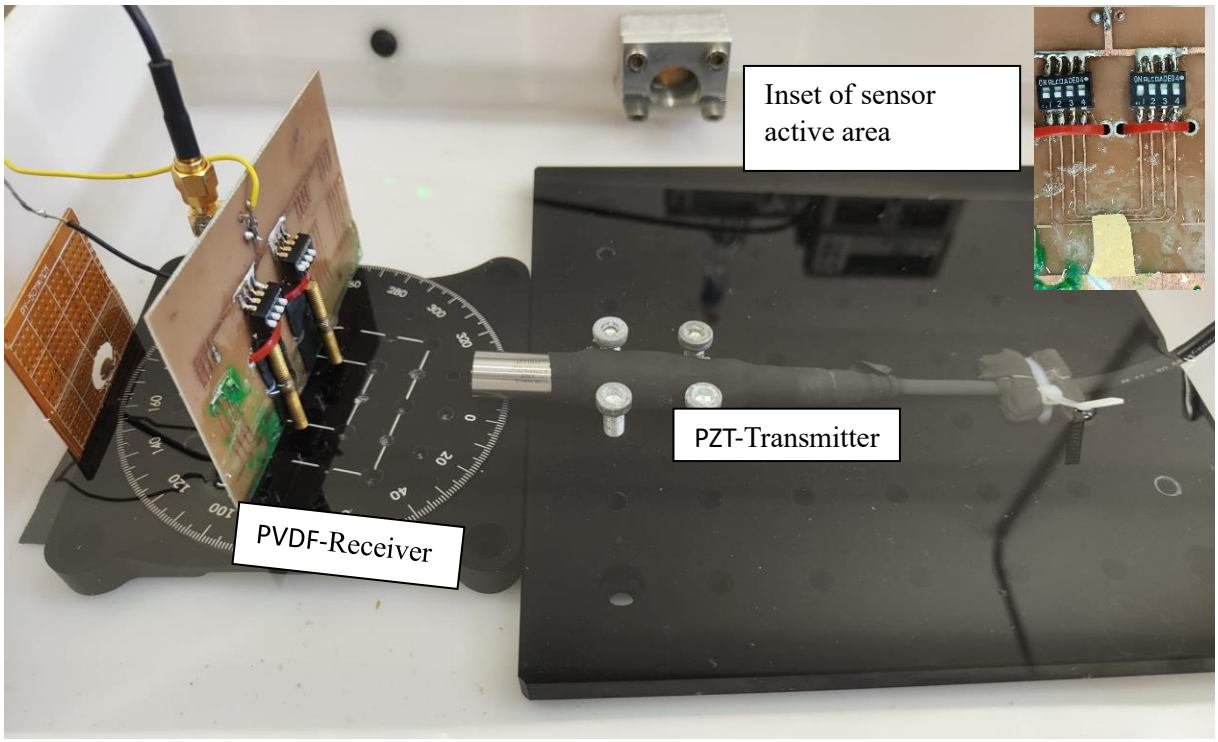

Figure 38: Acoustic test setup

4.11 Time Domain acoustic signal

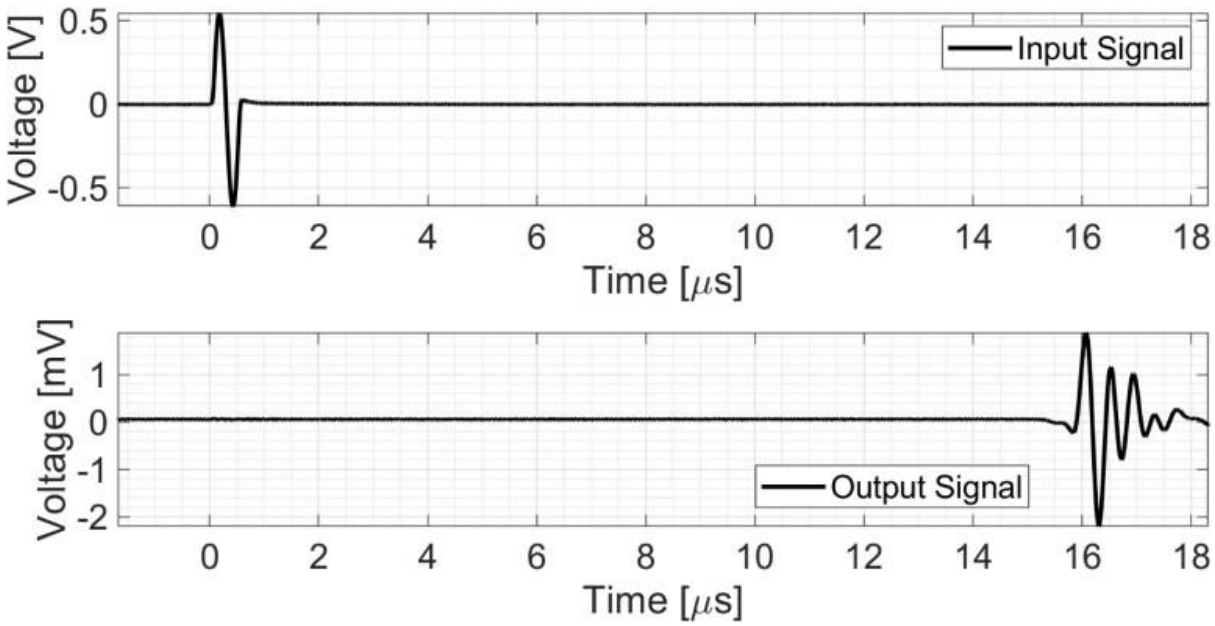

Figure 39: Acoustic signal Flight (Time vs voltage)

Figure 39. shows the input and output voltage signals in the time domain. A single pulse signal of 500 mV0peak and an equivalent frequency of 2 MHz from a signal generator is used to stimulate the transmitter. The PVDF receiver outputs a with 2 mV0peak amplitude, where the difference in amplitude is due to the conversion (V-Pa and Pa-V) and propagation (1/r attenuation) losses. The ringing in the received signal has a bandwidth of 2 MHz and is due to the transmitter's high-quality factor, whereas no high-frequency oscillations (possibly due to the PVDF sensor) can be observed

In this work, an analytical design procedure and a FEM model are used to design a PVDF sensor array that exploits a low-cost PCB-based manufacturing method to minimize fabrication effort w.r.t. etching techniques [70, 71]. The sensor prototype has been characterized in terms of acoustic and electric parameters, highlighting the negligible impact of the glue layer required by the manufacturing process. Low-cost high-frequency ultrasound sensors could open to accessible high-resolution photoacoustic diagnostic tools [72].

4.12 Conclusion

PVDF (Polyvinylidene Fluoride) ultrasound sensors have been proposed as a high-precision and cost-effective replacement to traditional piezoelectric materials like PZT (Lead-Zirconate-Titanate). PVDF's acoustic impedance closely resembles that of water and biological tissues, reducing the need for complicated matching layers and enhancing signal transmission. This material's intrinsic features, such as broad bandwidth, low noise, and compatibility with PCB-based production, make it ideal for applications that need high spatial resolution and little signal distortion.

These PVDF-based arrays have demonstrated great sensitivity across a wide frequency range in thermoacoustic imaging, making them suitable for detailed tissue imaging with very easy and scalable production techniques. The directivity graphs shown in the research show that increasing PVDF thickness resulted in sharper directivity profiles and wider angle performance, strengthening its suitability for advanced medical imaging applications.

There are various opportunities to improve and broaden PVDF's applicability in medical imaging. First, optimizing PVDF thickness like 1.2mm to 0.1mm, might result in an optimal mix of sensitivity and bandwidth, improving directivity while keeping a small sensor footprint. Increasing the number of array channels and refining channel diameters may enhance spatial resolution 10µm, allowing for more detailed imaging capabilities, especially in biological diagnosis. Furthermore, merging PVDF sensors with CMOS technology may enable real-time processing, minimise noise, and improve acquisition fidelity. Such integration may also enable the creation of large-scale multi-channel systems adapted to complicated imaging requirements.

Beyond hadron treatment, PVDF arrays show potential in photoacoustic or thermoacoustic imaging while using thickness 20 µm for early cancer diagnosis. PVDF sensors' cost-effectiveness makes them attractive candidate for diagnostic equipment in low-resource situations, increasing access to refined imaging. Furthermore, developments in PCB technology enable flexible PVDF arrays, which may be configured in non-planar ways to adapt to complicated anatomical features. Flexible arrays may improve imaging accuracy for organs and tissues with uneven surfaces, such as the brain and liver. Future research and development efforts aimed at improving sensor characteristics, integrating advanced electronics, and expanding geometric configurations could help to unlock PVDF's application potential, positioning it as a next-generation solution in medical diagnostics.

Publications

PVDF Ultrasound Array Design for Ionoacoustic Tomography of Particle Beams in Hadron Therapy.

DOI**:** 10.1109/PRIME61930.2024.10559694

56-MHz-Bandwidth 2.4-3.5 µV/Pascal-Sensitivity-Range Polyvinylidene Fluoride Ultrasound Sensor Array for Biomedical Thermoacoustic Imaging.

DOI: 10.1109/PRIME58259.2023.10161987

Low-cost PVDF High-Frequency Ultrasound Sensor Design and Manufacturing for Thermoacoustic Imaging Applications

DOI: 10.1109/ICECS202256217.2022.9971002

Acknowledgment.

I would like to express my heartfelt gratitude to my colleagues whom I had the privilege of working alongside during my three years in the Ph.D. program. In particular, I extend my sincere thanks to Andrea La Gala for their invaluable guidance, which significantly enhanced my understanding of various concepts in simulation work. I am deeply indebted to Prof. Marcello De Matties and Prof. Giuseppe Chirico for granting me the opportunity to contribute to such an exciting and challenging project and for their unwavering support and mentorship throughout my doctoral journey. Special thanks to Elia A. Vallicelli for their important role as Co-supervisor of the project, whose expertise and contributions were instrumental to its success.

I would like to express my profound appreciation to my family for their steadfast support and encouragement throughout my academic endeavors, from my undergraduate and master's studies to my Ph.D. program. Their belief in my aspirations has been an enduring source of motivation and strength.

.

References.

1. Oralkan, O., et al., *Capacitive micromachined ultrasonic transducers: Next-generation arrays for acoustic imaging?* IEEE transactions on ultrasonics, ferroelectrics, and frequency control, 2002. **49**(11): p. 1596-1610.
2. Blow, E.C., *Microwave Photonic Interference Cancellation: RF Analysis, III-V and Silicon Integration, Development of Balanced and Hybrid Architectures*. 2024, Princeton University.
3. Cummins, T., et al. *Backscattering analysis of high frequency ultrasonic imaging for ultrasound-guided breast biopsy*. in *Medical Imaging 2017: Ultrasonic Imaging and Tomography*. 2017. SPIE.
4. Shung, K.K., J. Cannata, and Q. Zhou, *Piezoelectric materials for high frequency medical imaging applications: A review.* Journal of Electroceramics, 2007. **19**: p. 141-147.
5. Vallicelli, E., *Design of Mixed-Signal Electronic Instrumentation for Proton Sound Detectors.* 2021.
6. Wu, D., et al., *Contrast agents for photoacoustic and thermoacoustic imaging: a review.* Int J Mol Sci, 2014. **15**(12): p. 23616-39.
7. Vallicelli, E.A., et al. *Low-cost PVDF High-Frequency Ultrasound Sensor Design and Manufacturing for Thermoacoustic Imaging Applications*. in *2022 29th IEEE International Conference on Electronics, Circuits and Systems (ICECS)*. 2022. IEEE.
8. Baig, M.H., et al. *56-MHz-Bandwidth 2.4-3.5 μV/Pascal-Sensitivity-Range Polyvinylidene Fluoride Ultrasound Sensor Array for Biomedical Thermoacoustic Imaging*. in *2023 18th Conference on Ph. D Research in Microelectronics and Electronics (PRIME)*. 2023. IEEE.
9. Dogra, V.S., et al., *Multispectral photoacoustic imaging of prostate cancer: preliminary ex-vivo results.* Journal of clinical imaging science, 2013. **3**.
10. Wang, L.V. and S. Hu, *Photoacoustic tomography: in vivo imaging from organelles to organs.* science, 2012. **335**(6075): p. 1458-1462.
11. Lee, W., et al., *A 10-Fr ultrasound catheter with integrated micromotor for4-D intracardiac echocardiography.* IEEE transactions on ultrasonics, ferroelectrics, and frequency control, 2011. **58**(7): p. 1478-1491.
12. Qiu, Y., et al., *Piezoelectric micromachined ultrasound transducer (PMUT) arrays for integrated sensing, actuation and imaging.* Sensors, 2015. **15**(4): p. 8020-8041.
13. Dangi, A., et al. *Evaluation of high frequency piezoelectric micromachined ultrasound transducers for photoacoustic imaging*. in *2018 IEEE SENSORS*. 2018. IEEE.
14. Kim, K.Y., et al., *Measurements of the longitudinal wave speed in thin materials using a wideband PVDF transducer.* J Acoust Soc Am, 2003. **114**(3): p. 1450-3.
15. Uchino, K., *The development of piezoelectric materials and the new perspective*, in *Advanced Piezoelectric Materials*. 2017, Elsevier. p. 1-92.
16. Guerin, S., S.A. Tofail, and D. Thompson, *Organic piezoelectric materials: milestones and potential.* NPG Asia Materials, 2019. **11**(1): p. 10.
17. Lee, H.S., et al., *Flexible inorganic piezoelectric acoustic nanosensors for biomimetic artificial hair cells.* Advanced Functional Materials, 2014. **24**(44): p. 6914-6921.
18. Ramadan, K.S., D. Sameoto, and S. Evoy, *A review of piezoelectric polymers as functional materials for electromechanical transducers.* Smart Materials and Structures, 2014. **23**(3): p. 033001.
19. Guerin, S., et al., *Control of piezoelectricity in amino acids by supramolecular packing.* Nature materials, 2018. **17**(2): p. 180-186.

20. Mokhtari, F., et al., *Recent advances of polymer-based piezoelectric composites for biomedical applications.* Journal of the Mechanical Behavior of Biomedical Materials, 2021. **122**: p. 104669.
21. Lai, Y.-H., et al., *Oxygen-producing composite dressing activated by photothermal and piezoelectric effects for accelerated healing of infected wounds.* Chemical Engineering Journal, 2023. **476**: p. 146744.
22. Capuana, E., et al., *Poly-L-lactic acid (PLLA)-based biomaterials for regenerative medicine: A review on processing and applications.* Polymers, 2022. **14**(6): p. 1153.
23. Azimi, S., et al., *Self-powered cardiac pacemaker by piezoelectric polymer nanogenerator implant.* Nano Energy, 2021. **83**: p. 105781.
24. Chernozem, R., et al., *Piezoelectric 3-D fibrous poly (3-hydroxybutyrate)-based scaffolds ultrasound-mineralized with calcium carbonate for bone tissue engineering: inorganic phase formation, osteoblast cell adhesion, and proliferation.* ACS applied materials & interfaces, 2019. **11**(21): p. 19522-19533.
25. Xie, L., et al., *Properties and applications of flexible poly (vinylidene fluoride)-based piezoelectric materials.* Crystals, 2021. **11**(6): p. 644.
26. Foster, F., *<History of_PVDF_transducers(R).pdf>*. IEEE transactions on ultrasonics, ferroelectrics, and frequency control, 2000. **47**: p. 6.
27. Brown, L.F. *Ferroelectric polymers: current and future ultrasound applications*. in *IEEE 1992 Ultrasonics Symposium Proceedings*. 1992. IEEE.
28. Zipparo, M.J., K.K. Shung, and T.R. Shrout, *Piezoceramics for high-frequency (20 to 100 MHz) single-element imaging transducers.* IEEE transactions on ultrasonics, ferroelectrics, and frequency control, 1997. **44**(5): p. 1038-1048.
29. Kawai, H., *The piezoelectricity of poly (vinylidene fluoride).* Japanese journal of applied physics, 1969. **8**(7): p. 975.
30. Park, C., et al., *Soft Ferroelectrics Enabling High-Performance Intelligent Photo Electronics.* Advanced Materials, 2021. **33**(47): p. 2004999.
31. Aksel, E. and J.L. Jones, *Advances in lead-free piezoelectric materials for sensors and actuators.* Sensors, 2010. **10**(3): p. 1935-1954.
32. Ribeiro, C., et al., *Electroactive poly (vinylidene fluoride)-based structures for advanced applications.* Nature protocols, 2018. **13**(4): p. 681-704.
33. Laudari, A., et al., *Tuning charge transport in PVDF-based organic ferroelectric transistors: status and outlook.* ACS applied materials & interfaces, 2020. **12**(24): p. 26757-26775.
34. Soulestin, T., et al., *Vinylidene fluoride-and trifluoroethylene-containing fluorinated electroactive copolymers. How does chemistry impact properties?* Progress in Polymer Science, 2017. **72**: p. 16-60.
35. Shirinov, A.V. and W.K. Schomburg, *Pressure sensor from a PVDF film.* Sensors and actuators A: Physical, 2008. **142**(1): p. 48-55.
36. Sharma, T., et al., *Patterning piezoelectric thin film PVDF–TrFE based pressure sensor for catheter application.* Sensors and Actuators A: physical, 2012. **177**: p. 87-92.
37. Maity, K., et al., *Self-powered human-health monitoring through aligned PVDF nanofibers interfaced skin-interactive piezoelectric sensor.* ACS Applied Polymer Materials, 2020. **2**(2): p. 862-878.
38. Khan, A., et al., *The potential of organic piezoelectric materials for next-generation implantable biomedical devices.* Nano Trends, 2024: p. 100032.

39. Guo, Z., et al., *Self-powered sound detection and recognition sensors based on flexible polyvinylidene fluoride-trifluoroethylene films enhanced by in-situ polarization.* Sensors and Actuators A: Physical, 2020. **306**: p. 111970.
40. Wong, C.M., *Study of high-frequency ultrasound transducers for advanced biomedical imaging.* 2022.
41. Manbachi, A. and R.S. Cobbold, *Development and application of piezoelectric materials for ultrasound generation and detection.* Ultrasound, 2011. **19**(4): p. 187-196.
42. Kang, B.J., Q. Zhou, and K.K. Shung, *High-frequency ultrasonic transducers to uncover cardiac dynamics.* Interfacing Bioelectronics and Biomedical Sensing, 2020: p. 185-192.
43. Basavarajappa, G., *Tunable Band Pass Filters for Communication Systems.* 2021.
44. Alvarez-Arenas, T.G., *Acoustic impedance matching of piezoelectric transducers to the air.* IEEE transactions on ultrasonics, ferroelectrics, and frequency control, 2004. **51**(5): p. 624-633.
45. Fazlyyyakhmatov, M. *Sensitivity and directivity measurement of ultrasonic transducer with polymer-powder matching layer*. in *Journal of Physics: Conference Series*. 2018. IOP Publishing.
46. Zhou, Q., et al., *Piezoelectric single crystal ultrasonic transducers for biomedical applications.* Progress in materials science, 2014. **66**: p. 87-111.
47. Ozeri, S. and D. Shmilovitz, *Ultrasonic transcutaneous energy transfer for powering implanted devices.* Ultrasonics, 2010. **50**(6): p. 556-66.
48. Kelly, S., G. Hayward, and T. Gomez. *An air-coupled ultrasonic matching layer employing half wavelength cavity resonance*. in *2001 IEEE Ultrasonics Symposium. Proceedings. An International Symposium (Cat. No. 01CH37263)*. 2001. IEEE.
49. Otto, C.M., *Textbook of clinical echocardiography*. 2013: Elsevier Health Sciences.
50. Foster, F.S., K.A. Harasiewicz, and M.D. Sherar, *A history of medical and biological imaging with polyvinylidene fluoride (PVDF) transducers.* IEEE transactions on ultrasonics, ferroelectrics, and frequency control, 2000. **47**(6): p. 1363-1371.
51. Cannata, J.M., et al., *Design of efficient, broadband single-element (20-80 MHz) ultrasonic transducers for medical imaging applications.* IEEE transactions on ultrasonics, ferroelectrics, and frequency control, 2003. **50**(11): p. 1548-1557.
52. Turnbull, D.H., et al., *A 40–100 MHz B-scan ultrasound backscatter microscope for skin imaging.* Ultrasound in medicine & biology, 1995. **21**(1): p. 79-88.
53. Fleischman, A., et al., *Miniature high frequency focused ultrasonic transducers for minimally invasive imaging procedures.* Sensors and Actuators A: Physical, 2003. **103**(1-2): p. 76-82.
54. Alves, C.H., et al. *High-frequency single-element and annular array transducers incorporating PVDF*. in *Medical Imaging 2000: Ultrasonic Imaging and Signal Processing*. 2000. SPIE.
55. Sherar, M. and F. Foster, *The design and fabrication of high frequency poly (vinylidene fluoride) transducers.* Ultrasonic imaging, 1989. **11**(2): p. 75-94.
56. Carey, S.J., et al., *PVdF array characterisation for high frequency ultrasonic imaging*, in *IEEE Ultrasonics Symposium, 2004*. 2004. p. 1930-1933.
57. Lockwood, G.R. and C.R. Hazard. *Miniature polymer transducers for high-frequency medical imaging*. in *Medical Imaging 1998: Ultrasonic Transducer Engineering*. 1998. SPIE.
58. Carey, S., C. Gregory, and J. Hatfield. *Electronics for high impedance ultrasound transducers*. in *World Congress on Ultrasonics, Paris*. 2003.

59. Xing, J., et al., *An integral wavy shaped P (VDF-TrFE) transducer for audio directional system.* Sensors and Actuators A: Physical, 2024. **375**: p. 115533.
60. Ritter, T.A., et al., *A 30-MHz piezo-composite ultrasound array for medical imaging applications.* IEEE transactions on ultrasonics, ferroelectrics, and frequency control, 2002. **49**(2): p. 217-230.
61. Smith, W.A. *The role of piezocomposites in ultrasonic transducers*. in *Proceedings., IEEE Ultrasonics Symposium*. 1989. IEEE.
62. Geng, X., *Numerical modeling and experimental study of piezocomposite transducers*. 1997: The Pennsylvania State University.
63. Ballandras, S., et al. *A periodic finite element formulation for the design of 2-2 composite transducers*. in *1999 IEEE Ultrasonics Symposium. Proceedings. International Symposium (Cat. No. 99CH37027)*. 1999. IEEE.
64. Kirkbright, G., *Photoacoustics and photoacoustic spectroscopy. Allan Rosencwaig. published by Wiley/Interscience.* Spectrochimica Acta, 1981. **36**(10): p. 1030-1030.
65. Zharov, V.P. and V.S. Letokhov, *Laser optoacoustic spectroscopy*. Vol. 37. 2013: Springer.
66. Riva, M., et al., *Acoustic analog front end for proton range detection in hadron therapy.* IEEE transactions on biomedical circuits and systems, 2018. **12**(4): p. 954-962.
67. De Matteis, M., et al., *64 dB dynamic-range 810 μW 90 MHz fully-differential flipped-source-follower analog filter in 28nm-CMOS.* IEEE Transactions on Circuits and Systems II: Express Briefs, 2021. **68**(9): p. 3068-3072.
68. Harris, G. and D. Shombert, *A pulsed near-field technique for measuring the directional characteristics of acoustic receivers.* IEEE transactions on sonics and ultrasonics, 1985. **32**(6): p. 802-808.
69. Chivers, R., *The definition and use of effective geometrical parameters for radiating transducers in experimental ultrasonics.* Acta Acustica united with Acustica, 1990. **70**(3): p. 215-222.
70. Arditi, M., et al., *An annular array system for high resolution breast echography.* Ultrasonic Imaging, 1982. **4**(1): p. 1-31.
71. Hurrell, A. and F. Duck, *A two-dimensional hydrophone array using piezoelectric PVDF.* ieee transactions on ultrasonics, ferroelectrics, and frequency control, 2000. **47**(6): p. 1345-1353.
72. Zou, W., et al., *Wideband high-frequency line-focus PVDF transducer for materials characterization.* Ultrasonics, 2003. **41**(3): p. 157-161.

Figure References

1- Y. Chen, M. Ye, L. Song, J. Zhang, Y. Yang, S. Luo, M. Lin, Q. Zhang, S. Li, Y. Zhou, A. Chen, Y. An, W. Huang, T. Xuan, Y. Gu, H. He, J. Wu, X. Li, Appl. Mater. Today 20 (2020) 100756.

2- Yuan, X.; Gao, X.; Shen, X.; Yang, J.; Li, Z.; Dong, S. A 3D-printed, alternatively tilt-polarized PVDF-TrFE polymer with enhanced piezoelectric effect for self-powered sensor application. Nano Energy 2021, 85, 105985.